UNIVERSIDADE DE BRASÍLIA-UnB
INSTITUTO DE GEOCIÊNCIAS-IGD
PROGRAMA DE PÓS-GRADUAÇÃO EM GEOLOGIA

CLEVERTON CORREIA SILVA

PETROGRAFIA, GEOQUÍMICA E GEOCRONOLOGIA DAS ROCHAS VULCÂNICAS EFUSIVAS E PIROCLÁSTICAS DA FORMAÇÃO ARRAIAS, GRUPO ARAÍ, NORDESTE DE GOIÁS

Orientador: Valmir da Silva Souza
Coorientador: Nilson Francisquini Botelho

TESE DE DOUTORADO N° 163

Brasília-DF
2020

UNIVERSIDADE DE BRASÍLIA-UnB
INSTITUTO DE GEOCIÊNCIAS-IGD
PROGRAMA DE PÓS-GRADUAÇÃO EM GEOLOGIA

CLEVERTON CORREIA SILVA

PETROGRAFIA, GEOQUÍMICA E GEOCRONOLOGIA DAS ROCHAS VULCÂNICAS EFUSIVAS E PIROCLÁSTICAS DA FORMAÇÃO ARRAIAS, GRUPO ARAÍ, NORDESTE DE GOIÁS

Orientador: Valmir da Silva Souza
Coorientador: Nilson Francisquini Botelho

Tese de Doutorado apresentada ao Instituto de Geociências da Universidade de Brasília, como parte dos requisitos para a obtenção de título de Doutor em Geologia.

Comissão Examinadora:
Prof. Dr. Valmir da Silva Souza (Presidente-UnB)
Dr. Jaime Estevão Scandolara (CPRM)
Dra. Joseneusa Brilhante Rodrigues (CPRM)
Profa. Dra. Natalia Hauser (UnB)

Brasília-DF
2020

FICHA CATALOGRÁFICA

Silva, Cleverton Correia

SS579p Petrografia, Geoquímica e Geocronologia das Rochas Vulcânicas Efusivas e Piroclásticas da Formação Arraias, Grupo Araí, Nordeste de Goiás / Cleverton Correia Silva; orientador Valmir da Silva Souza; co-orientador Nilson Francisquini Botelho. -- Brasília, 2020.
119 p.

Tese (Doutorado - Doutorado em Geologia) -- Universidade de Brasília, 2020.

1. Vulcanismo Paleoproterozoico. 2. Vulcanismo Bimodal. 3. Grupo Araí. 4. Formação Arraias. 5. Faixa Brasília. I. Souza, Valmir da Silva, orient. II. Botelho, Nilson Francisquini, co-orient. III. Título.

AGRADECIMENTOS

Ao longo desses últimos anos pude contar com o apoio de diversas pessoas e instituições que contribuíram para que eu pudesse concluir o meu Doutorado em Geologia. Por isso, gostaria de agradecer:

De início, ao meu orientador Dr. Valmir da Silva Sousa pela orientação, pelos debates, pelos puxões de orelha, pela compreensão e pelos momentos de aprendizado durante o desenvolvimento do meu doutorado. Agradeço pela paciência e ajuda que me deu durante os momentos mais difíceis. Além disso, agradeço por não ter me deixado desistir, por confiar em meu trabalho e por me fazer refletir melhor sobre os caminhos que eu precisava seguir.

Ao meu coorientador o professor Dr. Nilson Francisquini Botelho por ter aceitado ser meu orientador quando participei da seleção para o doutorado no Programa de Pós-Graduação em Geologia. Além disso, agradeço por ter participado dos meus trabalhos de campo e pelas ajudas financeiras para o desenvolvimento da minha pesquisa.

Aos professores do Programa de Pós-Graduação em Geologia e convidados que me deram a honra de participar de suas aulas: Affonso Brod (UFG), Ana Maria Góes (USP), Benhard Buhun (*in* memória), Carlos Emanoel de Souza Cruz, Carlos José Souza de Alvarenga, José Marcelo Arnosio (Universidade de Salta, Argentina), Marcio Pimentel (*in* memória), Massimo Matteini, Natalia Hauser, Nilson Francisquine Botelho, Reinhardt A. Fuck, Sérgio Valente (UFRRJ), Sylvia Maria Araujo, Tiago Jalowitzki e Valmir da Silva Souza.

À Universidade de Brasília, que mesmo passando por momentos de cortes orçamentários e ataques de diversas ordens, me deu todos os subsídios necessários para que eu pudesse concluir meu doutorado. Além disso, agradeço pelos auxílios da assistência estudantil que facilitou a minha permanência em Brasília.

Ao colegiado do Programa de Pós-Graduação em Geologia pelas diversas solicitações atendidas ao longo desses anos.

Ao corpo técnico dos laboratórios de Laminação, Geocronologia, Geoquímica, Microscopia e da Microssonda do Instituto de Geociências da UnB que sempre foram atenciosos e prestativos.

Ao Conselho Nacional de Desenvolvimento Científico e Tecnológico (CNPq) pela bolsa de estudo e a taxa de bancada, sem as quais não seria possível desenvolver essa pesquisa.

À Fundação de Apoio à Pesquisa do Distrito Federal pela ajuda de custo para divulgação de trabalho no 26° Godschimidt Conference na cidade de Paris, França.

Por fim, gostaria de agradecer aos amigos e familiares.

RESUMO

Localizado na porção norte da Faixa Brasília, o Grupo Araí apresenta na Formação Arraias um volumoso registro de rochas vulcânicas intercaladas com quartzitos, metarenitos, brechas e metaconglomerados. As rochas desse grupo encontram-se assentadas sobre os granitos peraluminosos da Suíte Aurumina e dos xistos grafitosos da Formação Ticunzal, e, juntamente com os granitos anorogênicos da Província Estanífera Pedra Branca, compõem um dos mais completos e bem preservados registros do desenvolvimento de um rifte intracontinental, que teve início durante o Estateriano, na região central do Brasil. Em razão do excelente grau de preservação das estruturas e texturas originais, foi possível reconhecer pelo menos três eventos vulcânicos distintos: piroclástico, efusivo félsico e efusivo máfico. Os depósitos piroclásticos ocupam extensas áreas do Grupo Araí e são classificados como depósitos piroclásticos de fluxo (ignimbritos) e depósitos piroclásticos de queda, com espessuras que chegam até 100 m. As rochas efusivas félsicas são porfiríticas, quanto ao aparecimento dos fenocristais de quartzo e feldspatos, com golfos de corrosão, imersos em sua matriz afanítica. Essas rochas são ácidas (66,10% a 76,60% de SiO_2), e possuem conteúdos variados de Al_2O_3 (10,79% a 14,25%), Ca (0,03% a 1,95%) e ΣK_2O+Na_2O (2,63% a 8,23%). Possuem afinidades com as rochas das séries alcalinas e subalcalinas, e são classificadas como dacito, riolito, álcali riolito e traquito peraluminosos. Em diagrama normalizado pelo condrito, essas rochas ácidas são enriquecidas em ETR_{Leves} em relação aos $ETR_{Pesados}$, com as suas expressivas anomalias negativas de Eu (Eu/Eu* = 0,26 a 0,53) indicando um importante fracionamento dos feldspatos. Nos diagramas para os ambientes tectônicos, por exemplo, Rb *versus* Y+Nb, o conjunto de rochas vulcânicas ácidas do Grupo Araí exibem afinidades com aquelas geradas em ambiente pós-colisional intraplaca (anorogênico). O vulcanismo máfico, por sua vez, é composto por rochas básicas afaníticas (49,72% a 54,70% de SiO_2), cujas colorações variam de cinza-esverdeadas, cinza-escuras a cinza-acastanhadas, e contém vesículas preenchidas por sílica. Classificadas como basalto, basalto alcalino, basalto andesítico e traquibasalto, essas rochas são formadas essencialmente por plagioclásio e clinopiroxênio, sendo este último substituído, quase completamente, por tremolita-actinolita. Apresentam conteúdos variados de MgO (5,29% a 7,17%) CaO (6,49% a 9,98%), K_2O (0,60% a 2,53%), Na_2O (1,88% a 3,59%), TiO_2 (0,65% a 1,51%), Ni (68 a 140 ppm) e V (112 a 240 ppm. No diagrama para ETRs normalizado pelo condrito, exibem um forte enriquecimento de ETR_{Leves} em relação aos $ETR_{Pesados}$, com anomalias pouco pronunciadas de Eu (0,80 a 0,99). Quando normalizadas pelo manto primitivo, essas rochas exibem anomalias positivas de Ba, Pb, Nd, e anomalias negativas de Rb, Nb, Sr e Ti. Os baixos valores de εNd(T), variando de -6,78 a -4,89, para uma idade de cristalização de 1,78 Ga, reforçam a importância da contaminação dos magmas responsáveis pela geração dos basaltos com as rochas da crosta continental, comum em regiões de crosta continental atenuada, como é caso do Rifte Intracontinental Araí.

Palavras-chave: Vulcanismo Paleoproterozoico; Grupo Araí; Formação Arraias; Faixa Brasília

ABSTRACT

Located in the northern portion of the Brasília Belt, the Araí Group presents in the Arraias Formation a voluminous register of volcanic rocks interbedded with quartzites, metasandstones, breccia, and metaconglomerates. The rocks of this group are located on the peraluminous granites of the Aurumina Suite and the schist of the Ticunzal Formation, and, together with the anorogenic granites of the Pedra Branca Province, they compose one of the most complete and well-preserved records of the development of a rift intracontinental, which started during the Estateriano, in the central region of Brazil. Due to the excellent degree of preservation of the original structures and textures, it was possible to recognize at least three distinct volcanic events: pyroclastic, felsic effusive and mafic effusive. The pyroclastic deposits occupy extensive areas of the Araí Group and are classified as flow pyroclastic deposits (ignimbrites) with thicknesses that reach up to 100 m. The felsic effusive rocks are porphyritic, as for the appearance of quartz and feldspar phenocrysts, with corrosion gulfs, immersed in their aphanitic matrix. These rocks are acidic (66.10% to 76.60% SiO2), and have varied contents of Al_2O_3 (10.79 wt.% to 14.25 wt.%), Ca (0.03 wt.% to 1.95 wt.%) and ΣK_2O+Na_2O (2.63 wt.% to 8.23 wt.%). They have affinities with the rocks of the alkaline and sub-alkaline series and are classified as peraluminous dacite, rhyolite, alkali rhyolite, and trachyte. In a diagram normalized by the chondrite, these acid rocks are enriched in LREE in relation to heavy HREE, with their expressive negative Eu anomalies (Eu/Eu * = 0.26 to 0.53) indicating an important fractionation of feldspars. In the diagrams for tectonic settings, for example, Rb versus Y + Nb, the set of acid volcanic rocks of the Araí Group exhibits affinities with those generated in a within-plate and/or post-collisional setting. Mafic volcanism, in turn, is composed of basic aphanitic rocks (49.72 wt.% to 54.70 wt.% SiO_2), whose colorings vary from greenish-gray, dark gray to brownish-gray, and contain vesicles filled with silica. Classified as basalt, alkaline basalt, andesitic basalt and trachybasalt, these rocks are formed essentially by plagioclase and clinopyroxene, the latter being replaced by tremolite-actinolite. They have varied contents of MgO (5.29 wt.% to 7.17 wt.%) CaO (6.49 wt.% to 9.98 wt.%), K_2O (0.60 wt.% to 2.53 wt.%), Na_2O (1.88 wt.% to 3.59 wt.%), TiO2 (0.65 wt.% to 1.51 wt.%), Ni (68 to 140 ppm) and V (112 to 240 ppm). In the diagram for REE normalized by the chondrite, exhibit a strong enrichment of LREE compared to HREE, with little pronounced anomalies of Eu (0.80 to 0.99), when normalized by the primitive mantle, these rocks exhibit positive anomalies of Ba, Pb, Nd, and negative anomalies of Rb, Nb, Sr, and Ti. εNd (T) values, ranging from -6.78 to -4.89, for a crystallization age of 1.78 Ga, reinforce the importance of the contamination of the magmas responsible for the generation of basalts with continental crust rocks, common in regions attenuated continental crust, as in the case of the Araí Intracontinental Rift.

Keywords: Paleoproterozoic volcanism; Araí Group; Arraias Formation; Brasília Belt

SUMÁRIO

LISTA DE FIGURAS

CAPÍTULO I– Introdução

CAPÍTULO II– Geologia da Área de Estudo

CAPÍTULO III- Artigo 1

CAPÍTULO IV- Artigo 2

LISTA DE TABELAS

CAPÍTULO III- Artigo 1

CAPÍTULO IV- Artigo 2

LISTA DE SIGLAS

AcmeLab® - *Acme Analytical Laboratories*

ALS® - *Australian Laboratory Services*

BR – Rodovia Federal

BSE - *Backscattered electrons*

DF – Distrito Federal

EPMA - Electron Probe Microanalyses

GO - Goiás

GO -118 – Rodovia Estadual

ICP-AES - *Inductively Coupled Plasma - Atomic Emission Spectrometry*

ICP-MS - *Inductively coupled plasma mass spectrometry*

IGD- Instituto de Geociências

LA-ICP-MS - *Laser Ablation Coupled to Inductively Coupled Plasma Mass Spectrometry*

LOI - *Loss on Ignition*

LST - Heterotungstato de Lítio e Sódio

MEV - Microscópio Eletrônico de Varredura

ppm – partes por milhão

SCLM – Subcontinental Lithospheric Mantle

TF-Trabalho Final de Graduação

TIMS-*Thermal Ionization Mass Spectrometry*

UnB - Universidade de Brasília

WDS - *Wavelength Dispersive Spectrometers*

CAPÍTULO I - INTRODUÇÃO

I.1 Estruturação da Tese

A presente Tese de Doutorado é composta por cinco capítulos que serão apresentados a seguir.

O primeiro capítulo aborda os tópicos introdutórios: apresentação e justificativas, objetivos, materiais e métodos e a geologia regional.

O capítulo II versa sobre a contextualização geológica da área de estudo. É apresentada, também, uma síntese das características texturais e mineralógicas dos litotipos vulcânicos (efusivos e piroclásticos), bem como suas relações de contato, expressas através de levantamentos litoestratigráficos.

Os capítulos III e IV apresentam os resultados obtidos durante o desenvolvimento da pesquisa, na forma de dois artigos científicos que foram submetidos ao periódico internacional ***Journal of South American Earth Sciences*** (artigos 1 e 2). O artigo 1 intitulado: "***Petrography and Geochemistry of Paleoproterozoic Volcanic Rocks from the Araí Intracontinental Rift in the Northern Portion of the Brasília Belt: A Review"*** faz revisão sobre os dados, petrográficos e geoquímicos, em especial aqueles provenientes de Trabalhos Finais de Graduação (TF), separando os diferentes depósitos vulcânicos do Grupo Araí. No artigo 2 intitulado: ***"Petrogenesis of the Paleoproterozoic Basaltic Magmatism from the Araí Rift, Central Brazil."*** são apresentados e discutidos dados petrográficos, química mineral, geoquímicos e isotópicos (Sm-Nd, Sr-Sr e U-Pb) das rochas basálticas do Grupo Araí com o intuito de reconhecer os processos petrogenéticos responsáveis pela gênese dessas rochas.

Por fim, o capítulo V mostra as considerações finais e conclusão sobre o tema estudado nessa Tese, seguida das referências bibliográficas utilizadas em todo o trabalho.

I.2 Apresentação e Justificativas

Riftes são feições geológicas que ocorrem em diversos ambientes tectônicos, como resultado da evolução contínua do mosaico de placas tectônicas do planeta Terra e/ou da interação entre os processos do manto e da litosfera sobrejacente (Buck et al., 1999; Olsen, 1995; Sengör & Burke, 1978). Representam o estágio inicial da ruptura continental (*break-up*), na qual a extensão pode levar ao rompimento da litosfera e a formação de uma nova bacia oceânica, com geração de crosta oceânica, marcando o intenso e contínuo tectonismo

continental (Buck, 2017; Allen & Allen, 2005; Buck et al., 1999; Friedmann & Burbank, 1995; Ruppel, 1995).

Segundo Buck et al. (1999), riftes intracontinentais clássicos são denominados de riftes estreitos ou discretos devido suas zonas de deformação extensional inferiores a 100 km (Bott, 1995). Alguns dos exemplos bem mais estudados de riftes estreitos ativos estão na região do Rifte do Leste Africano, zona do Rifte de Baikal, o Graben do Reno e o Rifte do Rio Grande (Buck, 2017; Kearey, 2013; Thybo & Nielsen, 2009; Leeman et al., 2008; Kieffer et al., 2004; Menzies et al., 2002; Ruppel, 1995; Daley & DePaolo, 1992). Em geral, os riftes se desenvolvem em crostas termicamente equilibradas e com espessura regular e são caracterizados por exibirem, comumente, magmatismo e falhas delimitadoras com mergulhos abruptos (45° a 70°) (Buck, 2017; Buck et al., 1999; Bott, 1995; Olsen, 1995; Ruppel, 1995; Sengör & Burke, 1978).

A presença de rochas ígneas é uma característica fundamental dessas regiões, pois elas refletem a energia despendida para a extensão da litosfera e ascensão da astenosfera (Allen & Allen, 2005; Huismans & Beaumont, 2003; Menzies et al., 2002; Bott, 1995). Essas rochas representam os produtos da crosta e do manto superior, portanto, carregam informações físicas e químicas únicas (Farmer, 2013; Mazumder & Arima, 2009; Bott, 1995; Friedmann & Burbank, 1995; Ruppel, 1995). Nesses locais ocorrem transferências de voláteis e fluidos magmáticos do manto para a superfície terrestre, através de derrames basálticos, e da superfície da Terra para o manto pela alteração superficial e sistemas hidrotermais (Bott, 1995; Friedmann & Burbank, 1995). Contudo, o pouco entendimento sobre a iniciação dos riftes, em especial nos riftes antigos, se dá, em parte, devido ao intenso alongamento (estiramento) da crosta, ao magmatismo *sin* e pós-rifte, e após o rompimento, a sedimentação que normalmente recobre o registro da extensão inicial dos riftes maduros e das margens passivas (Ring et al., 2014; Buck, 2004; Bott, 1995; Friedmann & Burbank, 1995; Olsen, 1995; Ruppel, 1995; Sengör & Burke, 1978). Nesse contexto, as rochas do Grupo Araí podem contribuir para o entendimento de tais processos iniciais.

A região nordeste do Estado de Goiás apresenta vários registros geológicos da dinâmica extensional envolvida no desenvolvimento de um rifte intracontinental durante o intervalo do Paleo ao Mesoproterozoico (Martins-Ferreira et al., 2018; Tanizaki et al., 2015; Fuck et

al., 2014; Pimentel, 2016; Pimentel & Botelho, 2001). Os registros desse importante evento geológico estão materializados na sedimentação e vulcanismo associado do Grupo Araí (Dardenne, 2000; Barbosa et al., 1969), além dos nos granitos intraplaca da Província Estanífera do Rio Paranã (Alvarenga et al., 2007; Botelho & Rossi, 1988; Marini & Botelho, 1986). No Grupo Araí são reconhecidas sequências sedimentares *sin*- a pós-rifte, intercaladas a episódios vulcânicos efusivos e piroclásticos *sin*-rifte, reunidos na sequência continental intermediária definida como Formação Arraias (Martins-Ferreira et al., 2018; Tanizaki et al., 2015; Marques, 2009; Alvarenga et al., 2007; Pimentel & Botelho, 2001; Pimentel et al., 1991; Dyer, 1970).

Levantamentos geológicos em escalas de 1:100.000, 1:50.000 e 1:25.000, realizados pelo Instituto de Geociências da Universidade de Brasília (IG-UnB) nas décadas de 1990 e 2000, através dos trabalhos finais de graduação (TF), identificaram a distribuição irregular e descontínua de um grande volume de rochas vulcânicas efusivas e piroclásticas intercaladas na fase rifte do Grupo Araí. Entretanto, esse vulcanismo ainda carecia de investigações litoestratigráficas, petrográficas, geoquímicas e isotópicas (Sr-Nd e U-Pb) complementares, que permitissem avançar na caracterização temporal, faciológica e as possíveis fonte desses pulsos vulcânicos.

I.3 Objetivos

A presente pesquisa teve por objetivo contribuir para o entendimento dos processos responsáveis pela geração das rochas vulcânicas que constituem a base do Grupo Araí. Assim, foram desenvolvidos estudos petrográficos, geoquímicos e isotópicos com o intuito de obter informações sobre fontes e mecanismos de geração desses magmas. Nesse sentido, essa pesquisa teve os seguintes objetivos específicos:

- Reunir o acervo dos dados geológicos, geoquímicos disponíveis em teses, dissertações, artigos e, principalmente, dos diferentes TF's realizados sobre as rochas vulcânicas da base do Grupo Araí;
- Realizar o empilhamento litoestratigráfico em exposições de rochas vulcânicas efusivas e piroclásticas, com o intuito de compreender a dinâmica desses eventos vulcânicos;
- Caracterização geoquímica de rocha total, objetivando identificação das séries magmáticas e afinidades tectônicas;

- Caracterização petrográfica das principais fases minerais presentes nessas rochas, acompanhado de estudo química mineral, com o intuito de caracterizar as fácies;
- Obtenção de dados de geoquímica isotópica U-Pb em zircão e Sm-Nd e Sr-Sr em rocha total dos diferentes pulsos vulcânicos, objetivando caracterizar tais eventos no tempo e obter informações petrogenéticas;
- Por fim, compreender qual o papel desse vulcanismo para a evolução do Grupo Araí.

I.4 Materiais e Métodos

Para alcançar os objetivos propostos na presente pesquisa foram realizados diversos procedimentos analíticos que serão descritos a seguir:

I.4.1 Petrografia e Química Mineral

Estudos petrográficos em lâminas delgadas e polidas foram realizados com o auxílio de microscópio petrográfico da marca OLYMPUS® modelo BX60FS no Laboratório de microscopia do Instituto de Geociências da Universidade de Brasília (IGD-UnB). Análises químicas pontuais em minerais foram obtidas em seções polidas em amostras representativas das rochas vulcânicas do Grupo Araí. Para tanto, utilizou-se da microssonda JXA-8230 *SuperProbe Electron Probe Microanalysis* (EPMA) da marca JEOL®, do Laboratório de Microssonda Eletrônica do IGD-UnB, cujo sistema *Wavelength dispersive* (WDS) foi configurado para operar com uma voltagem de 20 kV, corrente de 20 nA e tempo de contagem de 10s. Além disso, foram utilizados como padrões minerais: andradita (SiO_2 e CaO), albita (Na_2O), forsterita (MgO), topázio (F), coríndon (Al_2O_3), microclínio (K_2O), vanadinita (Cl e V_2O_3), pirofanita (TiO_2 e MnO), hematita (Fe_2O_3) e barita (BaO).

I.4.2 Geoquímica de Rocha Total

Dados geoquímicos inéditos e outros provenientes de Trabalhos Finais de Graduação (TF's), realizados pelo Instituto de Geociências da Universidade de Brasília (IGD-UnB) nas décadas de 1990 e 2000, são apresentados nesta pesquisa. No projeto Teresina (Botelho et al., 1995) as análises geoquímicas foram realizadas no laboratório de geoquímica do IGD-UnB, com o emprego de espectrometria de emissão atômica com plasma acoplado (ICP-AES), com o espectrômetro SPECTRO FYM03, para a obtenção de elementos maiores,

menores e alguns traços (Si, Al, Ti, Mn, P, Cu, Pb, Zn, Ni, Cr, Co, Y, Be, Sr e V), espectrometria de emissão com chama para Na e K, volumetria para Fe-ferroso, Ca e Mg, gravimetria: perda ao fogo. Enquanto os dados dos projetos Arraias (Campos et al., 2001) e Nova Roma-Porto Real (Fuck, 2005) foram obtidos na Acme Analytical Laboratories (Acme Lab®), no Canadá, por ICP-AES e Espectrômetro de Massa por Plasma Acoplado Indutivamente (ICP-MS).

Novas análises de rocha total para elementos maiores, menores, traços e terras raras foram realizadas no *Australian Laboratory Services* (ALS®) e *Activation Laboratories Ltd*. (Actlabs®). Os métodos empregados nesses laboratórios envolveram a abertura das amostras por fusão com meta/tetraborato de lítio seguida pela digestão em ácido nítrico. Para obtenção das concentrações de elementos maiores e menores, utilizou-se 0,100 g de amostra pulverizada, a qual foi adicionada ao metaborato de lítio/tetraborato de lítio e, em seguida fundida a 1000° C. O fundido gerado foi resfriado e dissolvido em 100 ml de ácido nítrico a 4% e ácido clorídrico a 2%. Esta solução foi então analisada por ICP-AES e os resultados corrigidos para interferências entre elementos com similaridades espectrais. Para o percentual de *loss on Ignition* (LOI), 1,0 g de amostra foi posta em forno a 1000° C durante uma hora, resfriada e depois pesada. Tal percentual é calculado a partir da diferença de peso. Para os elementos traços, incluindo as terras raras, 0,100 g de amostra foi adicionada ao metaborato de lítio/tetraborato de lítio, e depois fundida a 1025°C. Este fundido foi resfriado e dissolvido numa mistura ácida, contendo ácidos nítrico, clorídrico e hidrofluorídrico, e em seguida analisado no ICP-MS. Para a determinação da concentração de alguns metais-base no ICP-AES, as amostras foram dissolvidas em quatro ácidos (HCl, HNO_3, HF e $HClO_4$) (http://www.actlabs.com; https://www.alsglobal.com/en/services-and-products/geochemistry).

I.4.3 Geoquímica Isotópica Sm-Nd e Sr-Sr

Análises de Sm-Nd em rocha total foram realizadas no Laboratório de Geocronologia do IG-UnB. Para obtenção dos dados de Sm e Nd foram adotados os métodos descrito por Gioia & Pimentel (2000). Cerca de 50-100 mg da amostra pulverizada foi adicionada em cápsulas Savillex® e dissolvida em solução traçadora mista (*spike*) de ^{149}Sm e ^{150}Nd. Extrações de Sm e Nd foram realizadas pela técnica de troca catiônica convencional,

utilizando colunas de teflon contendo resina do tipo LN-Spec (HDEHP – ácido 2-tilexil fosfórico em PTFE). As frações de Nd e Sm foram depositadas em arranjos duplos de filamentos de rênio, com as razões isotópicas obtidas no espetrômetro de massa de fonte termal (*Thermal Ionization Mass Spectrometer*-TIMS) *Finnigan TRITON*® em modo estático. Incertezas para as razões $^{147}Sm/^{144}Nd$ e $^{143}Nd/^{144}Nd$ foram melhores que ±0.2% (2σ) e ±0.005% (2σ), respectivamente, com base nos padrões internacionais BHVO-2 e BCR-1. As razões $^{143}Nd/^{144}Nd$ foram normalizadas para o valor de $^{146}Nd/^{144}Nd$ de 0.7219 e a constante de desintegração (λ) usada é 6.54×10^{-12} a^{-1} (Lugmair & Marti, 1978). O tratamento dos dados foi realizado com auxílio de tabelas do Excel® e Isoplot 3.7® (Ludwig, 2008).

I.4.4 Geocronologia U-Pb LA-ICP-MS em Zircão

As análises isotópicas U-Pb em zircão foram realizadas no Laboratório de Geocronologia da Universidade de Brasília. Concentrados de zircão foram obtidos seguindo a rotina de peneiramento, concentração gravítica (bateia), separação magnética (*isodinamic Frantz*), separação com líquidos densos (bromofórmio e LST) e separação manual (lupa binocular e agulha). Os cristais de zircão das diferentes populações foram depositados em uma placa de vidro contendo fita dupla-face e embutidos resina *epóxi* (a frio) para a confecção dos *mounts*. Em seguida, esses *mounts* resinados foram lixados e polidos para exporem superfície homogênea dos cristais. As imagens do interior dos cristais de zircão foram obtidas por catodoluminescência no microscópio eletrônico de varredura (MEV) modelo FEI Quanta 450.

Os cristais de zircão foram analisados seguindo os procedimentos adotados por (Bühn et al., 2009) utilizando o equipamento de ablação a laser *New-Wave* UP213 Nd:YAG laser (λ = 213nm), acoplado ao ICP-MS *multicoletor Thermo Finnigan Neptune* (LA-ICP-MS). O laser incidente operou com frequência de 10 Hz, intensidade de energia variando de 2 a 3 J/cm^2, *spot* com diâmetro fixo de 30 μm e tempo de ablação de 40s. O padrão GJ-1 (Jackson et al., 2004) foi usado como fator de correção, em sequência de quatro análises, incluindo uma de branco laboratorial e uma do padrão. Para aferir a reprodutibilidade e acurácia da análise foram realizadas análises no padrão internacional 91500 (Wiedenbeck et al., 1995).

O *multicoletor Thermo Finnigan Neptune* é configurado para medir ^{238}U, ^{232}Th, ^{204}Pb, ^{206}Pb, ^{207}Pb, ^{208}Pb e ^{202}Hg em volts ou contagens por segundo (cps). Esses dados foram reduzidos em planilha Excel e o resultado, tratado e corrigido, fornece razões isotópicas cujo erro é expresso em 1σ%. Além disso, os dados foram trabalhados no ISOPLOT 3.75 (Ludwig, 2012), suplemento do Excel que permitiu a construção do diagrama da concórdia (Wetherill, 1956).

I.5 Localização e Acessos

A área de estudo está situada na porção nordeste do Estado de Goiás (GO), nas proximidades dos municípios de Nova Roma e Teresina de Goiás (Fig. 1), e dista cerca 370 km da capital federal (Brasília-DF). Ao tomar como ponto de partida a Universidade de Brasília, o acesso à área de estudo pode ser realizado por dois percursos que têm início pelas rodovias distritais Estrada Parque das Nações (DF-004; Via L4 Norte) e Estrada Parque do Torto (EPTT; DF-007). Em seguida, são utilizadas as rodovias federais BR-450, BR-010, BR-030 e BR-020, passando pelas cidades de Formosa-GO e Alvorado do Norte-GO até chegar ao município de Simolândia-GO. Logo após a entrada desta cidade, o percurso deve ser feito pela rodovia estadual GO-112 (Estrada Iaciara), sentido Iaciara-GO, até a cidade de Nova Roma-GO. O segundo percurso utiliza a rodovia GO-118, após a entrada para a cidade de Planaltina-DF, passando pelas cidades de São Gabriel-GO, Alto Paraíso de Goiás e Teresina de Goiás. Após a cidade de Teresina de Goiás, cerca de ~3,7 km, o trajeto deve ser realizado pela rodovia GO-241 até a cidade de Nova Roma-GO. Além disso, para se chegar aos afloramentos, foram utilizadas vias secundárias não pavimentadas.

I.6 Geologia Regional

A Província Tocantins (Almeida et al., 1981) é um importante orógeno neoproteozoico, localizada na região central do Brasil, que teve sua estruturação tectônica resultante das convergências e colisões entre os blocos paleocontinentais: Cráton do São Francisco-Congo (leste), Cráton da Amazônia (oeste) e Paranapanema (sul), este último encoberto pelas rochas da Bacia do Paraná (Valeriano, 2004). Tais colisões ocorreram durante o Ciclo Brasiliano (800-500Ma) (Brito Neves et al., 2014) e produziram as faixas de dobramentos e empurrões Araguaia, Paraguai, nas margens leste e a sudeste do Cráton da Amazônia,

respectivamente, e a Faixa Brasília na borda oeste do Cráton do São Francisco (Pimentel, 2016; Fuck et al., 2014; Valeriano et al., 2008; Pimentel et al., 2004; Bizzi et al., 2003; Delgado et al., 2003).

A Faixa Brasília é um orógeno alongado com direção norte-sul, que se estende por mais 1000 km (Fig. 2), sendo compartimentada nas zonas Interna e Externa, Maciço de Goiás e Arco Magmático de Goiás (Pimentel, 2016; Fuck et al., 20014; Pimentel et al., 2004). Inserido no contexto tectônico da Zona Externa, o Grupo Araí abrange uma área aproximada de 10.000 km^2 no nordeste do Estado de Goiás e sudeste do Tocantins (Pimentel, 2016; Fuck et al., 2014; Alvarenga et al., 2007; Pimentel & Botelho, 2001; Dardenne, 2000). As rochas desse grupo foram depositadas sobre os paragnaisses, quartzitos, conglomerados e xistos grafitosos, de idades 2,20 e 2,46 Ga, da Formação Ticunzal (Cuadros et al., 2017a), e dos granitos peraluminosos, com idade entre 2,17 e 2,12 Ga, da Suíte Aurumina (Cuadros et al., 2017b; Fuck et al., 2014; Alvarenga et al., 2007).

O Grupo Araí é composto por espessos pacotes de rochas metassedimentares, por vezes intercalados com depósitos vulcânicos, e é subdivido, da base para o topo, nas formações Água Morna, Arraias, Caldas e Traíras (Fig. 3). A Formação Arraias se caracteriza por hospedar volumosos depósitos vulcânicos intercalados aos espessos pacotes de rochas metassedimentares de origem fluvial e eólica e estão em contato tectônico com os granitos anarogênicos da Suíte Estanífera Pedra Branca (Martins-Ferreira et al., 2018; Tanizaki et al., 2015; Marques, 2009; Alvarenga et al., 2007; Pimentel & Botelho, 2001; Dyer, 1970).

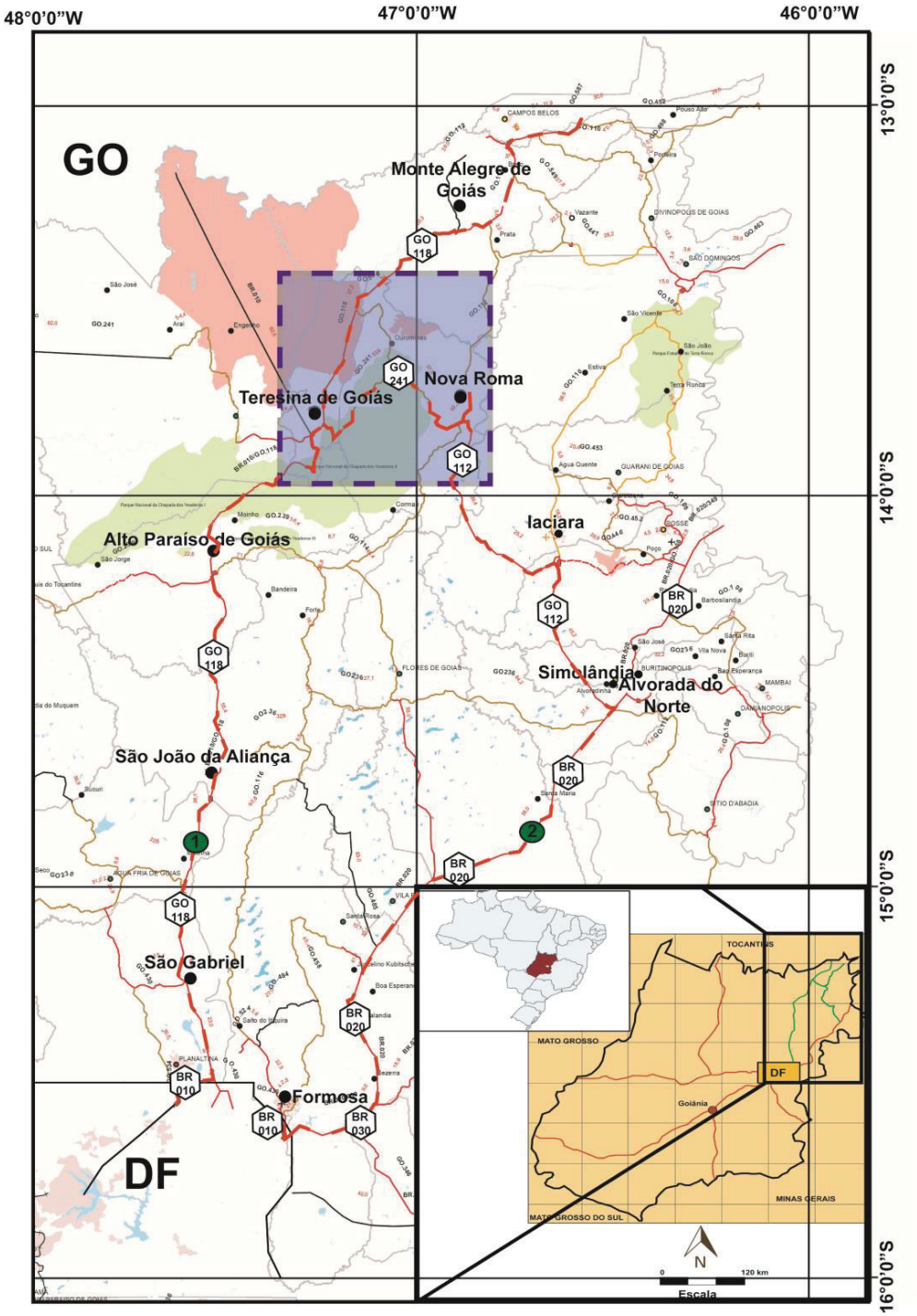

Figura 1. Mapa rodoviário simplificada com as principais vias de acesso e localização da área de estudo (Cristóvão,2017).

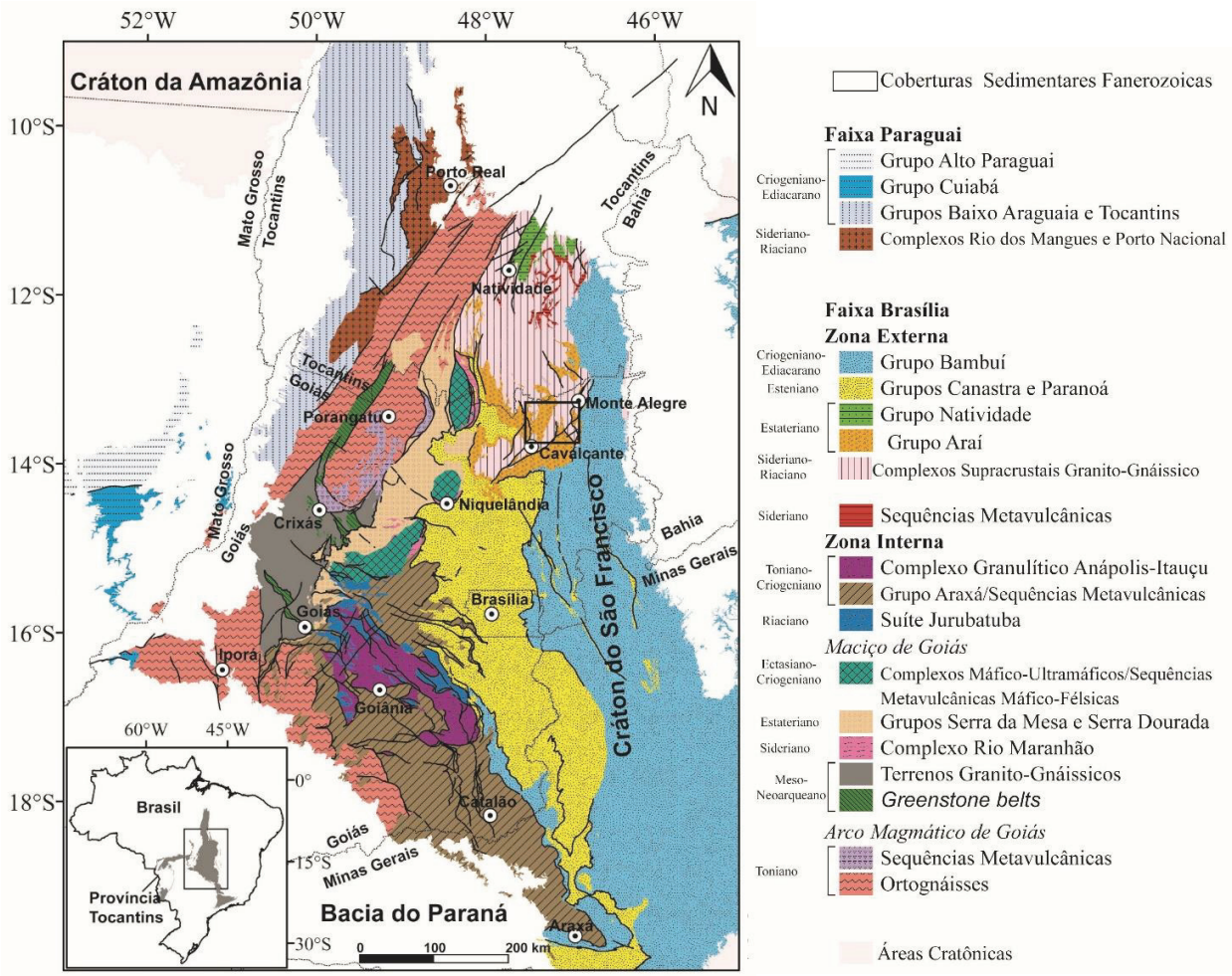

Figura 2. Mapa geológico da Faixa Brasília após Pimentel et al., (2004) *in* Cuadros et al., (2017a, 2017b) com a localização da área de estudo (retângulo preto).

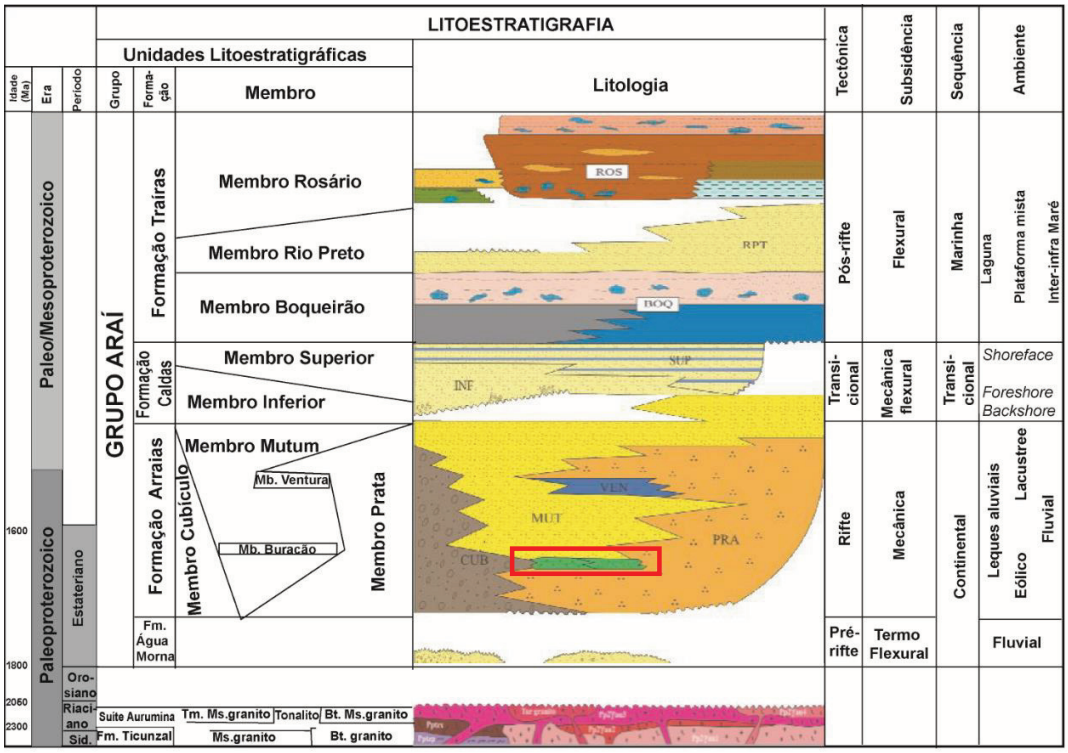

Figura 3. Estratigrafia integrada do Grupo Araí proposta por Tanizaki et al., (2015). Retângulo vermelho indica o posicionamento das rochas vulcânicas da Formação Arraias.

CAPÍTULO II-GEOLOGIA DA ÁREA DE ESTUDO

II.1 Contextualização Geológica da Área de Estudo

O Grupo Araí, localizado na região nordeste do Estado de Goiás, apresenta um dos mais completos e preservado registro do vulcanismo ocorrido durante o Paleoproterozoico (Alvarenga et al., 2007). Esse magmatismo é representado, na área de estudo, por grandes exposições de rochas vulcânicas efusivas e piroclásticas que podem chegar a centenas de metros, e estão distribuídas de forma irregular nos arredores das cidades de Teresina e Nova Roma de Goiás, próximo à divisa com o Estado do Tocantins (Fig. 1).

As rochas vulcânicas da Formação Arraias vêm sendo objeto de estudo desde a década de 1960 (e.g. Alvarenga et al., 2007; Pimentel & Botelho, 2001; Barbosa et al., 1960; Dyer, 1970), e são caracterizadas pelo excelente grau de preservação das suas texturas e estruturas originais. Essas rochas estão, por vezes, assentadas diretamente sobre o embasamento do Grupo Araí, que é representado, na região, pelos granitos peraluminosos da Suíte Aurumina (Cuadros et al., 2017b) e pelos xistos grafitosos da Formação Ticunzal (Cuadros et al., 2017a), ou em contato tectônico com os granitos anorogênicos da Suíte Pedra Branca.

Os depósitos vulcânicos da região representam os estágios iniciais de edificação da sequência vulcano-sedimentar que constitui o Rifte Intracontinental Araí. Ocorrem intercalados com quartzitos e/ou metarenitos, metassiltitos e metaconglomerados de origem fluvial e eólica na base da Formação Arraias. Seus afloramentos ocorrem, geralmente, sob as formas de blocos e lajedos, bem como nos leitos de rios e pequenas drenagens, onde são observadas estruturas de fluxos piroclásticos e derrame, com a presença de rochas maciças na base e aumento gradual de vesículas em direção ao topo. Esses depósitos foram submetidos a importantes deformações, representadas por expressivas zonas de cisalhamento, dobras e falhas (Fig. 2), durante o Brasiliano, que produziram descontinuidades nas relações de contato, dificultando assim, correlações estratigráficas precisas de espessuras dos diferentes depósitos vulcânicos da Formação Arraias. Nesse contexto, foram elaboradas seções geológicas e colunas estratigráficas que melhor representasse os depósitos efusivos e piroclásticos, cujas descrições serão apresentadas a seguir.

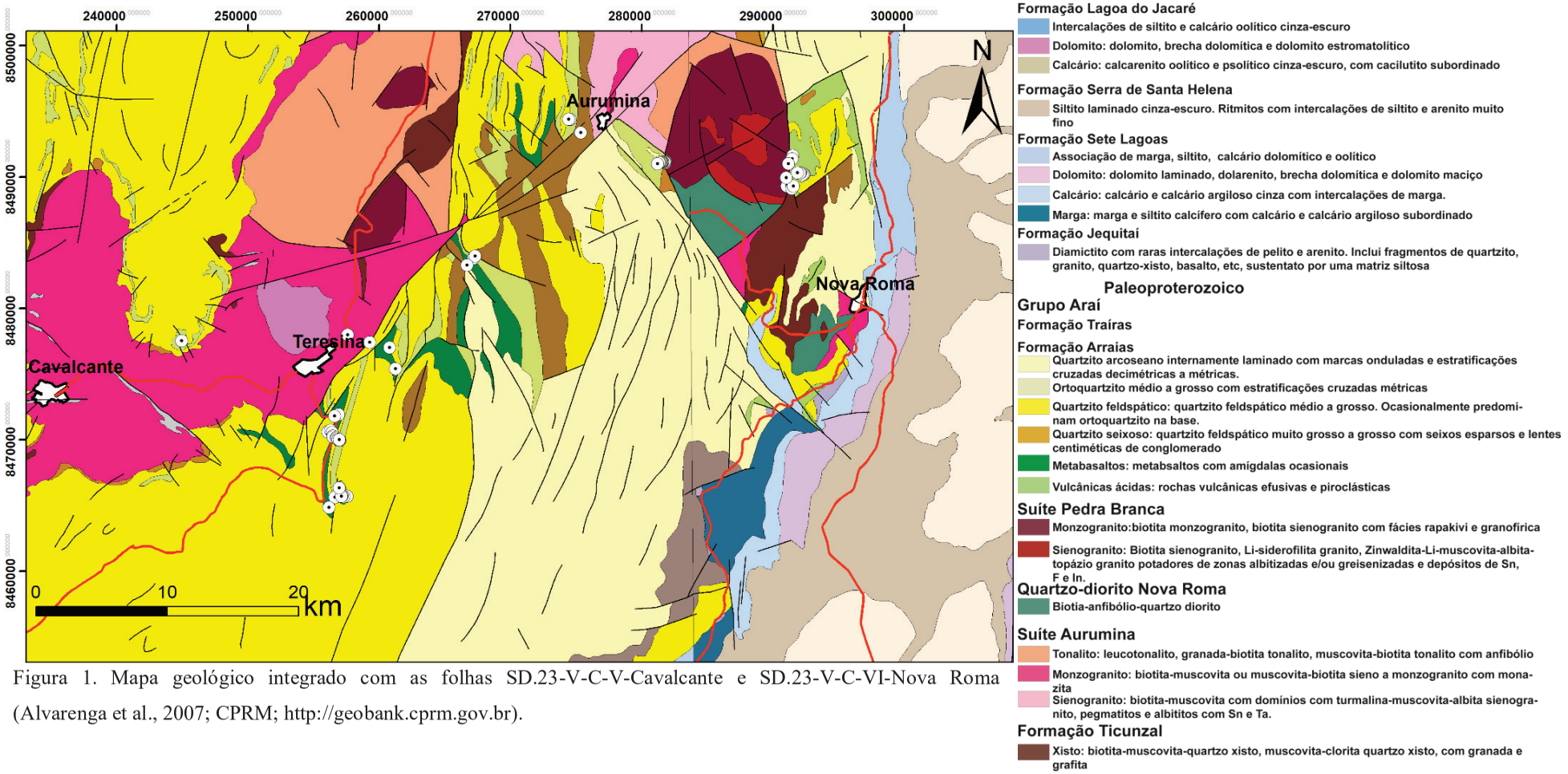

Figura 1. Mapa geológico integrado com as folhas SD.23-V-C-V-Cavalcante e SD.23-V-C-VI-Nova Roma (Alvarenga et al., 2007; CPRM; http://geobank.cprm.gov.br).

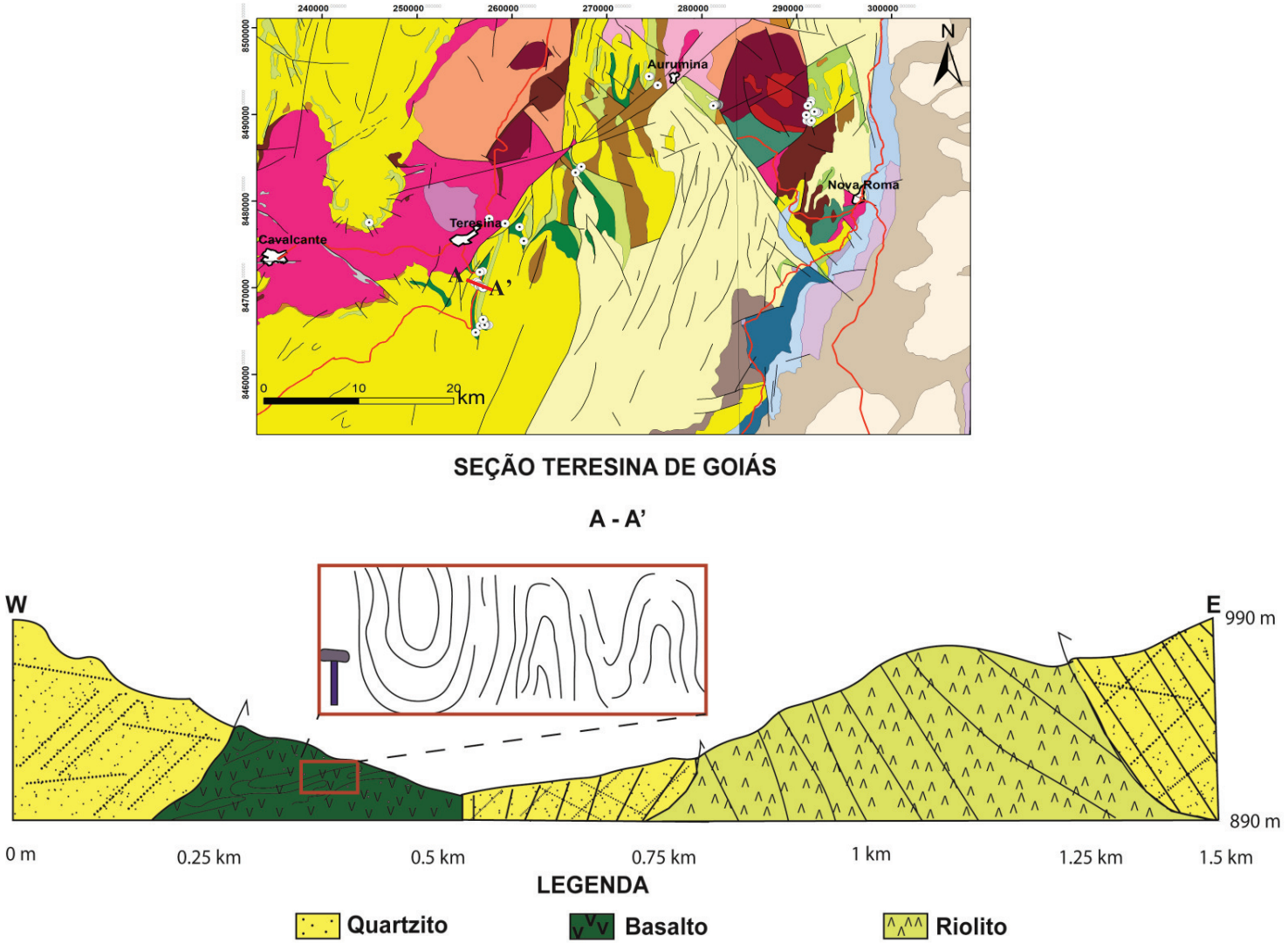

Figura 2. Seção geológica nas proximidades de Teresina de Goiás mostrando a distribuição das rochas vulcânicas da Formação Arraias.

II.2 Caracterização Textural e Mineralógica das Rochas vulcânicas da Formação Arraias

Nesse tópico é apresentada uma síntese das observações de campo, expressas através da construção de seções e perfis geológicos, que permitem compreender, pelo menos em parte, as relações de contato entre esses as rochas vulcânicas da Formação Arraias. Além disso, são adicionados dados petrográficos. Outras informações, tais como, geoquímica de rocha total, geoquímica isotópica e geocronologia dos litotipos estudados, estão materializadas nos dois artigos científicos submetidos ao periódico ***Journal of South American Earth Sciences***, os quais constituem os capítulos III e IV a seguir, e formam a base para a discussão e conclusão dessa pesquisa.

II.2.1 Rochas Vulcânicas Efusivas e Piroclásticas.

Os dados de campo e petrográficos possibilitaram reunir as rochas vulcânicas da Formação Arraias em depósitos vulcânicos distintos: efusivos e piroclásticos.

II.2.1.1 Rochas Efusivas.

Os depósitos efusivos possuem heterogeneidade composicional, são formados essencialmente, por rochas máficas e félsicas, produzidas por derrames de lavas, com importantes variações texturais. Essas rochas apresentam composição bimodal (basalto-riolito) e ocorrem, normalmente, em camadas de espessuras métricas e centimétricas, por vezes, dobradas e subverticalizadas, que estão intercaladas aos fluxos piroclásticos e as rochas metassedimentares da Formação Arraias.

Os litotipos ácidos são leucocráticos a mesocráticos, cujas cores variam de cor-de-rosa até vermelho-acastanhado a vermelho-acinzentado. Exibem arranjo textural porfirítico a glomoroporfirítico, ressaltados por fenocristais de quartzo, álcali-feldspato e plagioclásio, imersos em uma matriz de granulação fina a afanítica. Os fenocristais são euédricos a subédricos, pouco a moderadamente fraturados, ocupam entre 30-40% do volume das rochas e, frequentemente, se mostram orientados seguindo o fluxo magmático e exibem bordas corroídas e/ou reabsorvidas pela matriz, formando golfos de corrosão. Os feldspatos se mostram parcialmente serecitizados ou saussuritizados. Na matriz dessas rochas ocorrem proporções variadas de quartzo, feldspatos, muscovita, biotita, anfibólio, apatita,

magnetita, zircão, além de epidoto e carbonato. Ocasionalmente essas rochas hospedam também amígdalas ou vesículas preenchidas por agregados microcristalinos de quartzo, epidoto e carbonato.

As rochas básicas são melanocráticas, com cores variando de verde musgo a cinza esverdeado. Exibem arranjo textural porfirítico, ressaltado por fenocristais de plagioclásio, piroxênio e anfibólio, imersos em matriz afanítica a microcristalina. Esses fenocristais variam de anédricios a euédricos e ocupam entre 20-30% do volume da rocha. Os fenocristais de piroxênio exibem bordas uralitizadas, enquanto que plagioclásio se mostra parcialmente saussuritizados e anfibólio cloritizado. Ocasionalmente formam texturas ofíticas a subofíticas, e hospedam vesículas preenchidas por zeolita, carbonato e quartzo. Em general, a matriz é formada por agregados de clinopiroxenio, plagioclásio e anfibólio, tendo como minerais secundários quartzo, titanita, epidoto, clorita e opacos.

II.2.1.2 Rochas Piroclásticas.

Os depósitos de natureza piroclástica ocupam vasto volume de rochas dentro dos registros vulcânicos inseridos na Formação Arraias. Em geral, estão dispostos em camadas subhorizontais a subverticais intercaladas a rochas efusivas e sequencias siliciclásticas (Figs. 3 e 4). São depósitos formados por fluxos de massas, tração e suspensão, testemunhos de pulsos vulcânicos explosivos. Exibem cores que variam de cinza-claro a cinza-acastanhado, granulação fina a grossa, e são constituídos por fenocristais e cristaloclastos principalmente de quartzo e feldspatos, além de litoclastos variados, imersos em matriz de granulação fina a afanítica.

Os litoclastos exibem granulação que varia desde blocos angulares a subarredondados (quartzitos, metarenitos, riolito e granitos) até lapilli. Ocasionalmente, identifica-se a presença de rochas densamente vesiculadas contendo fragmentos elipsoidais de pumices e fiammes distribuídos em um arranjo textural do tipo eutaxítico. Textura do tipo parataxítica também é observada, a qual gera foliações planares com indicação de reomorfismo. Com base no arranjo textural, granulação e proporção de seus constituintes cristal e líticos, adotando a proposta de McPhie et al. (1993), Cas & Wright (1987) e Fisher & Schmincke (1984), esses depósitos podem ser classificados como: cristal-tuffo, lapilli-tuffo, surge e conglomerados ignimbríticos.

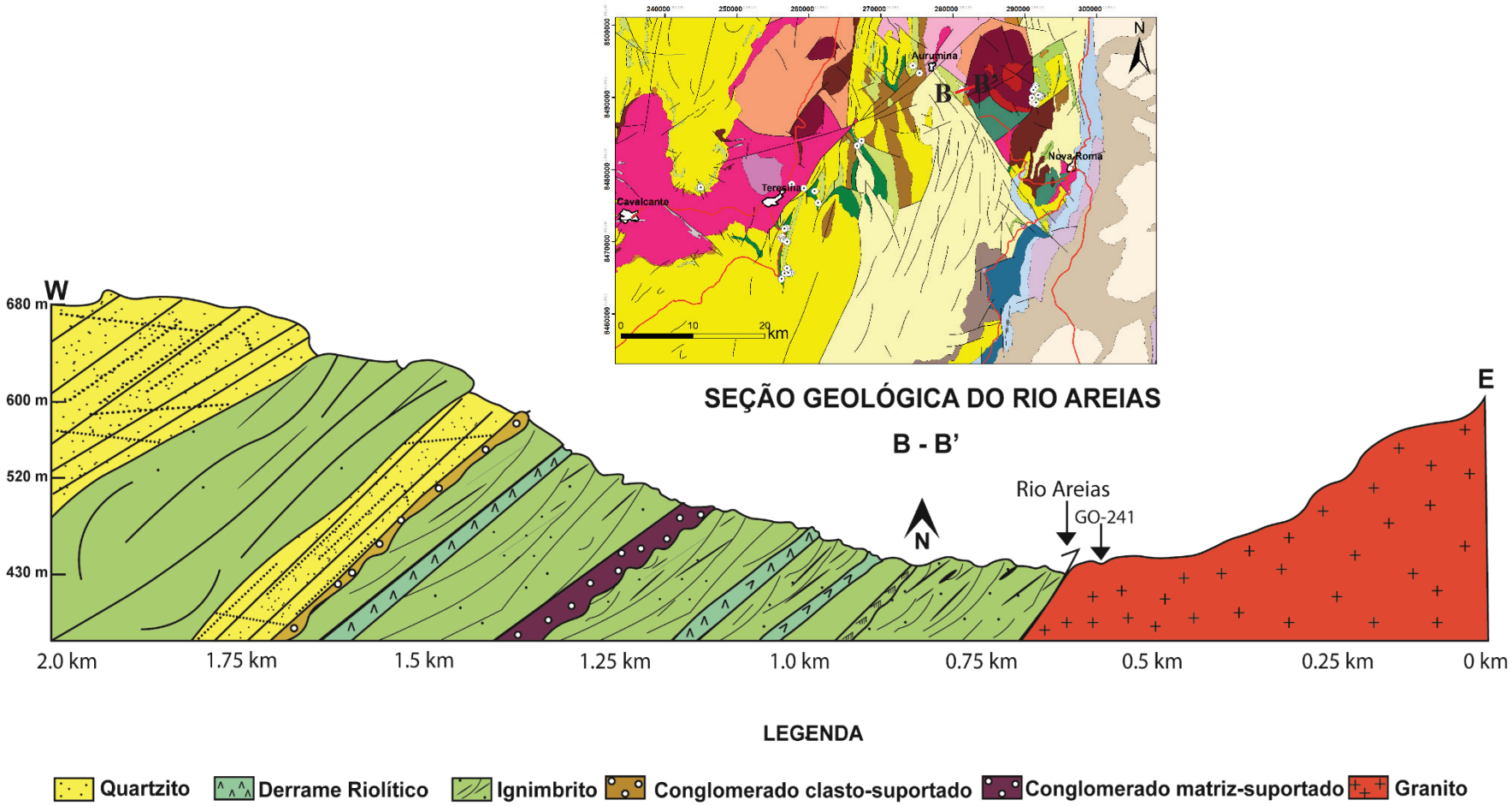

Figura 3. Seção Geológica B-B' no leito do rio Areias mostrando as relações de contato entre as rochas vulcânicas efusivas e piroclásticas da Formação Arraias com as rochas metassedimentares, da mesma formação, e o granito anorogênico da Suíte Pedra Branca.

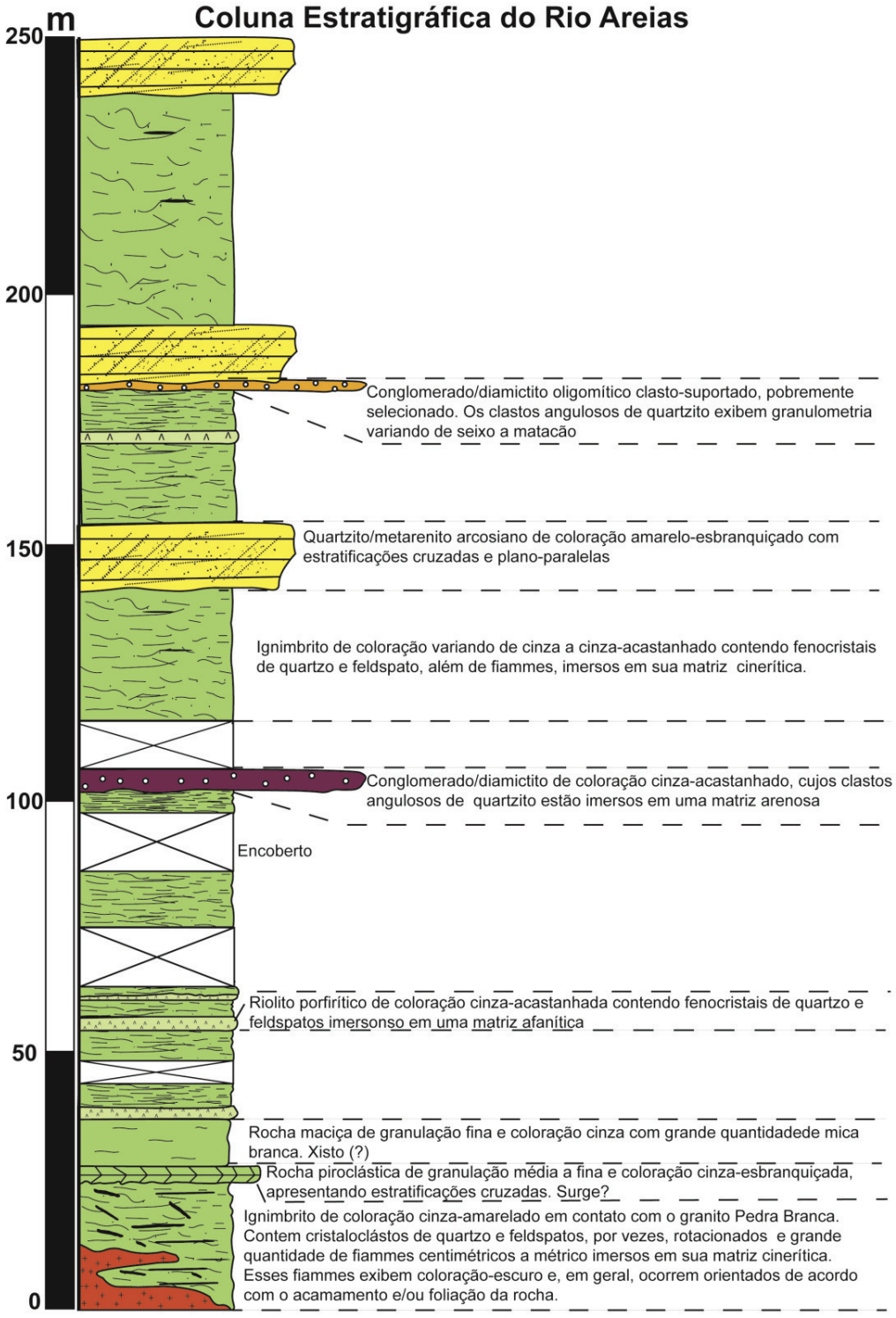

Figura 4. Coluna estratigráfica no leito do rio Areias exibindo as relações das rochas vulcânicas e metassedimentares da Formação Arraias, Grupo Araí.

II.3 Aspectos Geoquímicos e Geocronológicos.

As rochas vulcânicas ácidas da Formação Arraias apresentam conteúdos variados de SiO_2 (66,10% a 76,60%), Al_2O_3 (10,79% a 14,25%), Ca (0,03% a 1,95%) e ΣK_2O+Na_2O (2,63% a 8,23%). Possuem afinidades com as rochas das séries alcalinas e subalcalinas, e são classificadas como dacito, riolito, álcali riolito e traquito peraluminosos.

As rochas básicas, por sua vez, apresentam conteúdos variados de MgO (5,29% a 7,17%), SiO_2 (49,72% a 54,70%), CaO (6,49% a 9,98%), K_2O (0,60% a 2,53%), Na_2O (1,88% a 3,59%), TiO_2 (0,65% a 1,51%), Ni (68 a 140 ppm) e V (112 a 240 ppm), com baixas razões K_2O/Na_2O (0,10 a 0, 94), e são classificadas como basalto, basalto alcalino, basalto andesítico e traquibasalto. Além disso, apresentam baixos valores de εNd(T), variando de -6,78 a -4,89, para uma idade de cristalização, U-Pb em zircão, por volta de 1.78 Ga.

Capítulo III

Artigo 1: PETROGRAPHY AND GEOCHEMISTRY OF PALEOPROTEROZOIC VOLCANIC ROCKS FROM THE ARAÍ INTRACONTINENTAL RIFT IN THE NORTHERN PORTION OF THE BRASÍLIA BELT: A REVIEW

Gmail Cleverton Correia <cleverton.correia@gmail.com>

Confirming submission to Journal of South American Earth Sciences

Journal of South American Earth Sciences <em@editorialmanager.com>4 de fevereiro de 2020 17:18 Responder a: Journal of South American Earth Sciences <sames@elsevier.com>
Para: Cleverton Silva <cleverton.correia@gmail.com>

This is an automated message.

Petrography and Geochemistry of Paleoproterozoic Volcanic Rocks from the Araí Intracontinental Rift in the Northern Portion of the Brasília Belt: A Review

Dear Mr Silva,

We have received the above referenced manuscript you submitted to Journal of South American Earth Sciences.

To track the status of your manuscript, please log in as an author at https://www.editorialmanager.com/sames/, and navigate to the "Submissions Being Processed" folder.

Thank you for submitting your work to this journal.

Kind regards,
Journal of South

American Earth Sciences

Petrography and Geochemistry of Paleoproterozoic Volcanic Rocks from the Araí Intracontinental Rift in the Northern Portion of the Brasília Belt: A Review

*Cleverton Correia Silva[1]; Valmir da Silva Souza[1,2]; Nilson Francisquini Botelho[1,2]

[1]Programa de Pós-Graduação em Geologia, Instituto de Geociências, Campus Asa Norte, 70910-900, Brasília-DF, Brazil, E-mail: cleverton.correia@gmail.com

[2]Universidade de Brasília, Instituto de Geociências, Campus Asa Norte, 70910-900, Brasília- DF, Brazil

Abstract

In the early stages of development of the Araí intracontinental rift, around 1.77 Ga, large volumes of effusive and pyroclastic volcanic rocks, anorogenic granites and dikes were produced in the northern portion of the Brasília Belt in central Brazil. These volcanic rocks occur interbedded with quartzite, metasandstones, metasiltstone, breccia, and conglomerates of fluvial-eolic origin and are irregularly distributed at the base of the Arraias Formation. The pyroclastic deposits occupy extensive areas and have varying thicknesses. In general, they have a high content of brittle and poorly selected crystaloclasts and phenocrysts of quartz and feldspars, lithoclasts and angular pumice and fiammes and are classified as tuff with or without crystals, lapilli-tuff, and block-and-ash flow. The basic (SiO_2 = 47.60-54.50 wt.%) and acid (SiO_2 = 66.11-75.72 wt.%) effusive volcanic rocks are sub-alkaline, and exhibit transitional features positioned in the fields of the Tholeiitic and Calc-alkaline series, with acidic rocks more alkali enrichment. These rocks are classified as basalt, basaltic andesite, dacite/rhyodacite, rhyolite, and alkali rhyolite. In the Harker diagrams, the composition intervals and dispersions in the evolutionary tendencies indicated the bimodal composition of this volcanism. For rare earth elements (REE), spectra with distinct curves between basic and acidic rocks are noted, with enrichment of LREE in relation to the HREE, with ratios $(La/Yb)_N$ ranging from 3.30 to 10.56 and from 4.72 to 56.57 in the basic and acidic volcanic rocks, respectively. In the same diagram, it is possible to observe expressive negative anomalies of Eu (Eu/Eu*= 0.26 to 0.53), in the most differentiated rocks, contrasting with anomalies not very pronounced (Eu/Eu* = 0.79 to 0.99) of the basalts, when the normalized pattern of the primitive mantle the set of samples presents enrichment in HFSE and LILE. In for the tectonic setting diagrams, these volcanic rocks from the Arraias Formation exhibit affinities with the rocks generated in the within-plate settings. Also, this important volcano-plutonic magmatism presents in the region may have produced a Large Igneous Province (LIP) of the bimodal type.

Keywords: Paleoproterozoic Volcanic Rocks; Bimodal; Intracontinental Rift; Araí Group; Brasília Belt

1. Introduction

Intracontinental rifts are generally linear tectonic structures limited by faults with dip angles greater than 45° that host thick sedimentary sequences associated with magmatism, in the early development stages especially (Allen and Allen, 2005; Olsen, 1995; Ruppel, 1995; Sengör and Burke, 1978). Such magmatism contributes to the intense transfers of volatiles and magmatic fluids from the mantle to the Earth surface through basaltic flow and, from the planet surface to the mantle, through hydrothermal processes and surface changes (Corti, 2009; Olsen, 1995; Ruppel, 1995).

On the modern rifts, lithosphere extension processes occur as a response to the convective heat flow of the mantle and/or the action of mantle plumes installed at the base of the lithosphere (Lavecchia et al., 2017; Allen and Allen, 2005; Buck, 2004; Buck et al., 1999; 1991; Ruppel, 1995; Sengör and Burke, 1978), generating forces, such as slab pull and ridge push, capable of breaking and moving the tectonic plates (Ring et al., 2014; Kearey, 2013; Buck, 2004). These mechanisms favor the thinning of the lithosphere, which is controlled by transcrustal faults (Gerya, 2013; Cloetingh and Van Wees, 2005; Corti et al., 2003), facilitating subsidence and sedimentation (Kearey, 2013; Allen and Allen, 2005; Olsen, 1995; Burke et al., 1977), as well as the rise of mantle rocks, which contribute to the magmatism of these regions (Ring et al., 2014; Schmeling, 2010; Olsen, 1995; Wilson, 1989). However, such initial records are difficult to observe due to the intense stretching of the continental crust, post-rift sedimentation, and subsequent tectonic events (Friedmann and Burbank, 1995; Olsen, 1995; Ruppel, 1995). Therefore, studying the volcanic rocks of these rifts can provide unique physicochemical information on the stages of lithosphere extension and mantle rise, because their volumes and compositions depend on the heterogeneity, thickness, resistance, and composition of the pre-existing lithosphere (Ring et al., 2014; Bosworth et al., 2005; Olsen, 1995; Ruppel, 1995). Also, it helps to understand the extension and fragmentation processes of large continental masses that were agglutinated in previous orogenic cycles (Pirajno and Santosh, 2015, 2014; Fuck et al., 2014; Condie, 2004; Olsen, 1995).

The Araí Intracontinental Rift, located in the domain of the regional geotectonic unit known as the Tocantins Province (Almeida et al., 1981), was developed during the Paleo-Mesoproterozoic and produced voluminous effusive and pyroclastic volcanic deposits

inserted in the regional unit called Arraias Formation, which make up the base of the Araí Group (Martins-Ferreira et al., 2018; Pimentel, 2016; Tanizaki et al., 2015; Fuck et al., 2014; Brito Neves, 2011; Alvarenga et al., 2007; Pimentel and Botelho, 2001). However, much of the information on these volcanic deposits is available in internal reports conducted by the undergraduate students of the Geosciences Institute of the Brasília University, Brazil, during the 1990s and 2000s. The purpose of this review is to organize the available information and complementing it with new data to define the current stage of lithostratigraphic, petrographic and geochemical knowledge on the volcanic rocks, as well as discussing the petrogenetic aspects involved.

2. Regional Geology

A large part of central Brazil lies within an important regional geotectonic unit named Tocantins Province (Marini et al., 1984; Almeida et al., 1981). The Tocantins Province tectonic structuring resulted from the convergences and collisions of three paleocontinental blocks, the São Francisco-Congo Craton (east), the Amazon Craton (west), and the Paranapanema block (south), during the Neoproterozoic Brasiliano-Pan African orogeny at 800-500 Ma (Pimentel, 2016; Brito Neves et al., 2014; Fuck et al., 2014; Bizzi et al., 2003). These collisions produced three mobile belts, named of Araguaia and Paraguay, on the east and southeast borders of the Amazon Craton, respectively, and the Brasilia Belt on the western border of the São Francisco Craton (Pimentel, 2016; Fuck et al., 2014; Valeriano et al., 2004).

The Brasília Belt (Fig. 1), where the Araí Group rocks are distributed, forms along north-south orogenic system, which extends for more than 1000 km, being subdivided into Internal and External zones, Goiás Massif and Goiás Magmatic Arc (Pimentel, 2016; Fuck et al., 2014). The Araí Group, inserted in the tectonic context of the External Zone, occupies approximately 10,000 km^2 in the northeast of Goiás State and southeast of Tocantins (Pimentel, 2016; Tanizaki et al., 2015; Fuck et al., 2014; Alvarenga et al., 2007; Dardenne, 2000). This group consists of thick pockets of metasedimentary rocks, sometimes interbedded with volcanic deposits. Rocks of this group overlain paragneiss, quartzites, conglomerates and graphitous schist of the Ticunzal Formation, that show ages between 2.20 and 2.46 Ga (Cuadros et al., 2017b), and peraluminous granites from the Aurumina Suite, that shows ages between 2.12 and 2.17 Ga (Cuadros et al., 2017b;

Tanizaki et al., 2015; Alvarenga et al., 2000). The Arraias Formation is characterized by the presence of large volcanic deposits interbedded with the thick layers of metasedimentary rocks of fluvial and eolian origin (Tanizaki et al., 2015; Alvarenga et al., 2007) and are in tectonic contact with the anorogenic granites of the tin-bearing Pedra Branca Suite (Alvarenga et al., 2007; Pimentel and Botelho, 2001). These volcanic deposits contain effusive and pyroclastic rocks of bimodal composition (basalt-rhyolite), with zircon U-Pb date of 1777 Ma (Pimentel et al., 1991), low values of εNd (-5.9 to -1.5), and model ages (T_{DM}) ranging from 2.59 to 2.20 Ga (Pimentel And Botelho, 2001).which were extruded in an intracontinental rift setting (Martins et al., 2018; Tanizaki et al., 2015; Alvarenga et al., 2007; Pimentel and Botelho, 2001).

3. Materials and Methods

The petrographic studies were accomplished at the Microscopy Laboratory of the Instituto de Geociências of the Universidade de Brasília (IGD-UNB). Geochemical data from the mapping from the Teresina (Botelho et al., 1995), Cavalcante (Botelho et al., 1998) and Monte Alegre de Goiás (Alvarenga et al., 1999) projects were obtained from Geochemistry Laboratory of the IGD-UNB by Inductively Coupled Plasma Atomic Emission Spectrometry (ICP-AES) and Inductively Coupled Plasma Mass Spectrometry (ICP-MS). Data from the Arraias (Campos et al., 2001) and Nova Roma-Porto Real (Fuck, 2005) projects were obtained at the Acme Analytical Laboratories® (AcmLab) by ICP-MS and Inductively Couple Plasma Optical Emission Spectrometry (ICP-OES).

New lithogeochemical analyses of major, minor, trace and rare earth elements were performed at the Australian Laboratory Services (ALS®), using ICP-OES to obtain major and minor elements and ICP-MS for traces and rare earth elements. To obtain the concentrations of the major and minor elements 0.100g of pulverized sample was used, which was added to lithium metaborate/lithium tetraborate and then melted at 1000°C. The melt generated was cooled and dissolved in 100 ml 4% nitric acid/2% hydrochloric acid. This solution was then analyzed by ICP-OES and the corrected results for interference between elements with spectral similarities. For the percentage of loss on ignition (LOI), 1.0 g of the sample was baked at 1000°C for one hour, cooled and then weighed. This percentage is calculated from the difference in weight. For trace elements, including rare earth elements. 0.100 g of the sample was added to lithium metaborate/lithium tetraborate

and then melted at 1025°C. This melt was cooled and dissolved in an acidic mixture containing nitric, hydrochloric and hydrofluoric acids, and then analyzed in ICP-MS.

Results

4. Local Geology and Stratigraphy

The volcanic rocks from the Araí Group are best exposed in the Goiás northeast region (Alvarenga et al., 2007), being irregularly distributed in the basal portion of the Arraias Formation and occurring sometimes in tectonic contact with the anorogenic granites of the Pedra Branca Suite (Fig. 2). These rocks form voluminous effusive and pyroclastic volcanic deposits, often occupying the base of large quartzite scarps up to 200 m thick while being associated with large shear zones crossing the region (Figs. 3A and 3B). These rocks occur as blocks, pyroclastic and lava flows in the hillside, riverbeds and small drainage (Figs. 3C-3H), and are, sometimes, interbedded with metasandstones, quartzites, metasiltstones, breccias, and conglomerates (Fig. 4). In the volcanic deposits from the Arraias Formation, the presence of folds and faults is common, however many of its rocks exhibit excellent degrees of preservation of their original textures and structures.

The effusive deposits consist of acidic and basic rocks with thicknesses reaching up to 20 m. The basic rocks are usually massive, dark to brownish-gray, with occasional centimetric columnar joints (Fig. 5A), textural gradation varying from microphaneritic to porphyritic at the base to amygdaloidal aphanitic at the top (Fig. 5B). The acidic effusive rocks, in turn, occurs as subvertical layers, varying from gray to brownish-gray, are anisotropic and porphyritic, enhanced by phenocrysts of quartz and feldspars immersed in the aphanitic groundmass (Fig. 5C and 5D).

The pyroclastic deposits represent the largest volume of volcanic rocks from the Arraias Formation. These deposits occur as pyroclastic flows with characteristics of those coming from traction, suspension and mass flows (McPhie et al., 1993), and are interbedded with the metasedimentary, acidic and basic volcanic rocks of the same formation. The rocks have colorings ranging from whitish gray to purplish gray. The main constituents are phenocrysts, crystalloclasts of quartz and feldspars, sometimes oriented and immersed in a very fine groundmass (tuff), as well as lithic fragments immersed in an aphanitic groundmass sometimes welded. These lithoclasts exhibit ranging sizes of blocks (quartzite and granite) to lapilli (quartzite and porphyritic volcanic rock). Quartzite fragments present

colors ranging from whitish gray to yellowish-white are angular to subrounded, and due to the high temperature, these quartzites sometimes appear as cooked. Other deposits are of densely vesiculated rocks, reddish-brown in color, containing angular fragments of whitish-gray pumice (Fig. 5E). At the top of this deposit, it is possible to observe that other pumice fragments are ellipsoidal in shape oriented along the direction of the pyroclastic flow. In some deposit, the high degree of welding of these rocks is observed from the eutaxitic texture, represented by the flattening and alignment of the fiammes, possibly during the transport and/or after the deposition of the same, whose compaction produced a foliation parallel to the bedding (Fig.5F). These fiammes exhibit dark gray coloration, whose width versus length ratios can reach 1:50, possessing a large number of crystalloclasts and/or quartz phenocrysts in their groundmass. Also, gas escape structures (pipes) can be observed by cutting off some of these pyroclastic deposits.

5. Petrography

The petrographic descriptions of the volcanic rocks from the Arraias Formation followed the recommendations proposed by Le Maitre (2002), McPhie et al., (1993), Cas and Wright (1987) and Fisher & Schmincke (1984). Due to the preservation of the textures of these rocks, it was chosen, in this work, not to add the prefix “meta” to designate samples that was submitted to the greenschist facies metamorphism, as will be presented below.

5.1 Pyroclastic rocks

Pyroclastic rocks show colorings dark gray, purplish gray, brownish-gray and yellowish gray, and are composed quartzite fragments, and accidental lithic pyroclasts and cognates of acid composition, crystalloclasts and phenocryst of plagioclase, alkali feldspar and quartz, as well as hornblende, epidote, chlorite, opaque minerals, titanite and carbonate in subordinate quantities immersed in their cineritic groundmass (Fig. 6A). Exhibit variations of sizes, selection, and morphologies of their main constituents. They are composed of fragments of the size blocks, lapilli, and ash, and can be classified as tuff with or without crystals, lapilli-tuff, block-and-ash flow and surge deposits. In these deposits, the pumice has forms that vary from angular to densely stretched (fiammes), suggesting that the process of welding by compaction acted in a significant way in these rocks. This process is responsible for the development of the eutaxitic texture. Also, we observe the parataxitic texture, with the generation of a planar foliation, with quartz crystals and rotated feldspar,

indicating a reomorphism during and/or after deposition (Fig. 6B). In these deposits, the crystalloclasts and phenocrysts of quartz and feldspars may exhibit corrosive embayment and fractures.

5.3. Effusive basic rocks

The basic rocks are usually porphyritic, marked by clinopyroxene phenocrysts (10-25%), plagioclase (10-30%), and amphiboles (10-20%) immersed in a recrystallized aphanitic groundmass (Fig. 6E). Few of these rocks have ophitic and sub-ophitic textures, and vesicles filled by zeolites, carbonate, and quartz. They are constituted essentially by clinopyroxene, plagioclase, and amphiboles, as well as quartz, epidote, titanite, chlorite and opaque minerals as accessories. The clinopyroxene occurs as anhedral to subhedral crystals, varying from 0.2 mm to 3 mm, 2 mm average exhibiting total and partial inclusions of euhedral plagioclase (Fig. 6F). Plagioclase occurs as subhedral to euhedral crystals, ranging from 0.2 mm to 1 mm, twinned according to the albite law, being sometimes altered to sericite and saussurite.

5.2. Effusive acid rocks

The acid effusive rocks are leucocratic, porphyritic to glomeroporphyritic (Figs. 6C and 6D), whose phenocrysts are essentially represented by quartz (5-10%), alkali feldspar (5-12%), plagioclase (3-8%) and, sometimes oriented and immersed in an felsophyric (quartz-feldspathic) to aphanitic groundmass (70-80%). Accessory minerals are muscovite, hornblende, apatite, zircon and magnetite, biotite, in addition to quartz, carbonate, and epidote filling the vesicles present in these rocks while the latter forms veins at some points. Quartz occurs as anhedral to subhedral crystals, usually fractured, ranging from 0.2 to 8 mm and exhibiting straight and undulating extinctions, and corrosion embayment on the edges of some crystals. The alkali feldspar is anhedral to subhedral, ranging from 0.2 mm to 8 mm, presenting corrosion embayment and fractures occasionally. Plagioclase occurs as anhedral to euhedral crystals, ranging from 0.5 mm to 5 mm, with albite type geminations, partially transformed in saussurite (epidote, carbonate, and white mica), exhibit corrosion embayment, and zircon, apatite and hornblende inclusions.

6. Whole-rock Geochemistry

Whole-rock compositions for volcanic rocks from the Arraias Formation are shown in table 1 (appendix 1). These rocks were separated into acidic and basic according to the SiO_2 and will be discussed below.

The basic volcanic rocks present variations of SiO_2 (47.60-54.57 wt.%), TiO_2 (0.65-2.91 wt.%), Al_2O_3 (13.12-16.35 wt.%), Fe_2O_{3t} (9.11-16.13 wt.%), MnO (0.12-0.71 wt.%), MgO (4.64-8.50 wt.%), CaO (4.93-9.98 wt.%), Na_2O (1.58-4.36 wt.%) K_2O (0.59-3.17 wt.%), and P_2O_5 (0.14-0.76 wt.%) contents with variable LOI (2.20-4.83 wt.%), $\sum Na_2O+K_2O$ (2.17-7.43) and Mg# (45.3-65.6). Also exhibit variations of trace elements such as Rb (20-62 ppm), Ba (244-1700 ppm), Th (1-5 ppm), Nb (3-16 ppm) La (9-74 ppm), Sm (3-8 ppm), Zr (48-168 ppm), Y(17-40 ppm) Ni (20-210 ppm) and V (112-240 ppm) (Tab.1).

The acidic volcanic rocks of the Arraias Formation show varied contents of SiO_2 (66.11-75.72 wt.%), TiO_2 (0.12-0.89 wt.%), Al_2O_3 (10.25-16.12%), Fe_2O_{3t} (1.18-10.61 wt.%), MnO (0.01-0.14 wt.%), MgO (0.01-2.85 wt.%), CaO (0.01-3.79 wt.%), Na_2O (0.03-3.79 wt.%), K_2O (2.12-8.70 wt.%) and P_2O_5 (0.03-0.47 wt.%), LOI (0.47-3.90 wt.%), and $\sum Na_2O+K_2O$ (2.15-12.49). Exhibit variations of Rb (61-315 ppm), Ba (260-2450 ppm), Th (1-115 ppm), Nb (2-105 ppm) La (10-506 ppm), Sm (3-62 ppm), Zr (84-920 ppm), Y (12-280 ppm) Ni (1-24 ppm) and V (1-132 ppm) (Tab.1).

According to the TAS diagram (ΣNa_2O+K_2O versus SiO_2; Le Maitre, 2002), basic volcanic rocks occupy mostly the fields of subalkaline and are classified as basalts and andesitic basalts, except for the samples R539, R586 and 05-XV-200, which are classified as trachybasalt, trachyandesite and alkaline basalt, respectively (Fig. 7A), while on the R1-R2 multicationic diagram (De La Roche et al., 1980) these rocks occupy the field of basalt, tholeiite, basaltic andesite, andesite, latite, and latibasalt (Fig. 7B). In these diagrams, acidic volcanic rocks are classified as dacite, rhyodacite, rhyolite, and alkali rhyolite (Figs. 7A-7B). To mitigate the effects of post-magmatic alterations, we use the Nb/Y versus Zr/TiO_2 immobile elements diagram (Winchester and Floyd, 1977, modified by Pearce, 1996). In this diagram, the studied volcanic rocks exhibit, essentially, affinities with the subalkaline series rocks, where basic rocks are classified as basalt and basaltic andesite, while acidic rocks are classified as rhyodacite/dacite, rhyolite, and alkali rhyolite (Fig. 7C).

In the diagram K_2O versus SiO_2 (Peccerillo and Taylor, 1976), the basic rocks show affinities with the tholeiitic to shoshonitic series rocks, while the acidic rocks are positioned in the fields of calc-alkaline of medium K to shoshonitic rocks (Fig. 7D). These rocks in the AFM diagram (Irvine and Baragar, 1971) exhibit transitional characteristics and are allocated in the rock fields of the Tholeiitic and Calc-alkaline series (Fig. 7E). Basic rocks are positioned exclusively in the field of metaluminous rocks, while acid rocks vary of metaluminous to strongly peraluminous with alumina saturation indices (ASI; A/CNK) ranging from 0.72 to 3.36 (Fig. 7F).

The set of studied rocks does not show clear trends of evolution in the Harker diagrams for major and trace elements (Fig. 8). These geochemical contrasts, marked by the compositional gap between 54.57 and 66.1 of SiO_2 indicate the bimodal character of this volcanism.

Differences between basic and acid rocks of the Arraias Formation are also exhibited in the distribution patterns of REE contents normalized to chondrite (Nakamura, 1974). Basic rocks show enriched in light rare earth elements (LREE) in relation to heavy rare earth elements (HREE) (Fig. 9A), whose ratios $(La/Yb)_N$ vary from 3.30 to 10.36, with less pronounced Eu anomalies (Eu/Eu* = 0.79 to 0.99). Acid rocks also are enriched in LREE compared to HREE, with high $(La/Yb)_N$ ratios (4.72-56.40), whereas the strong to moderate negative anomalies in Eu indicate the important role of plagioclase fractionation in these rocks (Fig. 9B). When normalized by the primitive mantle of Sun and McDonough (1989), basaltic rocks exhibit higher enrichment patterns than the basalts of the oceanic island and upper continental crust, with positive Ba, La, P and Nd anomalies, and negative Nb, Pb, Sr, Zr and Ti anomalies (Fig. 9C). The acidic rocks of the Arraias Formation are LILE-enriched (Fig. 9D), exhibiting expressive Ba, Sr, Nb, and Ti, negative anomalies and Th, La, Nd, Sm and Y positive anomalies.

In the discriminant diagrams for the tectonic settings Y/Nb versus TiO_2 (Winchester and Floyd, 1977) and Zr versus Zr/Y (Pearce and Nory, 1979) these basalts are preferably positioned in the field of continental and within-plate tholeiitic basalts, with other samples positioned in the Mid-Ocean Ridge Basalt (MORB) and Arc Island Basalt (AIB) field (Figs. 10A-10B). In the Y+Nb versus Rb diagram (Pearce et al., 1984), the dacite/rhyodacite, rhyolite, and alkali rhyolite from the Arraias Formation exhibit affinities

with rocks generated in within-plate and/or post-collision settings (Fig. 10C). On the other hand, in the diagram of Whalen et al. (1987), these rocks are positioned essentially in the field of type A granite, whose anorogenic character is emphasized by the high Zr contents, and high ratios of 10,000*Ga/Al_2O_3 (9.19-24.56) (Fig. 10D). Also, FeO_{Total}/(Fe_{OTotal}/MgO) ratios vary between 0.62 and 0.99, being mostly located in the Ferroan A-type granites field (Fig. 10E).

7. Discussion

The volcanic rocks from the Araí Group occupy large areas of northeast Goiás and southeast of Tocantins. These are interbedded with thick packages of metasedimentary rocks in the basal portion of the Arraias Formation in the north of the Brasília Belt (Tanizaki et al., 2015; Alvarenga et al., 2007; Pimentel and Botelho, 2001). These rocks have bimodal composition (basalt-dacite/rhyolite) that can be product of combinations of mantle rocks with crustal castings rich in silica and/or magma mix and are associated with the placement of large volumes of basaltic magmas at high temperatures inside the crust (Guo et al., 2018; Wang et al., 2017, 2016; Meade et al., 2014; Wilson, 1989). Also, excellent degrees of preservation of the original structures and textures, allowing us to recognize three distinct volcanic events: pyroclastic, acid effusive and basic effusive.

The pyroclastic deposits are classified as tuff with or without crystals, lapilli-tuff, block-and-ash flow, surge and occupy wide areas with varied thicknesses. In general, they have a high content of brittle and poorly selected phenocryst and crystalloclasts (quartz and feldspars), lithoclast (quartzite, granite, and acid volcanic rocks) and angular pumice, in addition to stretched and densely stretched fiammes. These characteristics indicate the explosive character, in which the source magmas were volatile-enriched and produced deposits of pumice pyroclastic flows (ignimbrites), with levels of welded ignimbrites and pipes indicating deposition under high temperatures (Gudmundsson, 2006; Sommer et al., 2003; McPhie et al.1993; Fisher and Schmincke, 1984).

Classified as basalt and basaltic andesite, essentially subalkaline, the basic rocks from the Arraias Formation have low Ni, V and Mg # contents (Tab.1), indicating that they do not represent primary magmas (Grove, 2000) and may have undergone the fractional crystallization process with the fractionation of olivine and/or pyroxene from the parental magmas in the magma chamber and/or during its rise to the surface in an within-plate

setting (Fig. 10B) (Farmer, 2013; Zhang et al., 2009; Wilson, 1995, 1989). Also, the positioning of the basalts from Arraias Formation in the Nb/Ba versus Nb/Zr diagram (Hooper and Hawkesworth, 1993), close to the Subcontinental Lithospheric Mantle (Fig. 11A), associated with the La/Yb_N (3.29 a 10.38) ratios, and the significant Nb negative anomalies observed in the diagram normalized by the Primitive Mantle (Fig. 9D) indicates that these rocks were subjected to crustal contamination processes, common characteristics observed in basaltic magmas extruding in intracontinental rift regions (Wang et al., 2017; Xu et al., 2017; Guo et al., 2016; Farmer, 2013; Pearce, 2008; Dusel-Bacon et al., 2004; Wilson, 1989).

The acidic volcanic rocks from the Arraias Formation are rich in SiO_2, being classified as dacite, rhyodacite/rhyolite to alkali rhyolite. These rocks show strong LREE and LILE enrichment, with high La/Yb_N (4.72-42.17) ratios with their expressive negative Sr and Eu anomalies indicate the great importance of the plagioclase crystallization in these rocks (Rollinson, 1993) and may have been generated from the partial melting of continental crust rocks and/or the fractional crystallization of basaltic magmas, as observed in the Nb/Y versus Zr/Y diagram (Fig. 11B), where they are positioned near the rocks the primitive mantle and of the continental crust (Wang et al., 2017; Aydin et al., 2014; Meade et al., 2014; Bonin, 2004; Dusel-Bacon et al., 2004). Also, these rocks were generated in an anorogenic and/or post-collisional settings, marked by the presence of rocks with affinities with those of type A1 and A2 of Eby (1992) (Fig. 11C).

The important volume of volcanic rocks in the Arraias Formation is associated with anorogenic granite bodies in the Province of Goiás, mafic and felsic dykes that intrude the Supracrustal Granite-gneissic Complexes on the west border of the São Francisco Craton (Cordeiro and Oliveira, 2017; Cuadros et al., 2017a, 2017b; Alvarenga et al., 2007; Tanizaki et al., 2015; Fuck et al., 2014; Pimentel and Botelho, 2001). This magmatism aged around 1.77 Ga (Pimentel and Botelho, 2001) may have formed a bimodal Large Igneous Province (LIP) similar to that of Dongargarh Group in central India (Sensarma, 2007) and is correlated with those responsible for the fragmentation of the Supercontinent Columbia in the Paleoproterozoic, generally, associated with mantle plume events (Pirajno and Santosh, 2015; Fuck et al., 2014; Brito Neves, 2011; Rogers and Santosh, 2009, 2004; Condie, 2001; Brito Neves et al., 1995). However, subsequent sedimentation, deformation,

and erosion make it difficult to calculate the volume of extruded melts. Also, the absence of isotopic data makes it impossible to verify whether volcanic rocks from the Arraias Formation were generated from mantle plumes or not. So, the authors are developing isotopic studies (Sm-Nd, Sr-Sr, Lu-Hf, and U-Pb), mineral chemistry, as well as obtaining new whole-rock geochemical data and construct stratigraphic sections. The objective is to understand the role of this volcanism in the fragmentation of the great Brazilian paleocontinental blocks, and the subsequent evolution of the Brasilia Belt.

8. Conclusions

The volcanic rocks from the Araí Group are irregularly distributed at the base of the Arraias Formation. These rocks occur interbedded with quartzite, metasandstones, metasiltstones, breccia, and conglomerate of fluvial-eolic origin and were subjected to metamorphism of the greenschist facies. However, the preservation of their original textures made it possible to recognize the pyroclastic and effusive deposits.

The pyroclastic rocks are classified as tuff with or without crystals, lapilli-tuff, block-and-ash flow, and surge deposited under high temperatures.

The geochemical data showed that the volcanic rocks of Arraias Formation have a bimodal composition, is composed of basalt, andesitic basalt, dacite, rhyodacite, rhyolite, and alkali-rhyolite, essentially subalkaline, generated in a within-plate setting.

The volcanic rocks From the Arraias Formation are associated with the anorogenic granites from the Goiás Province and with the mafic and felsic dikes that intrude the basement of the northern portion of the Brasília Belt. This important plutono-volcanic magmatism presents in the region may have produced a Large Igneous Province (LIP) of the bimodal type during the early stages of the formation of the Araí intracontinental rift around 1.77 Ga.

Acknowledgments

The authors would like to thank the Instituto de Geociências of the Universidade de Brasília (IGD-UNB) for the laboratories provided for this research. We would like to thank the CNPq (Conselho Nacional de Desenvolvimento Científico e Tecnológico) for financial assistance through the project: CNPq-Proc. n°443603/2014-6.

References

Allen, P.A., Allen J.R., 2005. Basins analysis: principles and applications. Oxford, Blackwell Scientific Publications Ltda, 560 p

Almeida, F.F.M., Hasui, Y., Brito Neves, B.B., Fuck, R.A., 1981. Brazilian structuralprovinces: an introduction. Earth-Science Reviews 17 (1), 1–29

Alvarenga, C.J.S., Botelho N.F., Dardenne M.A., Lima O.N.B., Machado M.A., 2007. Programa Levantamentos Geológicos Básicos do Brasil; Mapa Geológico da Folha Cavalcante (SD.23-V-C-V), escala: 1.100.000. Nota Explicativa Integrada com das folhas Monte Alegre de Goiás (SD.23-V-C-III), Cavalcante (SD.23-V-C-V) e Nova Roma (SD.23-V-C-VI). Goiás, UNB/CPRM, 67p

Alvarenga, C.J.S., Botelho, N.F., Campos, J.E.G., Moura, M.A., Meneses, P.R., Dardenne, M.A., Santos, R.V., 1999. Mapa Geológico da Região de Monte Alegre de Goiás, GO. Universidade de Brasília, Brasília.

Aydin, F., Schmitt, A.K., Siebel, W., Sönmez, M., Ersoy, Y., Lermi, A., Dirik, K., Duncan, R., 2014. Quaternary bimodal volcanism in the Niğde Volcanic Complex (Cappadocia, central Anatolia, Turkey): age, petrogenesis and geodynamic implications. Contrib. to Mineral. Petrol. 168, 1–24. https://doi.org/10.1007/s00410-014-1078-3

Bizzi, L.A., Schobbenhaus, C., Vidotti, R.M., Gonçalves, J.H., 2003. Geologia Tectônicae Recursos Minerais do Brasil. CPRM Serviço Geológico do Brasil, Brasília, 674 p

Bonin, B., 2004. Do coeval mafic and felsic magmas in post-collisional to within-plate regimes necessarily imply two contrasting, mantle and crustal, sources? A review. Lithos 78, 1–24. https://doi.org/10.1016/j.lithos.2004.04.042

Bosworth, W., Huchon, P., McClay, K., 2005. The Red Sea and Gulf of Aden Basins. J. African Earth Sci. 43, 334–378. https://doi.org/10.1016/j.jafrearsci.2005.07.020

Botelho, N.F., Alvarenga, C.J.S., Dardenne, M.A., Campos, J.E.G., 1998. Mapa Geológico da Região de Cavalcante, GO. Universidade de Brasília, Brasília.

Botelho, N.F., Alvarenga, C.J.S., Meneses, P.R., D'el-Rey Silva, L.J.H., 1995. Mapa Geológico da Região de Teresina de Goiás, GO. Universidade de Brasília, Brasília.

Brito Neves, B.B., Fuck, R.A., Pimentel, M.M., 2014. The Brasiliano collage in South America: a review. Brazilian J. Geol. 44, 493–518. https://doi.org/10.5327/Z2317-4889201400030010

Brito Neves, B.B., 2011. The Paleoproterozoic in the South American Continent: diversity in the geological time. Journal of South American Earth Sciences 32, 1–20. https://doi.org/10.1016/j.jsames.2011.02.004

Brito Neves, B.B., Sá, J.M., Nilson, A.A., Botelho, N.F., 1995. A Tafrogênese Estateriana nos Blocos Paleoproterozóicos da América do Sul e Processos Subsequentes. Rev. Geonomos. https://doi.org/10.18285/geonomos.v3i2.205

Buck, W.R., 2004. Rheology and deformation of the lithosphere at continental margins in Karner G et al. (eds), Columbia Univ. Press. https://doi.org/10.1177/004057368303900411

Buck, W.R., Lavier, L., Poliakov, A.N.B., 1999. How to make a rift wide. Philos. Trans. 357, 671–693. https://doi.org/10.1098/rsta.1999.0348

Buck, W.R.,1991. Yield Viscosity Straining. J. Geophys. Res. 96, 20161.

https://doi.org/10.1029/91JB01485

Burke, K., Dewey, J.F., Kidd, W.S.F., 1977. World distribution of sutures - the sites of former oceans. Tectonophysics. https://doi.org/10.1016/0040-1951(77)90030-0

Campos, J.E.G., Botelho, N.F., Alvarenga, C.J.S., Meneses, P.R., Moura, M.A., Dardenne, M.A., Nogueira, C., Souza, V.S., 2001. Mapa Geológico da Região de Arraias, TO. Universidade de Brasília, Brasília.

Cas, R.A.F., Wright, J.V (eds)., 1987. Volcanic Successions: Modern and Ancient. Allen and Unwin, London. 528p. http://dx.doi.org/10.1007/978-94-009-3167-1

Cloetingh, S., Van Wees, J.D., 2005. Strength reversal in Europe's intraplate lithosphere: Transition from basin inversion to lithospheric folding. Geology 33, 285–288. https://doi.org/10.1130/G21051.1

Condie, K.C., 2004. Supercontinents and superplume events: Distinguishing signals in the geologic record. Physics of the Earth and Planetary Interiors 146, 319–332. https://doi.org/10.1016/j.pepi.2003.04.002

Condie, K.C., 2001. Mantle Plumes and Their Record in Earth History. Cambridge: Cambridge University Press. doi:10.1017/CBO9780511810589

Cordeiro, P.F. de O., Oliveira, C.G. de., 2017. The Goiás Massif: Implications for a pre-Columbia 2.2–2.0 Ga continent-wide amalgamation cycle in central Brazil. Precambrian Res. 298, 403–420. https://doi.org/10.1016/j.precamres.2017.06.021

Corti, G., 2009. Continental rift evolution: From rift initiation to incipient break-up in the Main Ethiopian Rift, East Africa. Earth-Science Rev. 96, 1–53. https://doi.org/10.1016/j.earscirev.2009.06.005

Corti, G., Bonini, M., Conticelli, S., Innocenti, F., Manetti, P., Sokoutis, D., 2003. Analogue modeling of continental extension: A review focused on the relations between the patterns of deformation and the presence of magma. Earth-Science Rev. 63, 169–247. https://doi.org/10.1016/S0012-8252(03)00035-7

Cuadros, F.A., Botelho, N.F., Fuck, R.A., Dantas, E.L., 2017a. The peraluminous Aurumina Granite Suite in central Brazil: An example of mantle-continental crust interaction in a Paleoproterozoic cordilleran hinterland setting? Precambrian Res. 299, 75–100. https://doi.org/10.1016/j.precamres.2017.07.029

Cuadros, F.A., Botelho, N.F., Fuck, R.A., Dantas, E.L., 2017b. The Ticunzal Formation in central Brazil: Record of Rhyacian sedimentation and metamorphism in the western border of the São Francisco Craton. J. South Am. Earth Sci. 79, 307–325. https://doi.org/10.1016/j.jsames.2017.08.014

Dardenne, M.A., 2000. The Brasília Fold Belt. In: Cordani U.G., Milani E, J., Thomaz Filho A., Campos D.A. (eds.), Tectonic Evolution of South América. 31st International Geological Congress. Rio de Janeiro, 231-263

De La Roche, H., Leterrier, J., Grandclaude, P., and Marchal, M., 1980. A Classification of Volcanic and Plutonic Rocks Using R1R2-Diagram and Major Element Analyses—Its Relationships with Current Nomenclature. Chemical Geology, 29, 183-210. https://doi.org/10.1016/0009-2541(80)90020-0

Dusel-Bacon, C., Wooden, J.L., Hopkins, M.J., 2004. U-Pb zircon and geochemical evidence for

bimodal mid-Paleozoic magmatism and syngenetic base-metal mineralization in the Yukon-Tanana terrane, Alaska. Bull. Geol. Soc. Am. 116, 989–1015. https://doi.org/10.1130/B25342.1

Eby, G.N., 1992. Chemical subdivision of the A-type granitoids: petrogenetic and tectonic implications.Geology20,641–644.https://doi.org/10.1130/0091-7613(1992)020<0641:CSO TAT >2.3.CO;2

Farmer, G.L., 2013. Continental Basaltic Rocks, 2nd ed, Treatise on Geochemistry, 75–110 Second Edition. Elsevier Ltd. https://doi.org/10.1016/B978-0-08-095975-7.00303-X

Fisher, R.V., Schmincke, H.U., 1984. Pyroclastic Rocks, Geological Magazine. 472p. https://doi.org/10.1017/S0016756800031332

Friedmann, S.J., Burbank, D.W., 1995. Rift basins and supradetachment basins: Intracontinental extensional end-members. Basin Res. 7, 109–127. https://doi.org/10.1111/j.1365-2117.1995.tb00099.x

Frost, B.R., Barnes, C.G., Collins, W.J., Arculus, R.J., Ellis, D.J., Frost, C.D., 2001. A geochemical classification for granitic rocks. Journal of Petrology. 42, 2033–2048. https://doi.org/10.1093/petrology/42.11.2033

Fuck, R.A., Dantas, E.L., Pimentel, M.M., Botelho, N.F., Armstrong, R., Laux, J.H., Junges, S.L., Soares, J.E., Praxedes, I.F., 2014. Paleoproterozoic crust-formation and reworking events in the Tocantins Province, central Brazil: A contribution for Atlantica supercontinent reconstruction. Precambrian Res. 244, 53–74. https://doi.org/10.1016/j.precamres.2013.12.003

Fuck, R.A (Coord.)., 2005. Projeto Nova Roma-Porto Real. Escala 1:50.000. Brasília, Instituto de Geociências, Universidade de Brasília.

Gerya, T. V., 2013. Initiation of transform faults at rifted continental margins: 3D petrological-thermomechanical modeling and comparison to the Woodlark Basin. Petrology 21, 550–560. https://doi.org/10.1134/S0869591113060039

Grove, T.L., 2000. Origin of magmas. In: Sigurdsson H (ed.) Encyclopedia of Volcanoes, San Diego, CA: Academic Press,133–147

Gudmundsson, A., 2006. How local stresses control magma-chamber ruptures, dyke injections, and eruptions in composite volcanoes. Earth-Science Rev. 79, 1–31. https://doi.org/10.1016/j.earscirev.2006.06.006

Guo, P., Niu, Y., Sun, P., Wang, X., Gong, H., Duan, M., Zhang, Y., Kong, J., Tian, L., Wu, S., 2018. The Early Cretaceous bimodal volcanic suite from the Yinshan Block, western North China Craton: Origin, process and geological significance. J. Asian Earth Sci. 160, 348–364. https://doi.org/10.1016/j.jseaes.2017.10.023

Guo, P., Niu, Y., Sun, P., Ye, L., Liu, J., Zhang, Y., Feng, Y. xing, Zhao, J. Xin, 2016. The origin of Cenozoic basalts from central Inner Mongolia, East China: The consequence of recent mantle metasomatism genetically associated with seismically observed paleo-Pacific slab in the mantle transition zone. Lithos 240–243, 104–118. https://doi.org/10.1016/j.lithos.2015.11.010

Harker, A., 1909. The Natural History of Igneous Rocks. Methuen and Co., London, 344 p.

Hooper, P.R., Hawkesworth, C.J., 1993. Isotopic and geochemical constraints on the origin and evolution of the Columbia River Basalts. Journal of Petrology 34, 1203–1246. https://doi.org/10.1093/petrology/34.6.1203

Irvine, T.N., Baragar, W.R.A., 1971. A Guide to the Chemical Classification of the Common Volcanic Rocks. Canadian Journal of Earth Science, 8, 523-548.

Kearey, 2013. Global Tectonics, Journal of Chemical Information and Modeling. https://doi.org/10.1017/CBO9781107415324.004

Lavecchia, A., Thieulot, C., Beekman, F., Cloetingh, S., Clark, S., 2017. Lithosphere erosion and continental breakup: Interaction of extension, plume upwelling, and melting. Earth Planet. Sci. Lett. 467, 89–98. https://doi.org/10.1016/j.epsl.2017.03.028

Le Maitre R.W. 2002. Igneous Rocks: a Classification and Glossary of Terms: Recommendations of the International Union of Geological Sciences Subcommission on the Systematics of Igneous Rocks. Cambridge, Cambridge University Press, 236 p.

Marini, O.J., Fuck, R.A., Danni, J.C.M., Dardenne, M.A., Loguercio, S.O.C., Ramalho, R., Coutinho, M.G., 1984. As Faixas de Dobramentos Brasília, Uruaçu e Paraguai-Araguaia e o Maciço de Goiás. In: Schobbenhaus, C., Campos, D.A., Derze, G.R., Asmus, H.E. (Org.), Geologia do Brasil. Brasília, DNPM, pp.251–303

Martins-Ferreira, M.A.C., Chemale, F., Dias, A.N.C., Campos, J.E.G., 2018. Proterozoic intracontinental basin succession in the western margin of the São Francisco Craton: Constraints from detrital zircon geochronology. J. South Am. Earth Sci. 81, 165–176. https://doi.org/10.1016/j.jsames.2017.11.018

McPhie, J., Doyle M., Allen, R., 1993. Volcanic Textures. A Guide to the interpretation of textures in volcanic rocks. University of Tasmania, Australia, 198 p.

Meade, F.C., Troll, V.R., Ellam, R.M., Freda, C., Font, L., Donaldson, C.H., Klonowska, I., 2014. Bimodal magmatism produced by progressively inhibited crustal assimilation. Nat. Commun. 5, 1–11. https://doi.org/10.1038/ncomms5199

Nakamura, N., 1974. Determination of REE, Ba, Fe, Mg, Na, and K in Carbonaceous and Ordinary Chondrites. Geochimica et Cosmochimica Acta, 38, 757-775. http://dx.doi.org/10.1016/0016-7037 (74)90149-5

Olsen, K.H., 1995. Continental Rifts: Evolution, Structure, Tectonics (Developments in Geotectonics). Amsterdam, Elsevier Science, 490 p

Pearce, J.A., 2008. Geochemical fingerprinting of oceanic basalts with applications to ophiolite classification and the search for Archean oceanic crust. Lithos 100, 14–48. https://doi.org/10.1016/j.lithos.2007.06.016

Pearce, J.A., 1996. A User's Guide to Basalt Discrimination Diagrams. In: Wyman, D.A., Ed., Trace Element Geochemistry of Volcanic Rocks: Applications for Massive Sulphide Exploration, Geological Association of Canada, Short Course Notes, Vol. 12, 79-113.

Pearce, J.A., Harris, N.B.W., Tindle, A.G., 1984. Trace Element Discrimination Diagrams for the Tectonic Interpretation of Granitic Rocks. Journal of Petrology, 25, 956-983. http://dx.doi.org/10.1093/petrology/25.4.956

Pearce, J.A., Norry, M.J., 1979. Petrogenetic implications of Ti, Zr, Y, and Nb Variation in Volcanic Rocks. Contributions to Mineralogy and Petrology, 69, 33-47. http://dx.doi.org/10.1007/BF00375192

Peccerillo, A. and Taylor, S.R., 1976. Geochemistry of Eocene Calc-Alkaline Volcanic Rocks from the Kastamonu Area, Northern Turkey. Contributions to Mineralogy and Petrology, 58, 63-

81.http://dx.doi.org/10.1007/BF00384745

Pimentel, M.M., 2016. The tectonic evolution of the Neoproterozoic Brasília Belt, central Brazil: a geochronological and isotopic approach. Brazilian J. Geol. 46, 67–82. https://doi.org/10.1590/2317-4889201620150004

Pimentel, M.M., Jost, H., Fuck, R.A. 2004. O embasamento da Faixa Brasília e o Arco Magmático de Goiás. In: Mantesso-Neto, V., Bartorelli, A., Carneiro, C.D.R., Brito-Neves, B.B. (Eds.). Geologia do continente Sul-Americano: evolução da obra de Fernando Flávio Marques de Almeida. Ed. Beca. 355–368

Pimentel, M. M., Botelho N. F., 2001. Sr and Nd isotopic characteristics of 1,77-1,58 Ga rift-related granites and volcanic of the Goiás province, Central Brazil. Anais da Academia Brasileira de Ciências, 73: 263–276

Pimentel, M.M., Heaman, L., Fuck, R.A., Marini, O.J., 1991. U-Pb zircon geochronology of Precambrian tin-bearing continental-type acid magmatism in central Brazil. Precambrian Res. 52, 321–335. https://doi.org/10.1016/0301-9268(91)90086-P

Pirajno, F., Santosh, M., 2015. Mantle plumes, supercontinents, intracontinental rifting and mineral systems. Precambrian Res. 259, 243–261. https://doi.org/10.1016/j.precamres.2014.12.016

Pirajno, F., Santosh, M., 2014. Rifting, intraplate magmatism, mineral systems and mantle dynamics in central-east Eurasia: An overview. Ore Geol. Rev. 63, 265–295. https://doi.org/10.1016/j.oregeorev.2014.05.014

Ring, U., Livingstone, D., Stanley, H.M., Fischer, G., 2014. The East African Rift System. Aust. J. Earth sciences 107/1, 132–146

Rogers, J.J.W., Santosh, M., 2009. Tectonics and surface effects of the supercontinent Columbia. Gondwana Res. 15, 373–380. https://doi.org/10.1016/j.gr.2008.06.008

Rogers, J.J.W., Santosh, M., 2004. Continents and Supercontinents. Gondwana Res. 7, 653. https://doi.org/10.1016/s1342-937x(05)70827-3

Rollinson, H.R., 1993. Using Geochemical Data: Evaluation, Presentation, Interpretation. Longman Scientific and Technical, England, 352 p

Ruppel, C., 1995. Extensional processes in continental lithosphere. J. Geophys. Res. Solid Earth 100, 24187–24215. https://doi.org/10.1029/95JB02955

Schmeling, H., 2010. Dynamic models of continental rifting with melt generation. Tectonophysics 480, 33–47. https://doi.org/10.1016/j.tecto.2009.09.005

Sengör, A.M.C., Burke, K. 1978. Relative timing of rifting and volcanism on earth and tectonic implications. Geophysical Research Letters, 5:419-421

Sensarma, S., 2007. A bimodal large igneous province and the plume debate: The Paleoproterozoic Dongargarh Group, central India. Special Paper of the Geological Society of America 430, 831–839. https://doi.org/10.1130/2007.2430(38)

Shand, S.J., 1943, Eruptive rocks. Their genesis, composition, classification, and their relation to ore-deposits with a chapter on meteorite, 2nd edition: New York, NY, John Wiley & Sons, 444p.

Sommer, C. a., Lima, E.F., Nardi, L.V.S., Liz, J.D., Pierosan, P., 2003. Depósitos de Fluxo

Piroclástico Primários : Caracterização e Estudo de um Caso no Vulcanismo Ácido Neoproterozóico do Escudo Sul-rio-grandense. Pesquisa em Geociências 30, 3–26

Sun, S., McDonough, W.F., 1989. Chemical and isotopic systematics of oceanic basalts, implications for mantle composition and processes. In: Saunders, A.D., Norry, M.J. (Eds.), Magmatism in the Ocean Basins. Geological Society (Special Publications) 42, 313–345. doi.org/10.1144/GSL.SP.1989.042.01.19

Tanizaki, M.L.N., Campos, J.E.G., Dardenne, M.A., 2015. Estratigrafia do Grupo Araí: registro de rifteamento paleoproterozoico no Brasil Central. Brazilian J. Geol. 45, 95–108. https://doi.org/10.1590/23174889201500010007

Taylor, S.R., McLennan, S.M.,1995. The geochemical evolution of the continental crust. Reviews in Geophysics 33: 241-265. https://doi.org/10.1029/95RG00262

Valeriano, C.M., Dardenne, M.A., Fonseca, M.A., Simões, L.S.A., Seer, H.J., 2004. A evolução tectônica da Faixa Brasília. In: Mantesso Neto, V., Bartorelli, A., Carneiro, C.D.R., Brito Neves, B.B. (Org.), Geologia do Continente Sul-Americano– Evolução da obra de Fernando Flávio Marques de Almeida. São Paulo, Beca. 575–592

Wang, C., Ding, L., Liu, Z.C., Zhang, L.Y., Yue, Y.H., 2017. Early Cretaceous bimodal volcanic rocks in the southern Lhasa terrane, south Tibet: Age, petrogenesis and tectonic implications. Lithos 268–271, 260–273. https://doi.org/10.1016/j.lithos.2016.11.016

Wang, X.C., Wilde, S.A., Xu, B., Pang, C.J., 2016. Origin of arc-like continental basalts: Implications for deep-Earth fluid cycling and tectonic discrimination. Lithos 261, 5–45. https://doi.org/10.1016/j.lithos.2015.12.014

Whalen, J.W., Currie, K.L., Chappell, B.W., 1987. A-type granites: geochemical characteristics, discrimination, and petrogenesis. Contributions of Mineralogy and Petrology, 95, 407-419. doi: 10.1007/BF00402202

Wilson, M., 1995. Magmatic differentiation. Geol.Soc. London, Mem. 16, 205–218. https://doi.org/10.1144/GSL.MEM.1995.016.01.21

Wilson, M., 1989. Igneous petrology. A global tectonic approach, Unwin Hyman. Boston, 466p

Winchester, J.A., Floyd, P.A., 1977. Geochemical Discrimination of Different Magma Series and Their Differentiation Product Using Immobile Elements. Chemical Geology, 20, 325-343. http://dx.doi.org/10.1016/0009-2541(77)90057-2

Wood, A., 1979. A variably veined sub-oceanic upper mantle-genetic significance for mid-ocean ridge basalts from geochemical evidence. Geology, 7, 499-503.

Xu, Z., Zheng, Y.F., Zhao, Z.F., 2017. The origin of Cenozoic continental basalts in east-central China: Constrained by linking Pb isotopes to other geochemical variables. Lithos 268–271, 302–319. https://doi.org/10.1016/j.lithos.2016.11.006

Zhang, Z., Mao, J., Saunders, A.D., Ai, Y., Li, Y., Zhao, L., 2009. Petrogenetic modeling of three mafic-ultramafic layered intrusions in the Emeishan large igneous province, SW China, based on isotopic and bulk chemical constraints. Lithos 113, 369–392. https://doi.org/10.1016/j.lithos.2009.04.023

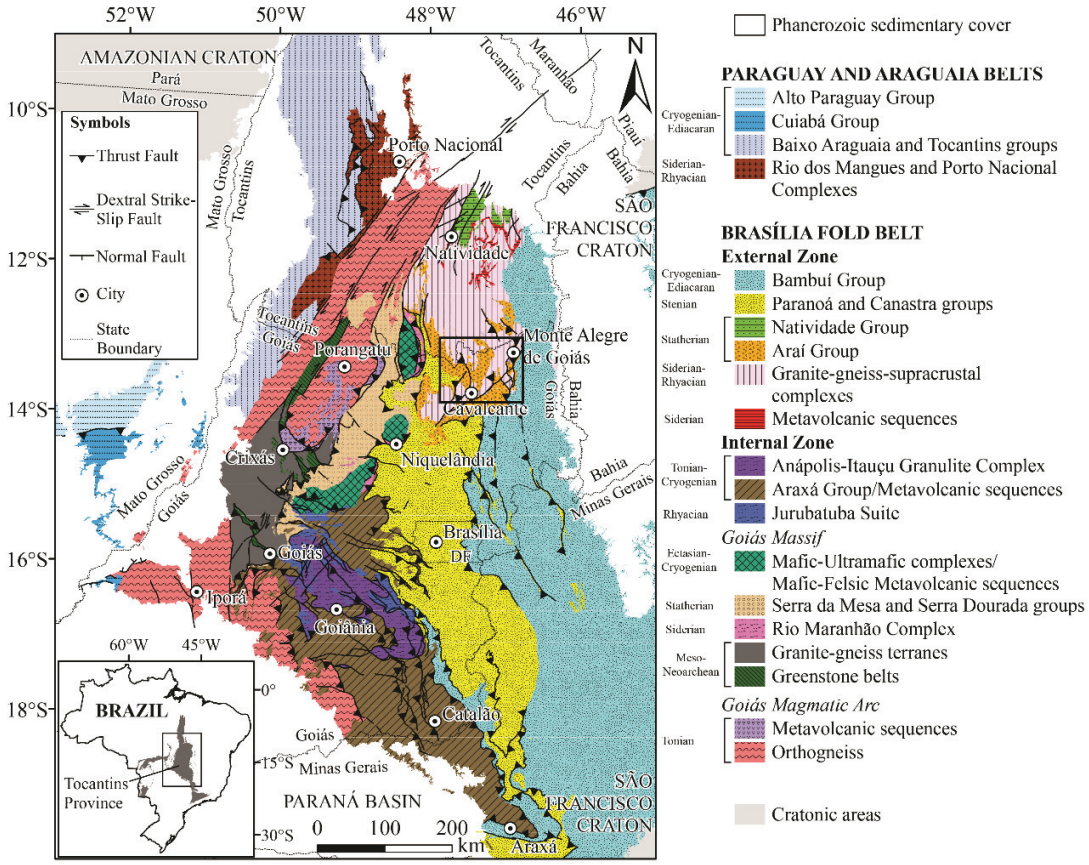

Figure 1. Geological map of the Brasília Belt with the location of the study area, black rectangle, (Pimentel et al., 2004 in Cuadros et al., 2017a).

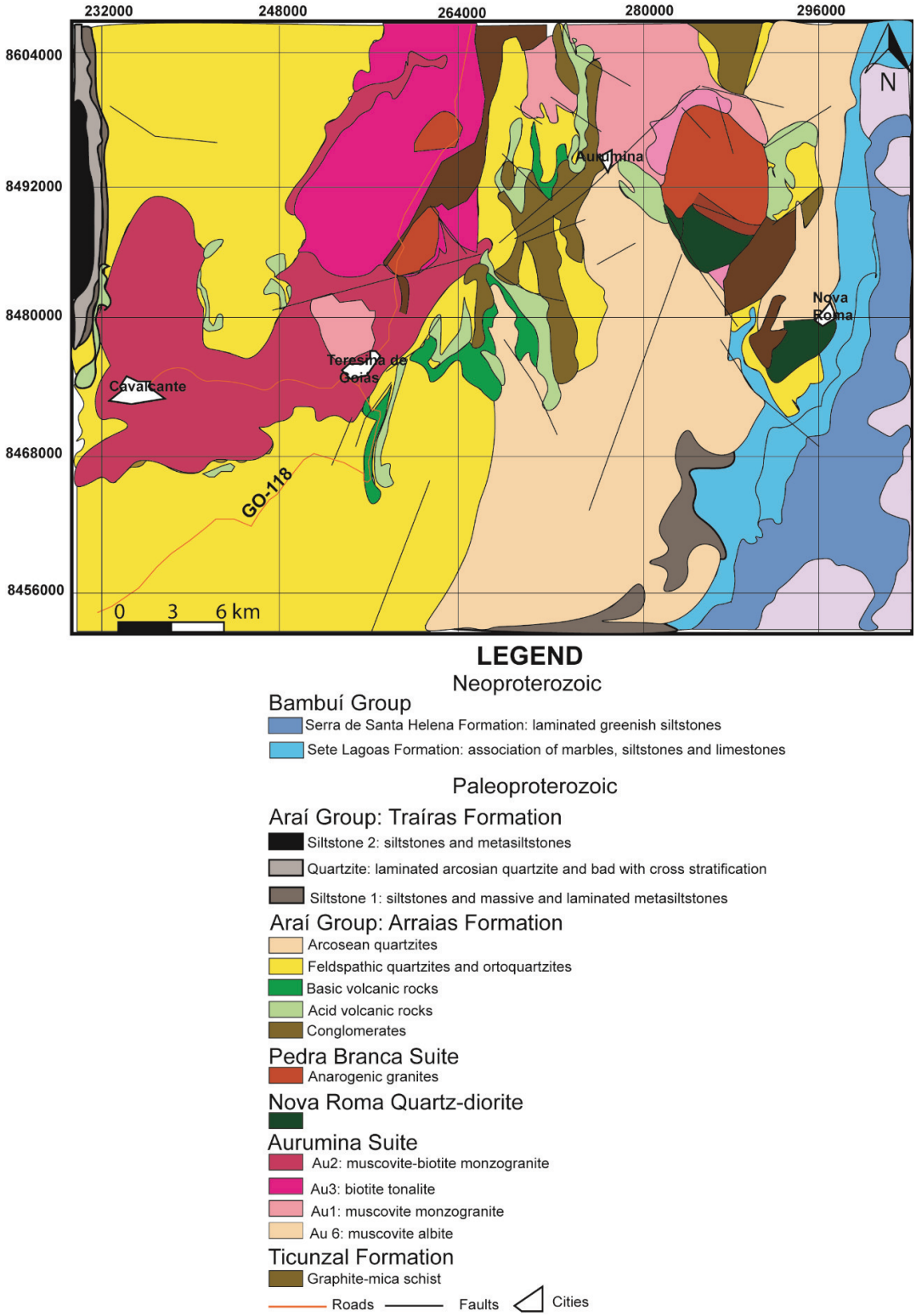

Figure 2. Geological map of the study area with the integration of the geological charts SD.23-VCV-Cavalcante and SD.23-VC-VI-Nova Roma showing the discontinuous distribution of the volcanic rocks from the Arraias Formation, Araí Group (Alvarenga et al., 2007).

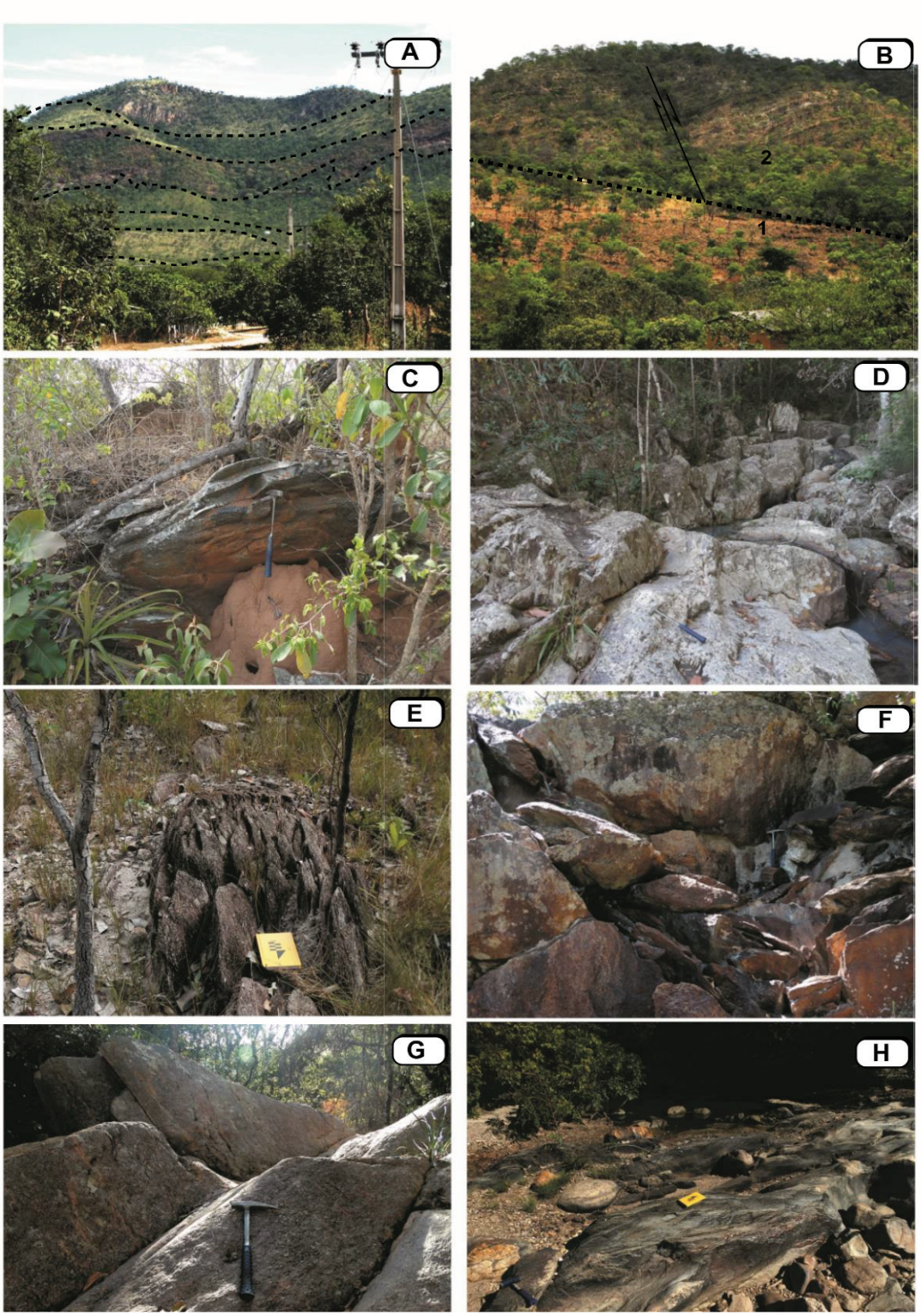

Figure 3. Outcrops of volcanic rocks from the Arraias Formation. In these outcrops interbedding between volcanic and metasedimentary rocks of the same formation are observed [A], with basaltic levels at the basis of stratified metasandstones [B]. The effusive (C and F) and pyroclastic [D, E, G, and H] rocks from the Araí Group can also exhibit subvertical layers in riverbeds [D and H] and/or as blocks [G, E, and H].

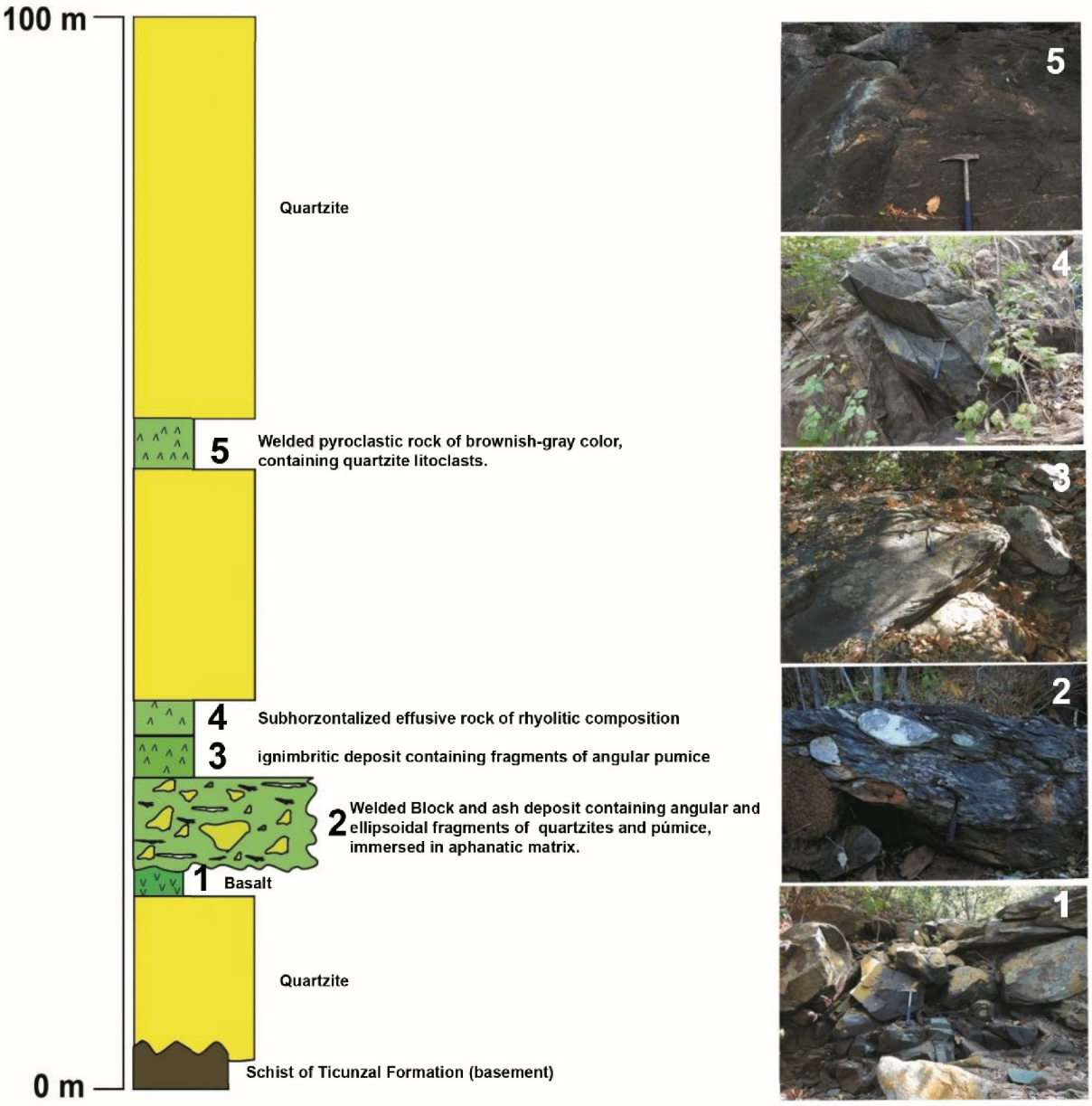

Figure 4. Stratigraphic column shown interbedding of the effusive and pyroclastic volcanic rocks with the metasedimentary rocks from the Arraias Formation, Araí Group.

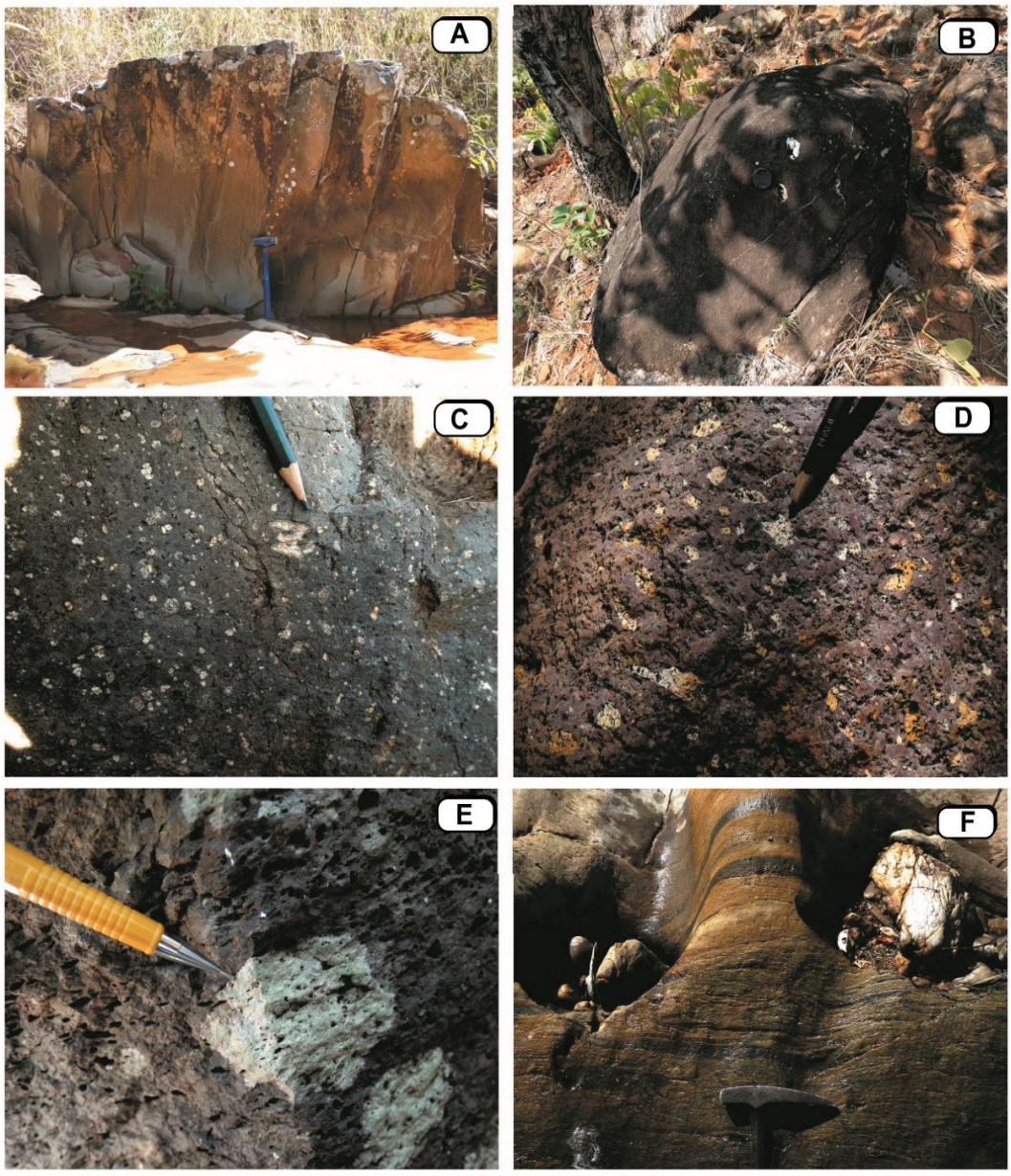

Figure 5. Field aspects of the effusive [A, B, C and D] and pyroclastic [E and F] volcanic rocks from the Araí Group. Basic effusive volcanic rocks [A and B], exhibiting centimetric columnar joints [A] and amygdaloidal structure [B]. Acidic effusive volcanic rocks containing feldspar phenocrysts immersed in an aphanitic groundmass [C and D]. Pyroclastic rock of gray-brownish color, densely vesiculated, containing angular fragments of pumice [E]. Ignimbrite with the parataxitic texture [F].

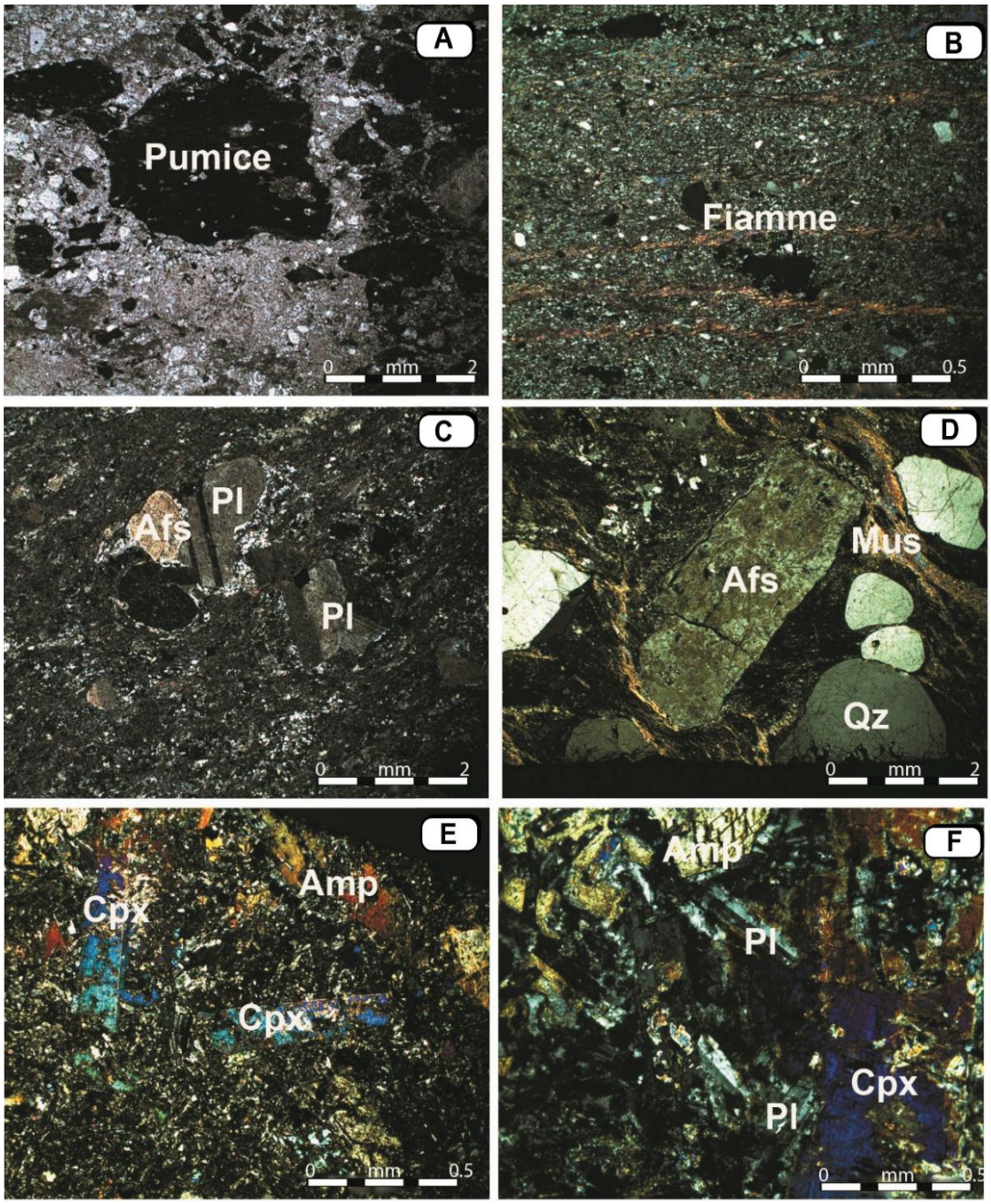

Figure 6. Photomicrographs of volcanic rocks of the Araí Group. Textural aspects of the pyroclastic deposits of the Arraias Formation, exhibiting fragments of angular pumice [A] and eutaxitic texture marked by the alignment of the fiammes [B]. Acid effusive rocks [C and D], with glomeroporphyrytic texture, with phenocrysts of plagioclase [C], alkali feldspar and quartz, sometimes oriented immersed in a feldspathic matrix [D]. Textural aspects of basic rocks, exhibiting clinopyroxene phenocrysts immersed in a very fine granulation groundmass [E]. Subophytic texture [F]. Clinopyroxene (Cpx); Plagioclase (Pl); amphibole (Amp); Quartz (Qz); Alkali feldspar (Afs), Muscovite (Mus).

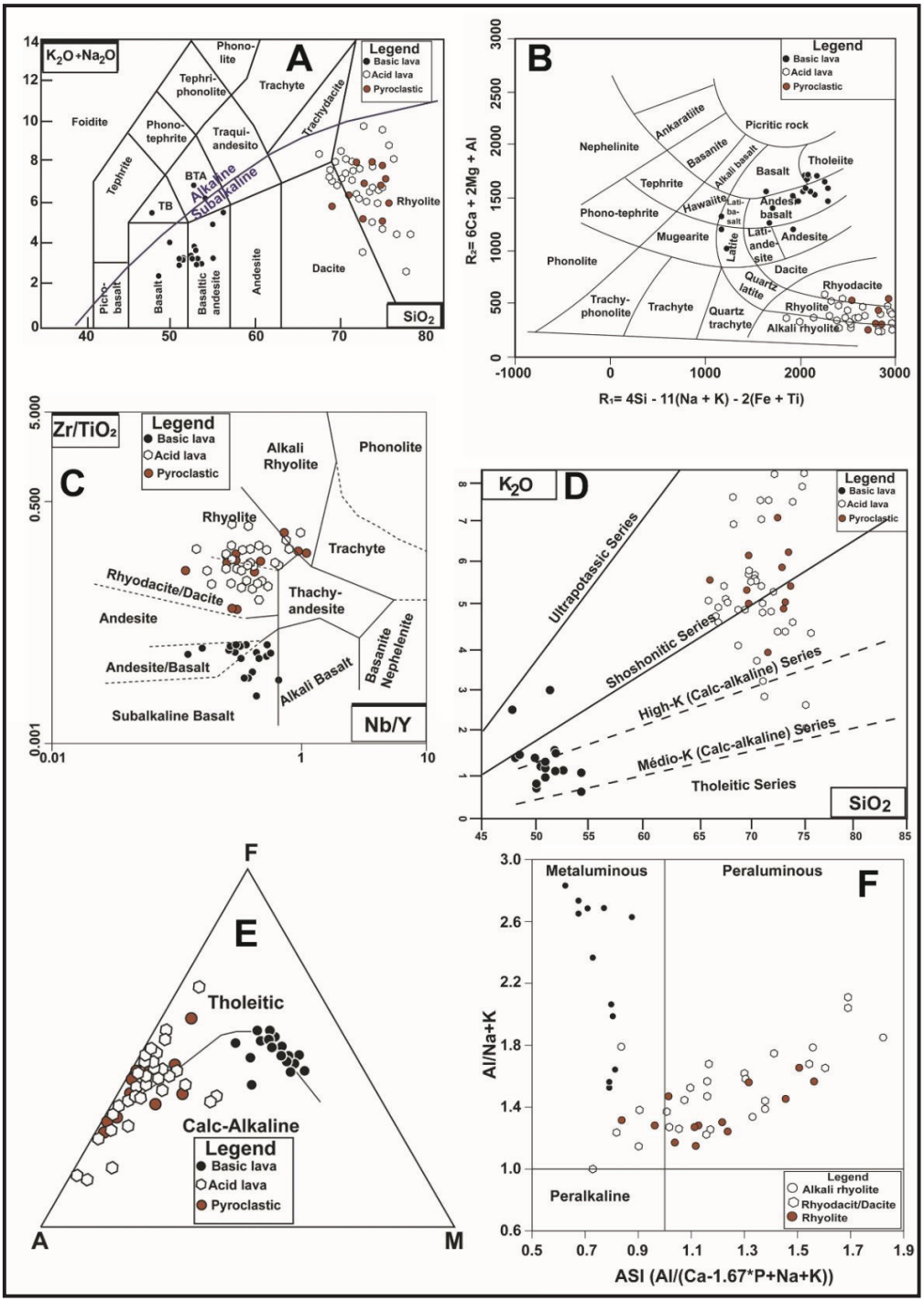

Figure 7. Classification and variation diagrams applied to the volcanic rocks of the Arraias Formation. TAS (SiO_2 *vs*. $\sum K_2O+Na_2O$; Le Maitre, 2002) [A], multicationic R1-R2 (De La Roche et al., 1980) [B], and Nb/Y *vs*. Zr/TiO_2 (Winchester and Floyd, 1977 modified by Pearce, 1996) [C] diagrams. SiO_2 *vs*. K_2O (Peccerillo and Taylor, 1976) [D], AFM (A = K_2O+Na_2O; Fe_2O_{3Total}; M = MgO) (Irvine and Baragar, 1971) [E] and Alumina Saturation Index (ASI) [Al/(Ca-1.67* P + Na + K)] vs. Al/Na+ K molecular rations (Frost et al., 2001 after Shand, 1943) variation diagrams [F].

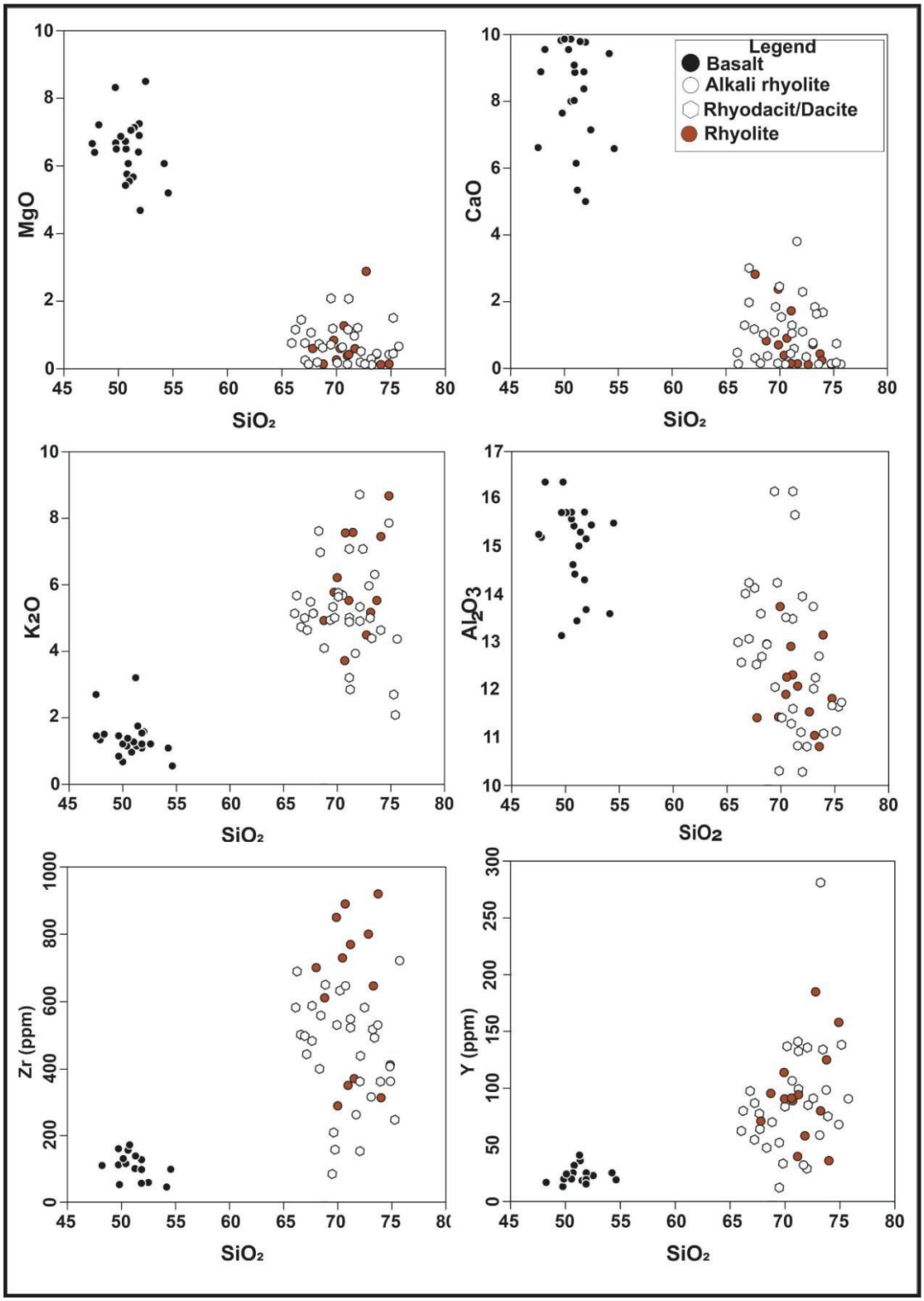

Figure 8. Haker diagrams (1909) for major (wt.%) and traces (ppm) elements applied to the volcanic rocks from the Arraias Formation, Araí Group.

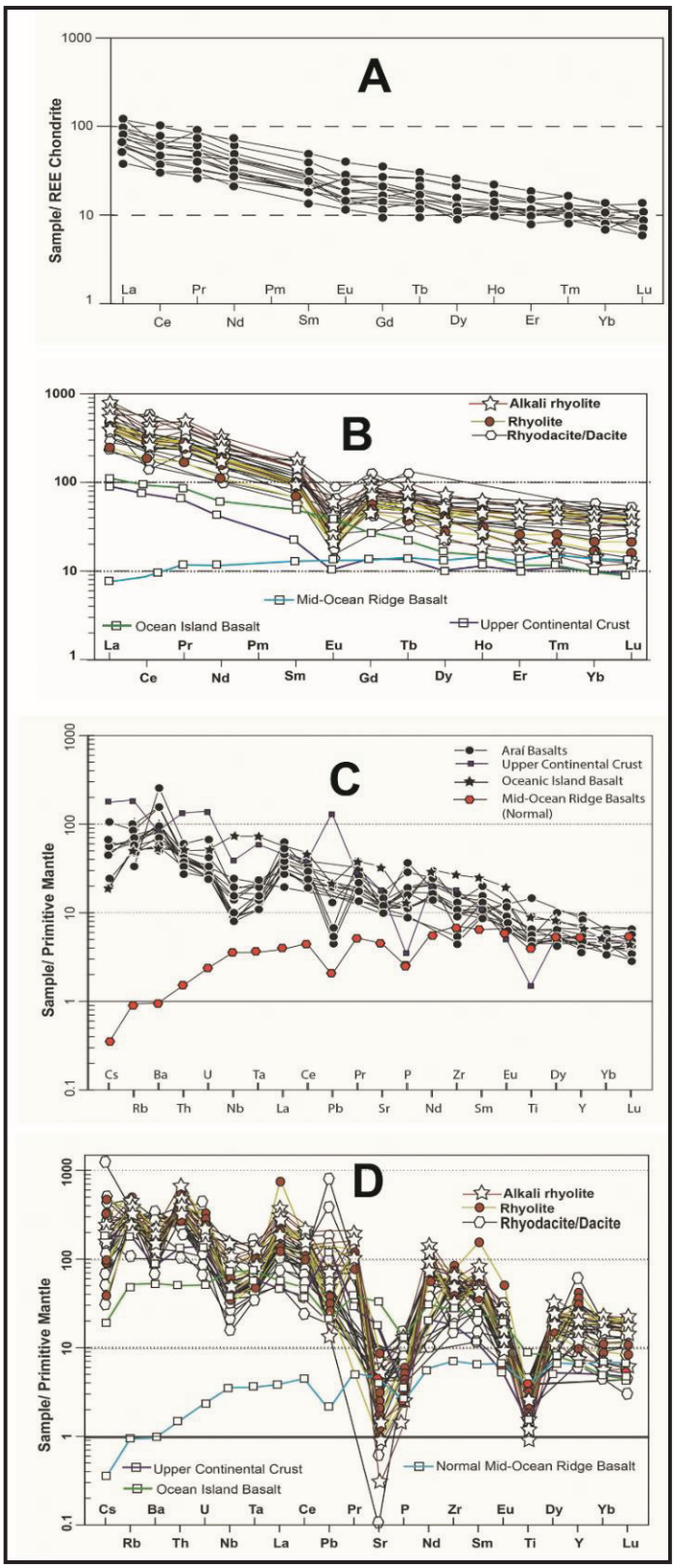

Figure 9. Rare earth elements (REE) diagrams normalized of the chondrite from the Nakamura (1974) [A, B]. Multielementar diagram normalized by the Primitive Mantle from the Sun & MacDonough (1989) (C, D). Data for Oceanic Island Basalt and Normal Mid-Oceanic Basalt Ridge (NMORB) by Sun and MacDonough (1989), and Upper Continental Crust by Taylor and McLennan (1995).

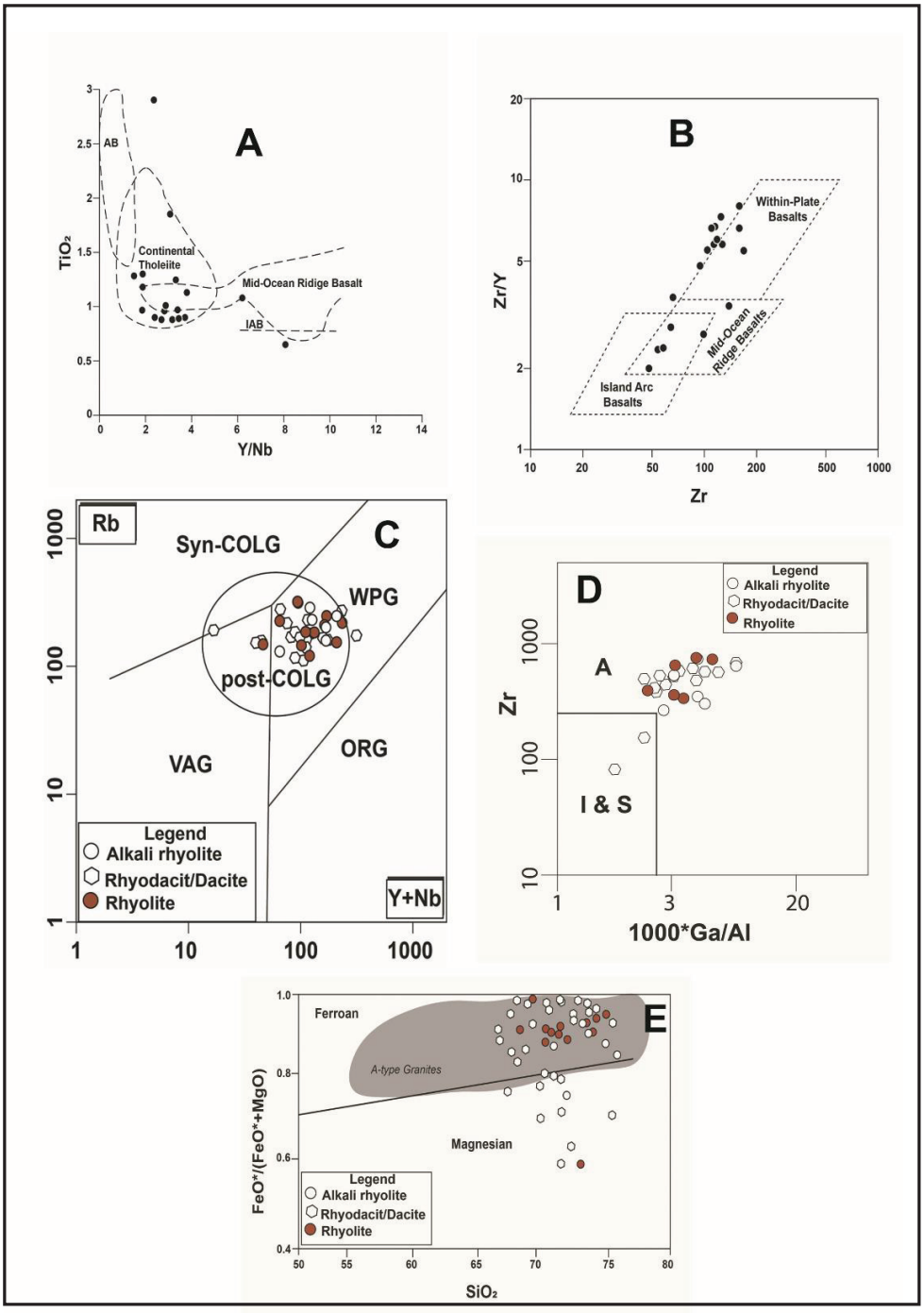

Figure 10. Tectonic settings diagrams applied to the volcanic rocks from the Arraias Formation. Y/Nb vs. TiO_2 (Winchester and Floyd, 1977) [A]. Zr vs. Zr/Y (Peace and Nory, 1977) [B], Y+Nb vs. Rb (Pearce et al.1984; Pearce, 1996) [C]; Zr vs. 10^4*Ga/Al (Whalen et al., 1987) [D], and FeO_{Total}/ (FeO_{Total}+MgO) (Frost et al., 2001) [E] diagrams. Volcanic Arc Granite (VAG); Within-plate Granite (WPG); Ocean-Ridge Granite (ORG); Syncollisional Granite (Syn-Colg). VAB: Volcanic arc basalt.

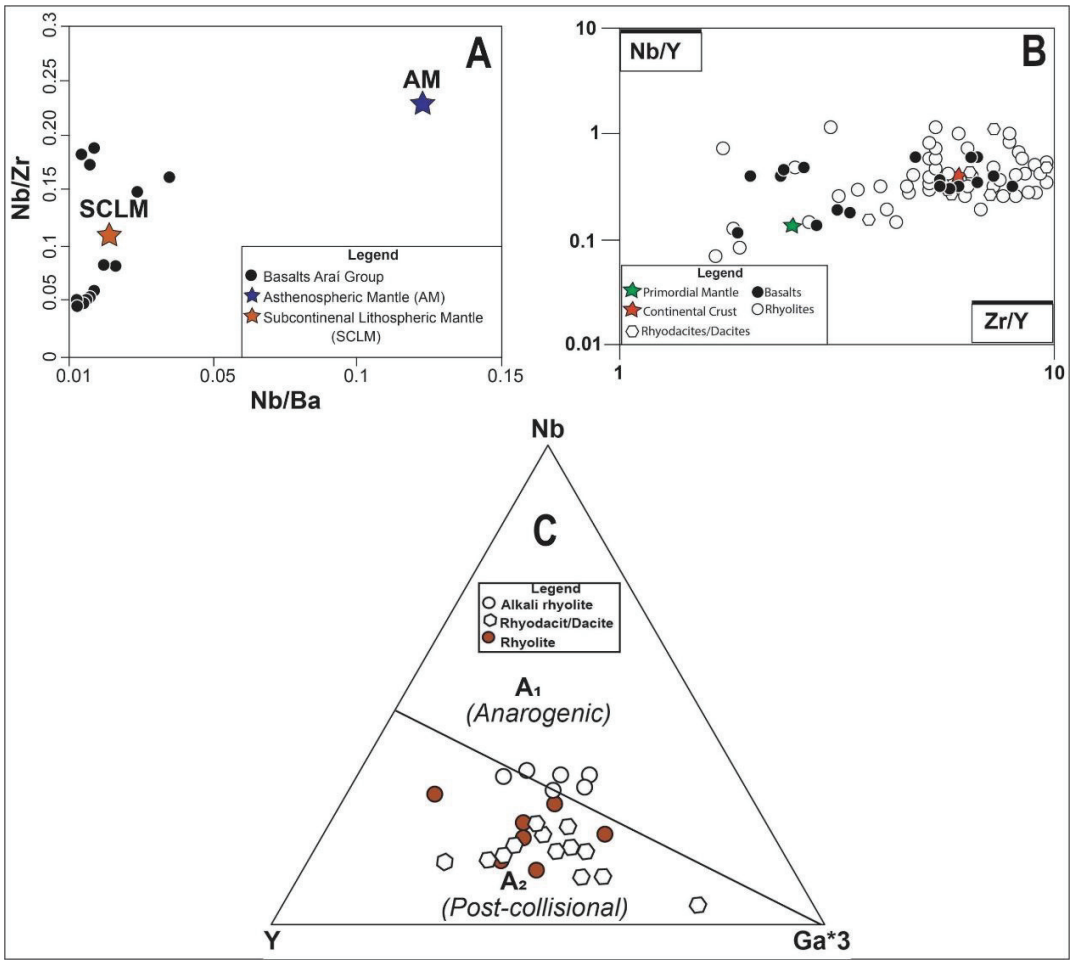

Figure 11. Nb/Zr *vs*. Nb/Ba diagram with the positions of the Subcontinental Lithospheric Mantle and Astenospheric Mantle from Hooper and Hawkesworth (1993) applied to the basalts of the Arraias Formation, Araí Group [A]. Nb/Y vs. Zr/Y diagram applied to the volcanic rocks of the Arraias Formation, with the positioning of Primordial Mantle by Wood (1979) and the Upper Continental Crust from Taylor and McLennan (1995) [B]. Ce versus Y versus Ga triangular diagram (Eby, 1992) [C].

Appendix 1.

***Table 1**. Whole-rock major and trace element compositions for the volcanic rocks from Araí Group. Fe2O3T = (1.11xFeO+Fe2O3). Lost on Ignition (LOI). Mg# = 100x (Mg/Fe+Mg). Eu/Eu* is a measure of the Eu anomaly when compared to Sm and Gd; Eu/Eu*=$Eu_N/(Sm_N*Gd_N)^{1/2}$; N = Chondrite normalized. ASI (Al/(Ca-1.67* P + Na + K).*

Sample N°	**R539**	**R583.1**	**CD-29A**	**CD-28**	**98-I-39**	**98-I-147**	**05-IV-77**	**CD-05**	**29B-16**	**01-III-27b**	**95-II-72**	**98-VI-20**	**R–626.2**	**R–626.1**	**98-VII-58**	**05-XV-200**
Rock type	Basalt	Basalt	Basalt	Basalt	Basalt	Basalt	Basalt	Basalt	Basalt	Basalt	Basalt	Basalt	Basalt	Basalt	Basalt	Basalt
Major elements (wt.%)																
SiO_2	47.60	47.77	48.20	49.72	49.73	49.86	50.16	50.40	50.60	50.78	50.80	50.90	50.90	51.00	51.24	51.30
TiO_2	0.92	0.96	0.88	1.25	1.18	1.01	1.13	0.89	1.30	1.85	1.29	0.85	0.73	0.70	2.91	1.08
Al_2O_3	15.20	15.18	16.35	15.70	13.12	16.34	15.71	15.70	15.55	14.58	14.34	15.40	14.41	14.41	13.43	14.97
Fe_2O_{3T}	16.13	11.69	9.45	9.83	11.50	9.52	10.06	9.97	10.55	11.57	11.65	12.28	11.17	11.08	12.39	10.04
MnO	0.18	0.17	0.13	0.15	0.12	0.16	0.13	0.15	0.15	0.16	0.14	0.14	0.16	0.15	0.15	0.16
MgO	6.65	6.40	7.22	6.66	8.32	6.52	6.84	6.75	6.50	5.44	7.09	6.06	5.75	5.57	5.67	7.10
CaO	6.60	8.87	9.53	9.89	9.87	7.61	9.98	9.57	9.85	7.99	8.95	8.01	8.90	9.07	6.11	5.29
Na_2O	2.75	2.53	1.58	1.81	2.10	2.63	1.96	2.13	1.87	2.96	1.92	2.86	2.48	1.89	2.35	3.49
K_2O	2.66	1.40	1.50	1.43	0.81	0.67	1.23	1.15	1.37	1.22	1.40	0.97	1.27	1.22	1.17	3.17
P_2O_5	0.30	0.33	0.23	0.39	0.32	0.22	0.35	0.23	0.40	0.59	0.39	0.29	0.15	0.15	0.76	0.31
LOI	-	-	3.28	2.43	2.72	4.83	2.20	2.37	2.91	2.50	2.26	2.51	-	-	2.91	2.90
Total	98.99	95.30	98.35	99.26	99.79	99.37	99.75	99.31	101.05	99.64	100.23	100.20	95.92	95.24	99.09	99.81
Mg#	44.93	52.01	60.20	57.29	58.89	57.55	57.37	57.27	54.95	48.21	54.64	49.42	50.48	49.89	47.53	58.33
Na_2O+K_2O	5.41	3.93	3.08	3.24	2.91	3.30	3.19	3.28	3.24	4.18	3.32	3.83	3.75	3.11	5.41	3.93
ASI	0.97	0.92	1.00	0.94	0.81	1.17	0.93	0.95	0.93	0.95	0.92	1.01	0.88	0.91	1.14	0.95
A/NK	1.22	1.12	1.13	1.06	0.94	1.51	1.07	1.12	1.06	1.20	1.05	1.31	1.08	1.07	1.40	1.30
Cs	-	-	0.95	1.20	-	-	-	1.30	1.04	0.40	2.20	9.30	-	-	-	-
Rb	-	-	44.90	40.00	-	52.00	28.60	34.10	37.30	34.60	51.00	38.00	-	-	29.00	59.70
Ba	1200.00	500.00	594.00	624.00	372.00	265.00	480.10	442.00	647.00	610.00	1020.00		420.00	340.00	387.00	1037.00
Th	-	-	2.28	3.00	-	1.10	3.10	3.09	3.80	3.40	3.30	0.90	-	-	-	3.60
U	-	-	0.50	0.70	-	-	0.60	0.58	0.84	0.60	0.60	-	-	-	-	0.60
Nb	-	-	5.20	6.00	9.00	8.00	5.80	5.80	13.00	10.00	12.00	-	-	-	16.00	6.50
Ta	-	-	0.40	0.40	-	1.10	0.50	0.40	0.70	0.50	0.80	0.90	-	-	-	0.60
K	2208.00	11621.00	12451	11870.00	6723.00	5561	10210.00	9546.00	11372.00	10127.00	11621.00	8051.00	10542.00	10127.00	9712.00	26313.00
La	34.00	-	18.90	26.00	-	9.00	23.50	20.50	28.10	31.40	25.00	17.00	-	74.00	-	39.80
Ce		-	36.40	52.60	-	19.00	50.10	42.30	59.10	64.30	42.00	26.00	-	-	-	51.80
Pb	62.00	11.00	-	-	-	-	0.80	-	2.00	-	-	-	10.00	10.00	-	1.00
Pr	-	-	4.61	6.28	-	-	5.88	4.85	6.97	8.18	-	-	-	-	-	9.73
Sr	230.00	430.00	228.00	229.00	176.00	326.00	243.50	260.00	268.00	337.60	212.00	-	300.00	230.00	240.00	196.70
P	1309.00	1440.00	1003.00	1702.00	1396.00	960.00	1527.00	1003.00	1745.00	2574.00	1702.00	1246.00	654.00	654.00	3316.00	1352
Nd	-	-	18.40	25.40	-	-	20.90	19.90	28.20	30.90	26.31	-	-	-	-	37.40
Sm	-	-	3.86	5.00	-	2.70	4.70	3.75	5.52	6.20	5.30	3.80	-	-	-	8.10
Zr	-	-	110.00	160.00	114.00	54.00	126.90	119.00	159.00	168.60	66.00	-	-	-	99.00	138.60
Hf	-	-	2.80	3.60	-	-	3.30	3.10	4.20	4.20	4.00	-	-	-		4.10

Ni	132.00	82.00	-	140.00	210.00	136.00	138.00	140.00	125.00	59.00	149.00	-	128.00	108.00	68.00	139.00
Cr	168.00	178.00	220.00	240.00	155.00	179.00	-	250.00	250.00	-	130.00	-	61.00	44.00	54.00	
V	-	-	170.00	177.00	155.00	176.00	171.00	184.00	203.00	200.00	190.00	-	-	-	170.80	181.00
Cu	84.00	78.00	-	-	141.00	35.00	42.80	-	-	46.00	56.00	-	84.00	55.00	39.00	64.30
Ga	-	-	16.20	17.00	-	-	16.30	18.00	17.80	15.80	-	-	-	-	-	15.50
Eu	-	-	1.02	1.43	-	-	1.19	1.18	1.44	1.80	1.00	2.00	-	-	-	2.04
Ti	3447.00	3597.00	3297.00	4669.00	4422.00	3785.00	4234.00	3335.00	4871.00	6933.00	4834.00	3185.00	2735.00	2623.00	10905.00	4047.00
Gd	-	-	3.63	4.70	-	-	4.40	3.95	5.40	6.29	-	-	-	-	-	7.47
Tb	-	-	0.59	0.70	-	-	0.67	0.62	0.81	0.85	0.90	0.70	-	-	-	1.21
Dy	-	-	3.46	4.30	-	-	3.76	3.40	4.41	5.30	-	-	-	-	-	7.17
Y	-	-	16.50	20.00	17.00	23.00	22.00	19.80	24.40	30.70	18.00	-	-	-	37.00	40.30
Ho	-	-	0.67	0.80	-	-	0.83	0.71	0.83	-	-	-	-	-	-	1.21
Er	-	-	1.80	2.30	-	-	2.57	2.20	2.50	-	-	-	-	-	-	3.32
Tm	-	-	0.26	0.32	-	-	0.33	0.31	0.36	-	-	-	-	-	-	0.49
Yb	-	-	1.89	2.00	-	-	1.51	1.80	2.29	2.66	-	-	-	-	-	2.83
Lu	-	-	0.24	0.31	-	0.20	0.34	0.29	0.38	0.32	0.20	0.30	-	-	-	0.45
Eu/Eu*	-	-	0.82	0.89	-	-	0.79	0.93	0.80	0.88	0.99	-	-	-	-	0.79
$La/Yb_{(N)}$	-	-	6.69	8.69	-	-	10.41	7.62	8.21	7.89	-	-	-	-	-	9.40
Nb/Ba	-	-	0.01	0.01	0.02	0.03	0.01	0.01	0.02	0.02	0.01	-	-	-	0.04	0.01
Nb/Zr	-	-	0.05	0.04	0.08	0.15	0.05	0.05	0.08	0.06	0.18	-	-	-	0.16	0.05
Nb/Y	-	-	0.32	0.30	0.53	0.35	0.26	0.29	0.53	0.33	0.67	-	-	-	0.43	0.16
Y/Nb	-	-	3.17	3.33	1.89	2.88	3.79	3.41	1.88	3.07	1.50	-	-	-	2.31	6.20
Zr/Y	-	-	6.67	8.00	6.71	2.35	5.77	6.01	6.52	5.49	3.67	-	-	-	2.68	3.44

Sample N°	**05-III-34**	**01-III-32**	**95–I-108**	**95-III-61B**	**R.586**	**01-IV-180**	**95-III-121**	**95-I-45A**	**D-PB179**	**NR-26**	**01-IV-74B**	**01-AR-15A**	**01-AR-18**	**05-IX-052**	**01-I-29B**	**95–II-11**
Rock type	**Basalt**	**Basalt**	**Basalt**	**Basalt**	**Basalt**	**Basalt**	**Basalt**	**Basalt**	**Rhy/Dacite**	**Rhy/Dacite**	**Rhy/Dacite**	**Rhy/Dacite**	**Rhy/Dacite**	**Rhy/Dacite**	**Rhy/Dacite**	**Rhyolite**
Major elements (wt.%)																
SiO_2	51.50	51.84	51.85	51.85	52.00	52.49	54.20	54.57	66.11	66.24	66.79	67.11	67.19	67.65	67.67	67.87
TiO_2	0.90	0.97	0.98	0.90	1.16	0.65	0.88	0.96	0.64	0.89	0.83	0.82	0.87	0.62	0.86	0.50
Al_2O_3	15.29	15.15	15.71	14.29	13.68	15.46	13.60	15.44	12.97	12.58	14.03	13.09	14.25	12.49	14.14	11.39
Fe_2O_{3T}	9.11	9.69	9.59	10.51	12.31	9.82	10.09	9.90	9.30	10.61	5.56	6.28	5.72	8.50	6.28	7.19
MnO	0.13	0.13	0.12	0.13	0.71	0.16	0.12	0.15	0.08	0.02	0.14	0.07	0.09	0.10	0.04	0.07
MgO	7.17	6.41	7.25	6.90	4.64	8.50	6.07	5.20	0.75	1.15	1.47	0.25	0.79	0.08	1.06	0.60
CaO	9.81	9.76	8.36	8.88	4.93	7.13	9.44	6.49	0.45	0.02	1.31	2.93	1.95	1.16	0.29	2.76
Na_2O	1.72	1.87	2.04	2.40	4.31	1.88	2.22	4.36	3.08	0.03	2.20	2.49	2.51	2.45	1.81	1.92
K_2O	1.67	1.12	1.57	1.20	1.60	1.19	1.08	0.59	5.15	5.65	4.74	4.98	4.63	5.48	5.17	5.12
P_2O_5	0.24	0.23	0.25	0.18	0.37	0.15	0.19	0.34	0.19	0.05	0.26	0.29	0.32	0.18	0.24	0.10
LOI	2.20	2.60	2.68	2.69	-	2.30	2.08	2.34	1.17	2.40	2.40	1.40	1.40	0.80	2.20	2.33
Total	99.74	99.77	100.40	99.93	95.71	99.73	99.97	100.34	99.89	99.64	99.73	99.71	99.72	99.51	99.76	99.85
Mg#	60.91	56.70	59.95	56.52	42.74	63.15	54.36	50.97	13.77	17.67	34.36	7.30	21.47	1.83	25.05	14.17

Na_2O+K_2O	3.39	2.99	3.61	3.60	5.91	3.07	3.30	4.95	8.23	5.68	6.94	7.47	7.14	7.93	6.98	7.04
ASI	0.89	0.92	1.01	0.88	0.98	1.17	0.83	1.06	1.07	1.49	1.23	0.92	1.15	0.98	1.39	0.84
A/NK	1.01	1.06	1.20	1.08	1.57	1.41	0.99	1.67	1.57	1.49	1.60	1.17	1.51	1.29	1.75	1.02
Traces and earth rare elements (ppm)																
Cs	-	0.50	-	-	-	3.70	1.20	-	-	10.30	5.50	0.60	3.60	-	4.20	-
Rb	42.60	30.10	-	37.00	-	62.80	38.00	20.00	114.30	206.50	179.20	166.60	223.90	135.60	171.70	-
Ba	529.20	365.00	590.00	664.00	255.00	244.00	553.00	1700.00	1472.20	756.00	924.00	814.00	840.00	1771.40	1064.00	1390.00
Th	3.20	2.60	-	3.00	-	2.20	2.90	4.80	20.00	28.70	33.20	31.70	37.00	20.70	34.50	-
U	0.60	0.50	-	0.50	-	0.90	0.50	1.40	3.00	3.80	6.00	8.50	5.20	2.40	3.90	-
Nb	5.20	5.60	6.00	10.00	-	2.80	9.00	11.00	26.30	34.30	27.40	27.50	29.50	28.40	29.40	38.00
Ta	0.60	0.50	-	-	-	0.10	0.80	0.60	-	1.80	1.60	1.60	1.80	2.40	1.70	-
K	13862.46	9296.98	13032.37	9961.05	13281.40	9878.04	8964.90	4897.52	42749.50	46899.93	39346.14	41338.35	38433.04	45488.78	42915.51	42500.47
La	20.60	18.30	-	20.00	-	12.70	20.00	31.00	49.30	108.70	101.10	81.40	91.00	95.50	70.30	-
Ce	41.80	36.30	-	33.00	-	26.80	35.00	53.00	109.30	201.10	156.60	158.50	187.80	206.70	145.20	-
Pb	0.70	-	-	-	11.00	3.00	-	-	4.10	22.00	121.00	14.00	10.00	58.90	4.00	-
Pr	4.94	4.44	-	-	-	3.36	-	-	-	23.65	24.85	19.00	21.27	21.39	17.97	-
Sr	282.50	244.70	11.00	194.00	150.00	538.80	222.00	233.00	84.60	11.40	123.00	167.30	156.10	111.00	50.50	89.00
P	1047.39	1003.75	1091.03	785.54	1614.73	654.62	829.19	1483.81	829.19	218.21	1134.67	1265.60	1396.52	785.54	1047.39	436.41
Nd	18.30	19.70	18.95	-	-	13.20	-	-	44.90	97.70	93.40	78.30	89.30	82.90	63.50	-
Sm	4.50	3.50	3.60	3.90	-	2.80	3.70	5.80	9.16	16.80	18.00	14.30	15.50	15.50	13.60	-
Zr	112.00	103.80	124.00	57.00	-	64.40	48.00	96.00	580.00	686.90	501.40	499.30	447.40	584.20	481.40	700.00
Hf	3.00	2.90	-	4.00	-	1.40	3.00	6.00	-	19.50	13.10	13.30	12.70	16.50	13.20	-
Ni	147.00	68.00	184.00	140.00	20.00	64.00	127.00	97.00	-	1.00	3.00	4.00	5.00	5.00	3.00	-
Cr	-	-	135.00	40.00	24.00	-	38.00	22.00	-	-	-	-	-	-	-	-
V	175.00	167.00	160.00	225.00		112.00	205.00	240.00	-	21.00	22.00	132.00	23.00	-	22.00	-
Cu	30.50	24.00	43.00	82.00	80.00	51.00	63.00	39.00	16.50	2.00	49.00	17.00	21.00	17.70	2.00	26.00
Ga	15.20	15.30	-	-	-	15.30	-	-	25.30	36.60	22.10	16.10	21.40	27.60	21.00	-
Eu	1.15	1.09	-	2.00	-	0.89	-	-	1.63	2.80	1.83	1.25	1.49	2.72	1.16	-
Ti	3372.89	3635.22	3672.70	3372.89	4347.28	2435.97	3297.93	3.597.75	2398.50	3335.41	3110.55	3073.07	3260.46	2323.54	3222.98	1873.83
Gd	3.29	3.70	-	-	-	2.75	-	-	-	14.33	17.82	10.97	13.27	12.68	11.71	-
Tb	0.65	0.59	-	0.80	-	0.46	-	1.20	-	2.32	2.49	1.72	2.02	2.48	1.76	-
Dy	3.02	3.54	-	-	-	3.49	-	-	9.25	13.92	14.38	9.70	11.96	12.07	9.93	-
Y	19.30	19.00	17.00	24.00		22.60	24.00	20.00	62.00	80.10	96.90	54.50	86.00	77.10	65.80	71.00
Ho	0.86	-	-	-	-	-	-	-	-	-	-	-	-	2.56	-	-
Er	2.17	-	-	-	-	-	-	-	-	-	-	-	-	7.53	-	-
Tm	0.38	-	-	-	-	-	-	-	-	-	-	-		1.07	-	-
Yb	1.80	1.81	-	-	-	2.57	-	2.00	6.89	7.94	6.38	4.36	5.60	7.49	5.03	-
Lu	0.27	0.26	-	-	-	0.37	-	0.20	-	1.32	0.83	0.70	0.89	1.15	0.80	-
Eu/Eu*	0.88	0.92	-	-		0.97	-	-	0.94	0.54	0.31	0.29	0.31	0.58	0.28	-
La/Yb(N)	7.65	6.76	-	-	-	3.30	-	10.36	4.78	9.15	10.60	12.48	10.87	8.53	9.35	-
Nb/Ba	0.01	0.02	0.01	0.02	-	0.01	0.02	0.01	0.02	0.05	0.03	0.03	0.04	0.02	0.03	0.03
Nb/Zr	0.05	0.05	0.05	0.18	-	0.04	0.19	0.11	0.05	0.05	0.05	0.06	0.07	0.05	0.06	0.05

Nb/Y	0.27	0.29	0.35	0.42	-	0.12	0.38	0.55	0.42	0.43	0.28	0.50	0.34	0.37	0.45	0.54
Y/Nb	3.71	3.39	2.83	2.40	-	8.07	2.67	1.82	2.36	2.34	3.54	1.98	2.92	2.71	2.24	1.87
Zr/Y	5.80	5.46	7.29	2.38	-	2.85	2.00	4.80	9.35	8.58	5.17	9.16	5.20	7.58	7.32	9.86

Sample N°	**PB-182-B**	**CD-29C**	**95- IV- 93**	**99-I-86**	**01-V154B**	**95-IV- 97**	**01-VIII-131**	**95-I-89**	**05-V148**	**95-IV-DI**	**95- IV-91B**	**CD-09**	**CD-16A**	**98- I-36B**	**CD-18**	**CD-01**
Rock Type	**Rhy/Dacite**	**Rhy/Dacite**	**Rhyolite**	**Rhy/Dacite**	**Rhy/Dacite**	**Rhy/Dacite**	**Rhy/Dacite**	**Rhyolite**	**Rhyolite**	**Rhy/Dacite**	**Rhy/Dacite**	**Rhyolite**	**Alk.Rhyo**	**Rhyolite**	**Rhyolite**	**Rhyolite**
Major elements (wt.%)																
SiO_2	68.32	68.44	68.79	68.90	69.53	69.59	69.77	69.90	69.92	70.01	70.21	70.44	70.60	70.70	71.01	71.10
TiO_2	0.73	0.66	0.60	0.71	0.15	0.66	0.50	0.55	0.27	0.62	0.58	0.55	0.30	0.66	0.35	0.54
$Al2O_3$	13.56	12.67	12.95	12.95	16.10	12.03	14.25	11.42	13.73	10.27	11.42	11.88	13.50	12.24	12.88	12.25
Fe_2O_{3T}	5.43	7.21	6.72	9.22	2.95	5.49	5.70	7.18	3.10	7.57	7.46	6.63	5.32	5.93	4.78	5.84
MnO	0.08	0.04	-	0.12	0.05	0.01	0.03	0.04	0.06	0.01	0.01	0.13	0.07	0.08	0.02	0.12
MgO	0.74	0.14	0.01	0.63	0.72	2.05	1.16	0.82	0.25	0.13	0.25	0.62	0.65	1.27	0.44	0.42
CaO	0.10	1.04	0.81	0.33	1.10	1.86	0.09	0.70	2.36	2.45	1.50	0.38	0.07	0.87	0.01	1.73
Na_2O	0.26	0.34	3.54	2.81	1.39	0.82	0.12	1.67	1.64	1.24	2.41	1.84	0.73	2.36	0.09	2.22
K_2O	7.62	6.95	4.93	4.08	4.95	5.39	5.05	5.80	6.20	5.80	5.62	5.71	5.67	3.71	7.51	5.53
P_2O_5	0.16	0.19	0.13	0.17	0.09	0.21	0.09	0.12	0.11	0.16	0.11	0.11	0.05	0.14	0.05	0.11
LOI	1.60	1.37	0.75	-	2.70	2.30	2.90	1.32	2.10	2.13	1.09	0.71	2.37	1.20	1.54	1.89
Total	98.60	99.05	99.23	99.92	99.73	100.41	99.66	99.52	99.74	100.39	100.66	99.01	99.33	99.16	98.68	101.75
Mg#	21.25	3.70	0.29	11.91	32.58	42.49	28.72	18.44	13.77	3.29	6.22	15.62	19.48	29.77	15.41	12.46
Na_2O+K_2O	7.88	7.29	8.47	6.89	6.34	6.21	5.17	7.47	7.84	7.04	8.03	7.55	6.40	6.07	7.60	7.75
ASI	1.16	1.06	1.00	1.29	1.53	1.07	1.85	0.98	0.96	0.77	0.85	1.05	1.42	1.27	1.14	0.92
A/NK	1.18	1.08	1.54	1.99	1.83	1.15	1.86	1.19	1.12	0.87	1.11	1.32	1.58	1.84	1.15	1.17
Traces and earth rare elements (ppm)																
Cs	25.30	2.20	-	1.30	10.60	8.70	9.70	-	-	1.90	4.90	3.80	4.42	-	3.50	1.78
Rb	231.00	184.00	-	120.00	180.10	280.00	157.40	-	247.10	110.00	160.00	185.00	251.00	118.00	233.00	179.50
Ba	1016.00	1976.00	1340.00	1413.00	975.00	1930.00	873.00	1351.00	1477.60	2450.00	1240.00	1247.00	860.00	1150.00	945.00	1180.00
Th	32.00	20.40	-	21.30	6.20	17.00	9.80	-	54.60	17.00	26.60	28.40	40.90	-	36.10	29.20
U	5.90	2.20	-	2.40	2.50	4.10	2.10	-	5.40	2.10	2.70	3.00	3.52	-	4.60	3.08
Nb	26.30	18.00	38.00	-	2.50	16.00	9.60	26.00	54.80	25.00	37.00	23.00	105.00	31.00	26.00	37.20
Ta	-	1.50	-	3.10	0.30	1.40	1.30	-	4.30	1.90	2.50	1.90	5.20	-	2.50	1.90
K	63252.65	57691.07	40923.30	33867.56	41089.32	4741.71	41919.41	48145.06	51465.41	48145.06	6650.91	7397.98	47065.95	30796.24	2339.56	45903.83
La	69.90	91.40	-	69.00	18.90	52.00	94.10	-	146.50	79.00	120.00	129.00	228.00	-	164.00	143.50
Ce	122.00	185.00	-	130.00	23.10	94.00	85.40	-	294.50	140.00	210.00	244.00	353.00	-	293.00	249.00
Pb	24.60	3.00	-	-	7.00	-	11.00	-	6.80	-	-	-	-	-	5.00	-
Pr	-	21.50	-	-	4.00	-	16.88	-	32.36	-	-	27.30	55.10	-	33.20	32.60
Sr	30.00	60.00	104.00	66.00	92.30	180.00	84.10	174.00	171.30	142.00	102.00	31.00	16.60	21.00	18.00	53.60
P	698.26	829.19	567.34	741.90	392.77	916.47	392.77	523.70	480.05	698.26	480.05	480.05	218.21	610.98	218.21	480.05
Nd	-	81.60	-	55.00	13.10		67.30	-	120.20			104.00	198.50	-	116.00	123.50
Sm	-	17.10	-	12.20	2.70	10.30	11.00	-	20.40	14.20	19.20	19.10	36.60	-	19.40	21.60
Zr	400.00	557.00	610.00	647.00	84.00	205.00	152.80	850.00	287.80	530.00	629.00	729.00	643.00	890.00	349.00	769.00

Hf	-	12.70	-	15.00	2.80	7.00	4.20	-	9.70	12.00	18.00	17.80	18.50	-	8.60	20.20
Ni	-		-	-	3.00	24.00	5.00	-	5.00	-	-	-	10.00	-	-	5.00
Cr	-	210.00	-	-	-	34.00	-	-	-	-	-	190.00	360.00	-	190.00	230.00
V	-	7.00	-	-	17.00	69.00	37.00	41.00	7.00	-	-	-	30.00	14.00	18.00	-
Cu	6.76	-	10.00	6.00	1.00	19.00	-	7.00	0.40	10.00	15.00	-	-	4.00	-	-
Ga	18.60	31.00	-	-	14.80	-	17.40	-	30.10	-	-	28.00	40.00	-	23.00	24.90
Eu	1.22	2.79	-	2.00	1.05	1.00	2.80	-	2.22	4.00	2.00	2.39	3.13	-	1.56	2.13
Ti	2735.79	2473.45	2.248.59	2660.83	562.15	2473.45	1873.83	2061.21	1011.87	2323.54	2173.64	2068.70	1124.30	2473.45	1311.68	2023.73
Gd	-	15.40	-	18.70	2.38		9.19	-	15.08	-	-	17.10	28.50	-	13.20	18.85
Tb	-	2.40	-	1.50	0.31	1.60	1.12	-	2.80	1.80	2.40	2.70	4.52	-	1.80	2.91
Dy	-	14.00	-	9.22	1.92		6.11	-	15.05	-	-	16.90	24.50	-	9.90	16.35
Y	46.50	71.00	95.00	70.00	12.30	51.00	33.30	93.00	113.30	82.00	135.00	89.00	106.50	89.00	41.00	93.00
Ho	-	2.70	-	-	-	-	-	-	3.40	-	-	3.50	4.27	-	1.80	3.25
Er	-	7.40	-	-	-	-	-	-	9.66	-	-	9.80	12.30	-	4.60	10.20
Tm	-	1.06	-					-	1.58		-	1.45	1.61	-	0.65	1.37
Yb	2.90	7.10	-	6.00	1.10	3.00	2.52	-	8.87	4.00	-	9.30	10.25	-	3.90	8.97
Lu	-	1.09	-	0.90	0.13	0.40	0.35	-	1.42	0.70	-	1.42	1.53	-	0.56	1.34
Eu/Eu*	-	0.52	-	0.41	-	0.51	0.83	-	0.37	-	0.55	0.40	0.29	-	0.28	0.32
$La/Yb_{(N)}$	16.12	8.61	-	7.69	11.49	11.59	24.97	-	11.04	13.21	-	9.28	14.87	-	28.12	10.70
Nb/Ba	0.03	0.01	0.03	-	-	0.01	0.01	0.02	0.04	0.01	0.03	0.02	0.12	0.03	0.03	0.03
Nb/Zr	0.07	0.03	0.06	-	0.03	0.08	0.06	0.03	0.19	0.05	0.06	0.03	0.16	0.03	0.07	0.05
Nb/Y	0.57	0.25	0.40	-	0.20	0.31	0.29	0.28	0.48	0.30	0.27	0.26	0.99	0.35	0.63	0.40
Y/Nb	1.77	3.94	2.50	-	4.92	3.19	3.47	3.58	2.07	3.28	3.65	3.87	1.01	2.87	1.58	2.50
Zr/Y	8.60	7.85	6.42	9.24	6.83	4.02	4.59	9.14	2.54	6.46	-	8.19	6.04	10.00	8.51	8.27

Sample N°	**95-III-14**	**95- IV-85B**	**01-VI-101**	**98-VI-81**	**98-III-121**	**05-XI-116**	**CD-19**	**95-II-89**	**99-V-110**	**95-III-87**	**CD-27B**	**95- II-103**	**05-VI-249**	**95- IV-FSJ**	**CD-02**	**99-IV-132**
Rock Type	**Rhy/Dacite**	**Rhy/Dacite**	**Rhy/Dacite**	**Rhy/Dacite**	**Rhy/Dacite**	**Alk.Rhyo**	**Rhyolite**	**Rhy/Dacite**	**Rhy/Dacite**	**Rhy/Dacite**	**Rhy/Dacite**	**Rhyolite**	**Alk.Rhyo**	**Rhy/Dacite**	**Rhyolite**	**Rhy/Dacite**
Major elements (wt.%)																
SiO_2	71.11	71.13	71.18	71.20	71.33	71.64	71.70	72.08	72.10	72.17	72.50	72.77	73.09	73.19	73.23	73.40
TiO_2	0.69	0.67	0.86	0.34	0.79	0.19	0.39	0.40	0.23	0.69	0.55	0.56	0.25	0.62	0.53	0.35
Al_2O_3	11.30	11.59	13.45	16.12	15.64	10.79	12.04	11.05	13.95	10.24	10.85	11.50	13.73	12.01	11.06	12.26
Fe_2O_{3T}	8.27	7.71	5.25	3.39	1.18	3.41	5.12	2.34	3.33	8.57	6.72	4.76	3.03	5.56	4.77	3.89
MnO	0.05	0.00	0.06	-	0.02	0.07	0.01	0.04	0.07	0.03	0.02	0.10	0.06	0.04	0.05	0.05
MgO	0.08	0.14	1.16	2.03	0.41	0.97	0.56	1.19	0.15	0.50	0.06	2.85	0.19	0.11	0.31	0.15
CaO	1.30	0.43	0.12	1.04	0.54	3.79	0.02	2.26	1.10	1.12	0.33	0.11	0.77	1.81	0.69	1.63
Na_2O	2.14	1.00	0.08	0.33	3.79	1.10	0.09	1.07	1.64	0.77	0.75	0.32	0.78	2.05	1.96	2.28
K_2O	5.06	7.08	4.90	3.24	2.88	3.93	7.55	8.70	4.90	5.32	7.13	4.41	5.96	5.02	5.13	4.42

P_2O_5	0.15	0.16	0.11	0.47	0.17	0.05	0.07	0.08	0.10	0.17	0.15	0.08	0.29	0.14	0.11	0.07
LOI	0.59	0.80	2.60	2.41	2.52	3.90	1.68	1.26	-	0.83	0.84	3.12	1.60	0.47	0.91	-
Total	100.74	100.71	99.77	100.56	99.26	99.84	99.23	100.47	97.57	100.41	99.90	100.58	99.75	101.02	98.75	98.50
Mg#	1.88	3.47	30.43	54.26	40.80	36.03	17.80	50.17	8.19	10.36	1.74	54.26	11.04	3.77	11.40	7.09
Na_2O+K_2O	7.20	8.08	4.98	3.57	6.67	5.03	7.64	9.77	6.54	6.09	7.88	4.73	6.74	7.07	7.09	6.70
ASI	0.95	0.95	1.81	2.69	1.59	0.89	1.06	0.64	1.29	1.00	0.91	1.63	1.30	0.97	1.00	1.05
A/NK	1.22	1.04	1.80	2.61	3.13	1.00	1.06	0.69	1.60	1.09	0.98	1.71	1.39	1.22	1.29	1.41
Traces and earth rare elements (ppm)																
Cs	-	1.00	6.60	2.30	3.60	-	6.40	2.20	4.70	-	1.62	2.00	-	3.30	0.80	2.90
Rb	-	170.00	162.60	170.00	61.00	130.50	315.00	150.00	200.00	-	166.00	160.00	230.60	170.00	143.00	190.00
Ba	2030.00	2305.00	682.00	-	-	1057.00	1091.00	1345.00	520.00	2352.00	2050.00	890.00	1492.80	1905.00	1303.00	2000.00
Th	-	20.00	30.90	0.90	7.90	31.40	33.50	10.00	21.60	-	19.55	26.00	58.00	23.80	26.60	30.80
U	-	2.00	5.60	0.60	1.60	2.80	5.90	1.30	3.90	-	1.78	3.40	4.50	2.40	2.80	4.70
Nb	33.00	25.00	29.90	-	-	32.30	40.00	13.00	-	31.00	23.60	27.00	66.10	34.00	21.00	-
Ta	-	2.00	1.60	0.80	1.40	2.90	2.70	1.50	4.20	-	1.40	2.30	4.60	2.70	1.80	4.80
K	42002.42	58770.18	40674.28	26894.83	23906.51	32622.43	62671.59	72217.59	40674.28	44160.64	59185.22	36606.85	49473.20	41670.38	42583.48	36689.86
La	-	110.00	63.10	10.00	33.00	137.90	146.00	32.00	120.00	-	81.60	506.00	211.50	160.00	83.50	150.00
Ce	-	150.00	143.30	28.00	41.00	254.10	274.00	60.00	330.00	-	133.00	270.00	331.40	180.00	165.00	300.00
Pb	-	-	10.00	-	-	7.30	3.00	-	-	-	-	-	8.90	-	-	28.00
Pr	-	-	17.99	-	-	29.61	32.00	-	-	-	21.80	-	44.39	-	19.40	-
Sr	163.00	84.00	24.00	-	-	104.00	22.00	113.00	88.00	60.00	64.30	17.00	95.60	164.00	34.00	315.00
P	654.62	698.26	480.05	2060.87	736.45	218.21	305.49	349.13	436.41	741.90	654.62	349.13	1265.60	610.98	480.05	305.49
Nd	-	-	66.60	-	-	105.80	115.00	-	-	-	85.80	-	173.30	-	72.30	108.80
Sm	-	24.70	13.90	4.10	4.80	18.70	21.50	6.10	20.40	-	16.95	63.20	28.50	25.00	14.10	21.50
Zr	550.00	550.00	518.90	-	-	261.50	369.00	153.00	358.00	440.00	578.00	799.00	312.10	510.00	649.00	494.00
Hf	-	11.00	14.20	-	-	8.70	9.30	5.00	17.00	-	16.20	21.00	9.40	19.00	16.00	31.00
Ni	-	-	6.00	-	-	5.00	-	5.00	-	-	-	-	5.00	-	-	1.00
Cr	-	-	-	-	-	-	170.00	20.00	-	-	360.00	-	-	-	220.00	2.00
V	3.00	1.00	70.00	-	-	9.00	17.00	123.00	7.00	3.00	5.00	26.00	-	12.00	11.00	5.00
Cu	24.00	13.00	-	-	-	11.30	-	1.00	64.00	1.00	-	1.00	0.50	16.00	-	3.00
Ga	-	-	18.90	-	-	15.90	20.00	-	-	-	18.60	-	30.30	-	18.00	25.00
Eu	-	5.00	1.47	-	-	1.56	1.75	2.00	2.00	-	2.43	8.00	4.42	3.00	1.61	4.00
Ti	2585.88	2510.93	3222.98	1274.20	2960.64	712.05	1457.84	1499.06	861.96	2585.88	2061.21	2098.69	936.91	2323.54	1993.75	1311.68
Gd	-	-	16.67	-	-	12.82	16.40	-	-	-	16.40	-	24.55	-	14.60	25.77
Tb	-	4.00	2.30	1.00	-	2.05	2.20	0.80	2.60	-	2.60	5.20	3.22	4.50	2.40	2.70
Dy	-	-	15.24	-	-	8.02	12.20	-	-	-	15.30	-	12.81	-	14.70	17.36
Y	98.00	133.00	142.00	-	-	32.70	58.00	28.00	135.00	85.00	91.60	184.00	58.40	280.00	80.00	133.00
Ho	-	-	-	-	-	1.26	2.20	-	-	-	3.21	-	1.84	-	3.00	-
Er	-	-	-	-	-	3.61	5.90	-	-	-	8.95	-	4.32	-	8.40	-
Tm	-	-	-	-	-	0.50	0.80	-	-	-	1.33	-	0.44	-	1.23	-
Yb	-	-	8.92	-	-	3.06	4.80	2.00	8.00	-	8.25	8.00	2.50	9.00	8.00	10.00
Lu	-	-	1.27	0.20	0.30	0.43	0.75	0.20	1.10	-	1.12	1.40	0.41	1.30	1.30	1.40
Eu/Eu*			0.30			0.29	0.27		0.52		0.44	0.67	0.50	0.63	0.34	0.52
$La/Yb_{(N)}$	-	-	4.73	-	-	30.13	20.34	10.70	10.03	-	6.61	42.29	56.57	11.89	6.98	10.03
Nb/Ba	0.02	0.01	0.04	-	-	0.03	0.04	0.01	-	0.01	0.01	0.03	0.04	0.02	0.02	-

Nb/Zr	0.06	0.05	0.06	-	-	0.12	0.11	0.08	-	0.07	0.04	0.03	0.21	0.07	0.03	-
Nb/Y	0.34	0.19	0.21	-	-	0.99	0.69	0.46	-	0.36	0.26	0.15	1.13	0.12	0.26	-
Y/Nb	2.97	5.32	4.75	-	-	1.01	1.45	2.15	-	2.74	3.88	6.81	0.88	8.24	3.81	-
Zr/Y	5.61	4.14	3.65	-	-	8.00	6.36	5.46	2.65	5.18	6.31	4.34	5.34	1.82	8.11	3.71

Sample N°	**05-XII-262**	**95-III-130**	**05-IX-113**	**95-VI-50**	**CD-22**	**PB-41A**	**95-V-125**	**98-V61A**	**K6**
Rock Type	**Alk.Rhyo**	**Rhyolite**	**Rhyolite**	**Rhy/Dacite**	**Alk.Rhyo**	**Rhyolite**	**Rhy/Dacite**	**Rhy/Dacite**	**Alk.Rhyo**
Major elements (wt.%)									
SiO_2	73.65	73.70	74.03	74.04	74.83	74.85	75.28	75.31	75.72
TiO_2	0.25	0.71	0.12	0.70	0.19	0.25	0.68	0.77	0.51
Al_2O_3	12.68	10.85	13.14	11.04	11.65	11.80	11.09	11.61	11.74
Fe_2O_{3T}	3.87	5.43	1.79	6.13	3.45	3.24	6.80	4.16	4.41
MnO	0.04	0.01	0.02	-	0.04	0.01	0.04	0.04	0.01
MgO	0.34	0.45	0.10	0.20	0.41	0.14	0.44	1.48	0.67
CaO	0.02	0.41	0.19	1.65	0.03	0.02	0.11	0.73	0.01
Na_2O	1.45	0.38	2.05	1.39	0.14	0.13	0.51	1.73	0.07
K_2O	6.31	5.52	7.49	4.62	7.88	8.68	2.12	2.66	4.36
P_2O_5	0.06	0.12	0.05	0.15	0.05	0.10	0.09	0.15	0.03
LOI	1.10	1.58	0.90	0.78	1.09	0.68	3.18	1.63	2.20
Total	99.77	99.16	99.88	100.70	99.76	99.90	100.34	100.27	99.73
Mg#	14.82	14.08	9.96	6.06	19.05	7.88	11.35	41.30	23.12
Na_2O+K_2O	7.76	5.90	9.54	6.01	8.02	8.81	2.63	4.39	4.43
ASI	1.12	1.19	0.93	1.03	0.98	0.90	2.86	1.65	1.78
A/NK	1.34	1.24	1.15	1.22	0.99	0.91	3.35	2.36	1.80
Traces and earth rare elements (ppm)									
Cs	-	10.00	-	-	5.20	-	2.00	11.00	3.70
Rb	201.50	210.00	154.20	-	287.00	212.80	270.00	170.00	155.50
Ba	1355.30	1485.00	924.00	260.00	1088.00	743.00	570.00	419.00	683.00
Th	33.70	30.60	1.70	-	35.70	115.00	47.80	44.90	32.30
U	3.00	6.50	0.70	-	3.70	7.40	6.20	3.40	4.40
Nb	72.60	38.00	10.20	31.00	54.00	74.30	95.00	-	76.70
Ta	5.00	3.10	1.50	-	4.30	-	5.80	2.10	3.20
K	52378.51	45820.82	62173.54	38350.03	65410.88	72051.58	17597.85	22080.32	36191.81
La	258.50	90.00	52.70	-	194.00	213.00	160.00	88.00	127.40
Ce	425.20	200.00	70.10	-	248.00	1.480.00	310.00	210.00	232.70
Pb	11.10	-	2.70	-		30.00	-	8.00	2.00
Pr	51.62	-	10.61	-	42.20	-	-	-	27.73
Sr	27.80	47.00	62.80	88.00	30.00	19.60	2.00	65.00	5.80
P	261.85	523.70	218.21	654.62	218.21	436.41	392.77	657.50	130.92
Nd	172.80	-	41.30	-	153.00	-	-	-	109.60

Sm	29.70	17.40	6.60	-	28.80	-	29.90	13.10	20.00
Zr	528.10	920.00	312.40	360.00	358.00	406.00	240.00		722.90
Hf	15.70	22.00	9.40	-	9.20		10.00	21.00	21.00
Ni	5.00	-	5.00	-		-	-	-	-
Cr	-	-	-	-	180.00	-	-	-	-
V	15.00	25.00		3.00	20.00	-	-	47.00	12.00
Cu	1.00	12.00	0.90	13.00		23.20	6.00	3.00	< 1
Ga	20.80	-	-	-	24.00	14.90	-	11.00	24.30
Eu	2.64	-	5.04	-	2.00	0.24	-	2.00	1.88
Ti	936.91	2660.83	449.72	2623.36	727.04	936.91	2548.40	2885.69	1911.30
Gd	20.42	-	5.73	-	19.30	-	-	-	18.13
Tb	3.64	2.50	1.03	-	3.10	-	4.00	0.90	2.78
Dy	17.55	-	5.08	-	17.00	-	-	-	16.55
Y	97.50	125.00	35.50	75.00	68.00	158.00	138.00		91.30
Ho	3.32	-	1.01	-	3.00	-	-	-	-
Er	9.70	-	2.90	-	8.30	-	-	-	-
Tm	1.43	-	0.42	-	1.15	-	-	-	-
Yb	8.63	7.00	2.19	-	7.30	21.20	9.00		8.74
Lu	1.25	1.10	0.31	-	1.06		1.30	0.30	1.31
Eu/Eu*	0.31	-	-	-	0.25	-	-	0.80	0.30
La/Yb(N)	20.03	8.60	16.09	-	17.77	6.72	11.89	-	9.75
Nb/Ba	0.05	0.03	0.01	0.12	0.05	0.10	0.17	-	0.11
Nb/Zr	0.14	0.04	0.03	0.09	0.15	0.18	0.40	-	0.11
Nb/Y	0.74	0.30	0.29	0.41	0.79	0.47	0.69	-	0.84
Y/Nb	1.34	3.29	3.48	2.42	1.26	2.13	1.45	-	1.19
Zr/Y	5.42	7.36	8.80	4.80	5.26	2.57	1.74	-	7.92

Capítulo IV

Artigo 2: PETROGENESIS OF THE PALEOPROTEROZOIC BASALTIC MAGMATISM FROM ARAÍ RIFT, CENTRAL BRAZIL

Gmail

Successfully received: submission Petrogenesis of the Paleoproterozoic Basaltic Magmatism from Araí Rift, Central Brazil. for Journal of South American Earth Sciences

Journal of South American Earth Sciences <EviseSupport@elsevier.com> 1 de agosto de 2019 18:11 Responder a: sames@elsevier.com Para: cleverton.correia@gmail.com

This message was sent automatically.

Ref: SAMES_2019_329
Title: Petrogenesis of the Paleoproterozoic Basaltic Magmatism from Araí Rift, Central Brazil. Journal: Journal of South American Earth Sciences

Dear Mr. Silva,

Thank you for submitting your manuscript for consideration for publication in Journal of South American Earth Sciences. Your submission was received in good order.

To track the status of your manuscript, please log into EVISE® at: http://www.evise.com/evise/faces/pages/navigation/NavController.jspx?JRNL_ACR=SAMES and locate your submission under the header 'My Submissions with Journal' on your 'My Author Tasks' view.

Thank you for submitting your work to this journal.

Kind regards,

Journal of South American Earth Sciences

Have questions or need assistance?
For further assistance, please visit our Customer Support site. Here you can search for solutions on a range of topics, find answers to frequently asked questions, and learn more about EVISE® via interactive tutorials. You can also talk 24/5 to our customer support team by phone and 24/7 by live chat and email.

Petrogenesis of the Paleoproterozoic Basaltic Magmatism from the Araí Rift, Central Brazil.

Cleverton Correia Silva[1,2]; Valmir da Silva Souza[1,2,3]; Nilson Francisquini Botelho[1,2,3]

Elton Luiz Dantas[1,2,3]

[1]Programa de Pós-Graduação em Geologia da Universidade de Brasília (DF), BRAZIL

[2]Instituto de Geociências, Universidade de Brasília (DF), BRAZIL

[3]Universidade de Brasília-UNB (DF), BRAZIL

*Corresponding author: e-mail: cleverton.correia@gmail.com

Abstract

The Araí Group presents in its basal portion voluminous exposures of volcanic rocks with hundreds meters, whose composition varies from basic to acidic, and are interbedded with fluvial-eolian metasedimentary rocks from the Arraias Formation. The rocks of this group together with the anorogenic granites of the Staniferous Province of Goiás compose important and preserved records of the paleoproterozoic taphrogenetic processes in the northeast part of the Brasilia Belt, western border of the San Francisco Craton, in central Brazil. Basaltic lavas from the Arraias Formation occur discontinuously and interbedded with quartzite/meta-sandstones and acidic volcanic rocks (effusive and pyroclastic) of the same formation. Basalts are fine- to coarse-grained, usually massive, and vary from dark gray to greenish gray. Aphanitic textures are common, but in some outcrops basalts can exhibit porphyritic texture, with varying amounts of phenocrysts of plagioclase and augite in a fine-grained groundmass. Bulk geochemistry shows: SiO_2 = 48.20-54.80 wt.%, TiO_2 = 0.88-1.85 wt.%, Al_2O_3 = 13.90-16.35 wt.%, $Fe_2O_{3(T)}$ = 9.11-11.57 wt.%, MgO = 5.26-7.22 wt.%, CaO = 7.58-9.98 wt.%, Na_2O = 1.58-3.37 wt.%, K_2O = 0.34-2.25 wt.%, Mg# = 51.97-63.40, Ni (46-140 ppm), Cr (40-250 ppm), V (167-258 ppm), Sr (198-337 ppm), Nb (5-13 ppm), Y (16-31 ppm) and Zr (104-169 ppm). In classification diagrams, mafic volcanic rocks from the Arraias Formation occupy the field of subalkaline rocks and are classified as basalts and basaltic andesites. They exhibit a clear LREEs fractionation relative to HREEs, with $La/Yb_{(N)}$ ratios varying between 6.7 and 10.4, and slightly negative Eu anomalies (Eu/Eu* = 0.8-1.0). In multielementar diagram these rocks present positive Ba, U, K and Hf anomalies (Ba/Ba*= 1.1-1.8; U/U* = 1.3-1.6; K/K* = 1.0-2.3; Hf/Hf* = 1.0-1.2) and negative Nb, Ta, Th, Ti Sr and Zr anomalies (Nb/Nb* = 0.2-0.4; Ta/Ta* = 0.3-0.6; Th /Th* = 0.5-0.9; Ti/Ti* = 0.6-0.8; Sr/Sr* = 0.4-0.9; Zr/Zr* = 0.8-0.9). In tectonic discriminant diagrams, basalts exhibit similarities with rocks generated at a within-plate setting. Contamination is evidenced by the presence of inherited zircons with ages around 2221 ± 14 Ma, obtained by zircon U-Pb analysis (LA-ICP-MS), which differ from the age of crystallization at 1783 ± 17 Ma. In addition, the low εNd(T) values, between -6.78 and -4.89, obtained for the set of samples, confirms the contamination of basaltic magma from the Arraias Formation with rocks from the continental crust.

Keywords: Paleoproterozoic, basaltic rocks, intracontinental rift, Brasilia Belt

1. Introduction

In central Brazil, the Cavalcante-Natividade crustal block represents the sialic basement of late Paleoproterozoic to Neoproterozoic supracrustal sequences in the northeastern part of the Brasília Belt (Cordeiro and Oliveira, 2017; Cuadros et al., 2017a, 2017b; Fuck et al., 2014; Pimentel, 2016). In this region, the development of the Araí intra-continental rift during the Paleoproterozoic produced voluminous bimodal (basalt-rhyolite) volcanic rock deposits that occur associated anorogenic granites of Goiás Province (Tanizaki et al., 2015; Alvarenga et al., 2007; Pimentel and Botelho, 2001). The expressive volcano-plutonic magmatism generated during the early stages of development of the Araí intra-continental rift is synchronous to Columbia fragmentation (Pirajno and Santosh, 2015; Rogers and Santosh, 2009, 2011; Xia and Li, 2019), and may indicate the formation of a Large Igneous Province (LIP) in response to the action of mantellic plume in the regions.

The basaltic rocks from the Araí Group occupy extensive areas in the portion of the Brasília Belt. These rocks occur discontinuously and interbedded with acidic volcanic rocks (effusive and pyroclastic) and metasedimentary rocks in the Arraias Formation (Tanizaki et al., 2015; Alvarenga et al., 2007). However, the origin of the basaltic magmas that were responsible for producing these rocks is not known.

Basalts are formed by the crystallization of mafic magmas generated in the asthenosphere and/or subcontinental lithospheric mantle (SCLM), and their chemistry varies depending on the source reservoir and the melting conditions (Farmer, 2013; Pearce, 2008; Wang et al., 2016; Wood, 1980; Xia and Li, 2019). The chemical composition of basalts provides indirect information on the chemical and physical evolution of the subcontinental mantle. Therefore, basalts can be used to investigate the tectonic setting in which they formed, because specific tectonic settings yield distinctive geochemical characteristics (Bell et al., 2013, 2005; Fan et al., 2013; He and Santosh, 2014; Jia et al., 2017; Wang et al., 2016, 2011; Xia and Li, 2019; Xia et al., 2013).

Basaltic magmas from the modern intra-continental rifts are usually produced due to a local uplift of the asthenospheric mantle, in response to a lithospheric extension and to the action of mantle plumes located at the base of the lithosphere (Allen and Allen, 2005; Bailey, 2004; Bosworth et al., 2005; Buck, 2017; Buck et al., 1999; Caricchi and Blundy, 2015; Corti, 2009; Farmer, 2013; Kieffer et al., 2004; Niu and O'Hara, 2003; Pirajno and

Santosh, 2015; Ruppel, 1995; Sun and McDonough, 1989; Xu et al., 2017). Intra-plate continental basalt magmas often have OIB-like trace element signatures, but display relatively depleted Sr-Nd isotopic compositions (Li et al., 2016). Also, continental basalts may exhibit enrichment of fluid-mobile elements and depletion in the high-field-strength elements, similar to basalts produced in subduction environments (Arc-like intra-continental basalts; Wang et al., 2016).

In this paper we report new whole-rock geochemical, zircon U–Pb geochronological and Sr-Nd isotopic data of representative Palaeoproterozoic basaltic rocks from the Araí Group in order to determine the crystallization age of these rocks, understand their petrogenesis and possible magma sources.

2. Regional Geology

The Tocantins Province (Almeida et al., 1981) is a Neoproterozoic orogen located in the central region of Brazil whose tectonic structure results from the convergences and collisions between paleocontinental blocks of the São Francisco-Congo Craton (east), Amazonian Craton (west) and Paranapanema (south) during the Brasiliano/Pan-African Orogeny (Brito Neves et al., 2014; Pimentel, 2016). Araguaia and Paraguai belts located on the eastern and southeastern borders of the Amazonian Craton, respectively, and the Brasília Belt, located westwards of the São Francisco Craton (Almeida et al., 1981; Brito Neves, 2011; Brito Neves et al., 2014; Fuck et al., 2014; Pimentel, 2016; Valeriano et al., 2004).

The Brasília Belt is an elongated orogen (Fig. 1), with north-south direction, extending for more than 1,000 km in the central-northern portion of Brazil (Dardenne, 2000; Fuck et al., 2014; Pimentel, 2016). The belt can be tectonically divided into Internal and External zones, Goiás Massif and Goiás Magmatic Arc (Cuadros et al., 2017a; Fuck et al., 2014; Pimentel, 2016). In its northern portion, within the External Zone, important records of the Paleo-Mesoproterozoic extensional dynamics crop out: sedimentary and volcanic rocks of the Araí Group, which cover an approximate area of 10,000 km^2 in the northeast of Goiás and southeast of Tocantins (Alvarenga et al. 2007; Dardenne, 2000; Martins-Ferreira et al., 2018; Pimentel, 2016; Tanizaki et al., 2015).

The Araí Group is subdivided, from the base to the top, into the Água Morna, Arraias, Caldas and Traíras formations (Alvarenga et al., 2007; Tanizaki et al., 2015). Rocks of this

group overlain paragnaisses, quartzites, conglomerates and graphitic schists of the Ticunzal Formation, that show ages between 2.20 and 2.46 Ga (Cuadros et al., 2017b), and peraluminous granites from the Aurumina suite, that shows ages between 2.12 and 2.17 Ga (Alvarenga et al., 2007; Cuadros et al., 2017b; Tanizaki et al., 2015). The Arraias Formation is characterized by the presence of large volcanic deposits interbedded with the thick layers of metasedimentary rocks of fluvial and eolian origin (Alvarenga et al., 2007; Tanizaki et al., 2015) and are in tectonic contact with the anorogenic granites of the tin-bearing Pedra Branca Suite (Alvarenga et al., 2007; Pimentel and Botelho, 2001). These volcanic deposits contain effusive and pyroclastic rocks of bimodal composition (basalt-rhyolite) which are believed to be extruded in an intracontinental rift setting (Alvarenga et al., 2007; Pimentel and Botelho, 2001; Martins et al., 2018; Tanizaki et al., 2015).

3. Material and Methods

3.1. Petrography and Mineral Chemistry

Petrographic studies in thin and polished sections were performed at the Microscopy Laboratory of the University of Brasília. Mineral chemical analyses on plagioclase and pyroxene crystals were obtained in polished sections of representative basalt samples using a JEOL® JXA-8230 Electron Probe Microanalyzer (EPMA) at the Microprobe Laboratory of the University of Brasília. The wavelength-dispersive system (WDS) was configured to operate at an accelerating voltage of 15 kV, a beam current of 10 nA and counting time of 10 seconds. The standards used for calibration were the natural and synthetic minerals: microcline (Si, Al and K), andradite (Fe and Ca), albite (Na), forsterite$_{(Mg)}$, topaz (F), vanadinite (Cl and V), pyrophanite (Ti and Mn), barite (Ba), synthetic Cr_2O_3 (Cr) and NiO (Ni).

3.2. Geochemistry

Litogeochemical analyses of major and trace elements (including the rare earth elements) were performed at the Australian Laboratory Services (ALS®), using ICP-OES to obtain major and minor elements and ICP-MS for traces and rare earth elements. To obtain the concentrations of major and minor elements at the ALS, 0.100 g of pulverized sample was used, which was added to lithium metaborate/lithium tetraborate and then melted at 1000°C. The melt generated was cooled and dissolved in 100 ml 4% nitric acid/2%

hydrochloric acid. This solution was then analyzed by ICP-OES and results were corrected to remove spectral interferences. In order to determine the loss on ignition (LOI), 1.0 g of sample was weight, heated at 1000°C for one hour, cooled and then weight again. LOI is calculated from the difference in weight. For trace elements determination, including rare earth elements, 0.100 g of sample was added to lithium metaborate/lithium tetraborate, and then melted at 1025°C. This melt was cooled and dissolved in an acidic mixture containing nitric, hydrochloric and hydrofluoric acids, and then analyzed in ICP-MS.

3.3. U-Pb Geochronology

Extraction of zircon concentrates from rock samples of more than 50 kg was performed by crushing, milling and magnetic separating grains at the Geochronology Laboratory of the University of Brasilia. Zircon grains were then handpicked using a binocular microscope and mounted on epoxy resin. Mounts were then cleaned with dilute (ca.2%) HNO_3, mounted in an especially adapted laser cell and loaded into a New Wave UP213 Nd:YAG laser (= 213 nm), linked to a Thermo Finnigan Neptune Multi-collector ICPMS at the e Laboratory of Geochronology of University of Brasilia. A mixture of He and Ar composed the carrier gas running through the ICP. The laser beam was set to 30 μm with ~80% energy and 10 Hz frequency. Cathodoluminescence (CL) images were used to investigate the internal structure of the zircon crystals prior to each analysis. Data reduction was performed following Bühn et al. (2009). A standard sample bracketing technique was applied, comprising a cycle of analyzing a blank, a GJ-1 reference zircon (Jackson et al. 2004) and four samples. Often, between the analyzed samples, an internal standard consisting of the 91500 reference zircon (Wiedenbeck et al. 1995). Data reduction was performed by the Microsoft Excel add-in Chronus (Oliveira 2015), where raw data were corrected offline for background signals, common Pb, elemental fractionation and instrumental drift. The corrected data were plotted in the Wetherill concordia plot (Wetherill,1956) using ISOPLOT (Ludwig 2012). ^{238}U, ^{232}Th, ^{206}Pb and ^{208}Pb were measured in Faraday cups whereas ^{204}Pb, ^{207}Pb and ^{202}Hg were collected in ion counters. Errors are expressed at 1σ level.

3.4. Sr-Nd Isotopes

Sm-Nd analyses were performed at the Geochronology Laboratory (IG-UnB) applying the methods described by Gioia and Pimentel (2000) and using a Thermal Ionization Mass Spectrometer (TIMS) equipment. Whole-rock powders (ca. 50 mg) were mixed with a ^{149}Sm-^{150}Nd spike solution and dissolved in Savillex capsules. Sm and Nd extraction of whole-rock samples followed conventional cation exchange techniques, using Teflon columns containing LN-Spec resin ([di-(2-ethylhexyl)]) phosphoric acid (HDEHP) supported on PTFE powder. Sm and Nd samples were loaded on re-evaporation filaments of double filament assemblies and the isotopic measurements were carried out on a multi-collector Finnigan TRITON® mass spectrometer in static mode. Uncertainties for Sm/Nd and $^{143}Nd/^{144}Nd$ ratios are better than ± 0,2% (2σ) and ± 0.003% (2σ), respectively, based on repeated analyses of international rock standards BHVO-2 and BCR-1. $^{143}Nd/^{144}Nd$ ratios were normalized to $^{146}Nd/^{144}Nd$ of 0.7219 and the decay constant (λ) used was 6.54×10^{-12}.

The Sr-isotope ratio analyses were performed at the Geochronology Laboratory of the University of Brasília. Sr was separated using conventional ion-exchange technique. The Sr-isotope ratios were measured using a multi-collector thermal ionization Finnigan TRITON® mass spectrometer. The 1σ uncertainty on the measured $^{87}Sr/^{86}Sr$ ratios was better than 0.2% and the value obtained for the NBS-987 standard was 0.71026±0.00002.

4. Results

4.1. Local Geology

The studied area is located near the cities of Teresina de Goiás and Nova Roma in the northeast of the State of Goiás. Basaltic rocks from the Araí Group, in this region, are irregularly distributed in the basal part of the Arraias Formation (Fig. 2). Basaltic rocks occur in subvertical layers and are up to 20 m-thick. Basalts also crop out as *in situ* blocks (Fig. 3A) or rolled in river beds and small drainages. They are interbedded with effusive and pyroclastic volcanic rocks of acidic compositions (rhyolites and/or rhyodacites) and with quartzite/meta-sandstones of the same formation. Their contacts with metasedimentary

and acidic volcanic rocks are usually along faults and shear zones. The basalts usually exhibit lava flows features and present textural gradation, marked by microphaneritic texture at the base and amygdaloidal structure at the top of the layers (Figs. 3B-F). Amygdales observed in these rocks have sizes varying from 0.5 cm to 3 cm, with oval shapes and filled by quartz (Fig. 3D). In other regions, however, the presence of columnar joints and coarser textures may indicate that some of these basaltic rocks may also have crystallized in subvolcanic conditions (Fig. 3F). Near the shear zones, these rocks are folded and fractured and exhibit well developed foliation, indicating they were submitted to deformation in the greenschist facies after their formation (Figs. 3B-C).

4.2. Petrography and Mineral Chemistry

Basaltic rocks from the Arraias Formation are fine- to coarse-grained, usually massive, and vary in color from dark gray to greenish gray. When altered, they become yellowish to grayish-brown. Basalts have aphanitic and amygdaloidal structure, but can also exhibit porphyritic texture, with varying amounts of phenocrysts of plagioclase and pyroxene, in a fine groundmass, sometimes foliated, and composed of feldspars, chlorite, actnolite, hornblende, epidote, quartz, opaque minerals and carbonate (Fig. 4A). In general, the mineralogy of basalts from the Arraias Formation consists of pyroxene (5-20%), plagioclase (10-40%), hornblende (5%), tremolite-actinolite (5-20%) and secondary minerals, such as quartz, chlorite, carbonate and opaque minerals, which can occur filling amygdales, that sometimes, have elongated shapes (Fig. 4B).

Pyroxene crystals are anhedral to subeuhedral and occur as phenocrysts and/or xenocrysts immersed in a recrystallized groundmass, and as micro-phenocrysts (0.05mm - 3.5 mm) disseminated in the groundmass. In some samples pyroxene and plagioclase are in equilibrium and contacts are sharp, but in others, pyroxene phenocrysts and/or xenocrysts in contact with plagioclase exhibit corrosive embayment at the borders, or present a spongy aspect (Fig. 4C). Sub-ophitic texture is a common feature of these basalts, evidenced by partial inclusion of euhedral plagioclase on the edges of the pyroxene crystals (Fig. 4D). Some crystals show a high degree of alteration, observed in partial transformation to fibrous crystals of tremolite-actnolite. Results of mineral analyses performed in pyroxene using an electron microprobe are shown in Table 1 and Figure 5. According to the classification of the pyroxenes (Morimoto, 1988), all analyzed crystals belong to the Ca-

Mg-Fe pyroxene group (QUAD, no show) and are classified as augite (Fig. 5), when plotted in the Fs-Wo-En diagram (Morimoto, 1988).

Feldspar also occurs as phenocrysts and micro-phenocrysts within the groundmass, exhibiting subhedral to euhedral crystals, that range in size from 0.2 mm to 3 mm. They are twinned according to albite law and some crystals are partially saussuritized. Feldspar chemical composition obtained in electron microprobe are shown in Table 2. According to the results and regarding Ab-Or-An diagram (Deer et al., 1966) all analyzed crystals present sodic compositions and are classified as albite ($An_{0.8-4.2}$) (Fig. 6). These low levels of anorthite may reflect the rebalance during greenschist facies metamorphism.

Quartz occurs as 0.5 mm to 0.8 mm anhedral crystals disseminated in the groundmass and is also observed filling amygdales (Fig.4B). Hornblende and tremolite-actinolite are possibly transformations from augite and form subeuhedral to anhedral crystals, which size varies between 0.5 mm and 2.5 mm. Subeuhedral epidote and euhedral opaque minerals are 0.1 to 0.4 mm. These minerals, products of secondary reactions, make up a mineral paragenesis indicative of greenschist facies metamorphism.

4.3. Whole-rock Geochemistry

Concentration of major, minor and trace elements of basaltic rocks from the Arraias Formation are shown in Table 3. Major element contents are SiO_2 = 48.20-54.80 wt.%, TiO_2 = 0.88-1.85 wt.%, Al_2O_3 = 13.90-16.35 wt.%, $Fe_2O_{3(T)}$ = 9.11-11.57 wt.%, MgO = 5.26-7.22 wt.%, CaO = 7.58-9.98 wt.%, Na_2O = 1.58-3.37 wt.%, K_2O = 0.34-2.25 wt.% and P_2O_5 = 0.23-0.59 wt.%. Magnesium numbers (Mg#) are between 51.97-63.40 and loss on ignition (LOI) vary between 2.20 and 3.28 wt.%. Other important elements for tectonic classification are Ni (46-140 ppm), Cr (40-250 ppm), V (167-258 ppm), Ba (123-745 ppm), Sr (198-337 ppm), Th (2-4ppm), Nb (5-13 ppm), Ta (0.4-0.7 ppm), La (18-31ppm), Gd (3-6 ppm), Sm (3-6 ppm) Zr (103-168 ppm), Hf (3-4 ppm), Y (16-31 ppm), and Yb (1.5-2.6 ppm).

In R1-R2 (De la Roche et al., 1980) and Nb/Y versus Zr/Ti (Winchester and Floyd, 1977; modified by Pearce, 1996) classification diagrams, basalts from the Arraias Formation occupy the field of silica-oversaturated and are classified as andesite-basalt and tholeiite (Fig. 7), and basalt and basaltic andesite (Fig. 8), respectively. Variation on the content of MgO, $Fe_2O_{3T,}$ TiO_2, $SiO_{2,}$ Ni, Cr and Mg# (Tab. 3) as well as Fenner diagrams

(Fig. 9) suggest that studied basaltic rocks may have been formed by fractional crystallization processes (Fan et al., 2013, Wilson, 1995). In these diagrams, have MgO on x-axis, despite slight scatter, it is possible to observe positive correlations for CaO, Al_2O_3 and K_2O, with significant R^2 values (Fig. 9). On the other hand, SiO_2 (R^2= 0.43), TiO_2 (R^2= 0.57), $Fe_2O_{3(T)}$ (R^2= 0.73) and P_2O_5 (R^2= 0.53) correlate negatively with MgO. Negative correlations with MgO are also observed for La (R^2 =0.43), Sm (R^2 = 0.41), Y (R^2 = 0.53), Nb (R^2 = 0.24) and Zr (R^2 = 0.59). Sr data are strongly scattered in the Fenner diagram (R^2 = 0.08).

When normalized for the Nakamura chondrite (1974) basalts show fractionation of light rare earth elements (LREEs) relative to heavy rare earth elements (HREEs), marked by moderate $La/Yb_{(N)}$ (6.68 to 10.38), $La/Sm_{(CN)}$ (2.82-3.37) and $Dy/Yb_{(CN)}$ (1.04-1.59) ratios (Tab. 3). In addition, Eu negative anomalies (Eu/Eu* = 0.78-1.0) are indicative plagioclase fractionation (Rollinson, 1993).

Normalization for the Primitive Mantle (Sun and McDonough, 1989) shows that these basalts present positive Ba (Ba/Ba*= 1.11-1.84), U (U/U* = 1.27-1.59), K (K/K* = 1.0-2.97) and Hf (Hf/Hf* = 1.05-1.20) anomalies, and negative Nb (Nb/Nb* = 0.23-0.43), Ta (Ta/Ta* = 0.28-0.62), Th(Th /Th* = 0.49-0.88), Ti (Ti/Ti* = 0.60-0.80), Sr (Sr/Sr* = 0.42-0.92) and Zr (Zr/Zr* = 0.84-0.97) anomalies. P anomalies vary from slightly negative values to positive values (P/P *=0.78-1.40) (Fig.11). The enrichment in lithophile elements is similar to what is observed in OIB type basalts contaminated by continental crust (Rudnick and Gao, 2013) and in volcanic arc basalts (Jia et al., 2017, Kieffer et al., 2004, Sun and McDonough, 1989, Xia et al., 2013).

4.4. U-Pb zircon Geochronology

Twenty-two zircon crystals from basalt sample CD-05-15 (coordinates: 256412E/8470563N, 23S) were selected for the geochronological studies (U-Pb). Samples are dark gray, fine-grained and may contain amygdales and fractures filled with amorphous silica. Results are shown in Table 4 and Figure 12. Zircon crystals are colorless, prismatic, elongated or bipyramidal, range in length from 80μm to 250μm and have length-by-width ratios from 1:1 to 3:1. Cathodoluminescence images revealed a magmatic internal zonation of the grains (Figs.12A and 12F). Their high Th/U ratios (0.2 to 1.14) (Table 4), except for

spot 05 (U/Th = 0.09), are suggestive of magmatic origin (Corfu et al., 2003; Rubatto, 2002).

The analyzed grains resulted in a Discordia linea, whose ages vary from Archean to Paleoproterozoic, providing two concordant $^{206}Pb/^{238}U$ ages (Fig. 12B). The younger is interpreted as the crystallization age, around 1783 ± 17 Ma, in the Statherian (Fig. 15C). The other age suggests crustal contamination, represented by inherited Rhyacian zircon crystals of 2221 ± 14 Ma (Fig. 15D). In addition, these grains produced apparent $^{206}Pb/^{207}Pb$ ages of 3093-1660 Ma (Tab. 4) and in population density diagram can be grouped into three distinct populations (Fig. 12E). The first population is composed of Archean zircons (age 7/6 = 3093-2492 Ma, n = 3), the second is composed of zircons from Rhyacian to Orosirian (age 7/6 = 2227-1987 Ma, n = 10) and the third population comprises Statherian zircons (age 7/6 = 1813-1660 Ma, n = 9).

4.5. Sr-Nd Isotopes

Sm-Nd isotopic data of the basaltic rocks are listed in Table 5. Sm and Nd concentrations range from 3.6-6.0 ppm and 19.9-31.3 ppm, respectively (Tab. 5). These rocks show few variations in the $^{147}Sm/^{143}Nd$ ratios (0.118-0.127) and for a crystallization age of 1783 Ma (Fig. 12), exhibit low initial ratios of $(^{143}Nd/^{144}Nd)_i$ = 0.509995-0.510101 (Tab.5). All samples show negative ε_{Nd} values (1783 Ma) = -6.58 to -4.46, and model ages (T_{DM}) range from 2.50-2.72 Ga (Tab. 5). Contents of Rb and Sr vary from 20-44 ppm and 198-284 ppm, respectively (Tab. 3). Initial $^{87}Sr/^{86}Sr$ ratios ($^{87}Sr/^{86}Sr_{(1783)}$ = 0.702400-0.708293).

5. Discussion and Conclusions

Secondary growth of chlorite, tremolite-actinolite, epidote, carbonate and clay minerals, observed in petrography and values of LOI (2.20-3.28 wt.%) suggest that basaltic rocks from the Arraias Formation were submitted to different stages of post-magmatic alterations. Some elements (e.g. Na, K, Cs, Rb, Ba and Sr) may have been removed by hydrothermal fluids and, as a result, have their initial concentrations modified. Zr is considered immobile during low and medium degrees of metamorphism (Polat et al., 2002; Rollinson, 1993). Therefore, it can be used in variation diagrams to test the mobility of other elements during

these post-magmatic alterations. Zr versus major and trace elements diagrams (Fig. 13), such as SiO_2, Al_2O_3, K_2O, Na_2O and CaO, Ba, Rb and Sr, produced low values of R^2 ($\leq$ 0.3) suggesting that the concentrations of these elements were modified during the post-magmatic processes (Polat and Hofmann, 2003). On the other hand, TiO_2, MgO, Fe_2O_{3T}, P_2O_5, La, Sm, Nb and Y exhibit good correlation with Zr ($R^2 \geq 0.50$), indicating minor mobilization of these elements during such processes (Pearce, 1996; Polat and Hofmann 2003; Whinchester and Floyd, 1977).

Low contents of Ni, Cr and Mg# of these basaltic rocks indicate these rocks do not correspond to primitive magmas (Farmer, 2013; Grove, 2000; Wilson, 1989). Parental magma was subjected to crystallization processes that fractionated mafic minerals (olivine and/or pyroxene) in the magma chamber and/or during its ascent to the surface (Farmer, 2013; Wilson, 1995, 1989; Zhang et al., 2009). In addition, inclined patterns of REEs, with fractionation of LREEs relative to HREEs (Fig. 10) suggest that these basaltic rocks were produced by low melting rates of an enriched mantle (Rollinson, 1993).

Assumptions on the degree of melting and on the composition of the mantle source can be made from $La/Sm_{(CN)}$ and $Dy/Yb_{(CN)}$ ratios (Srivastava and Gautam, 2014). High $La/Sm_{(CN)}$ ratios indicate low degrees of melting, while $Dy/Yb_{(CN)}$ ratio indicates whether a source retained garnet after partial melting or not (Srivastava and Gautam, 2014). Melting a lherzolitic mantle in the spinel stability field generates a melt with $Dy/Yb_{(CN)} \sim 1.0$. However, if this same source is melted in the garnet stability field it may produce melts with $Dy/Yb_{(CN)}$ rations ranging between ~1.1 and 2.5. Basaltic rocks from the Arraias Formation have high $Dy/Yb_{(CN)}$ (1.04-1.59) and $La/Sm_{(CN)}$ (2.82-3.37) ratios. When plotted in $La/Sm_{(CN)}$ versus $Dy/Yb_{(CN)}$ diagram (Mayborn and Lesher, 2004), it is possible to observe they occupy the garnet stability field (2.5 to 2.8 GPa) (Fig. 14) (Fram and Lesher, 1993; Mayborn and Lesher, 2004; Srivastava and Gautam, 2014). In Sm/Yb versus Sm diagram (Li and Chen, 2014) samples plot close to the Garnet-Spinel-Lherzolite field, in which melt rates vary between 8-15% (Fig. 15).

Paleoproterozoic magmatism that occurred in the Araí Group is rift-related and synchronous to Columbia (supercontinent) fragmentation. This global magmatic event has commonly been accredited to a plume or superplume activity, causing the rifting of a Paleoproterozoic supercontinent (Pirajno and Santosh, 2015; Rogers and Santosh, 2009,

2011; Xia and Li, 2019). Records of the same event can be recognized in Asia, Australia, North America (Fan et al., 2013; Pirajno and Santosh, 2015; Xia et al., 2013) and in different regions of Brazil, such as São Francisco Craton (Alkmim and Martins-Neto, 2012; Alkmim et al. 1993; Brito Neves, 2011; Brito Neves et al., 1995; Chemale et al., 2012; Danderfer Filho et al., 2014; Guadagnin et al., 2015; Martins-Ferreira et al., 2018) and the Amazonian Craton (Batata et al., 2008; Brito Neves et al., 1995; Danderfer Filho et al., 2014).

Basaltic rocks from the Arraias Formation occur interbedded with acidic volcanic rocks (rhyolites) and with quartzite/meta-sandstone of eolian and fluvial origin (Fig. 2) (Alvarenga et al., 2007; Fuck et al., 2014; Tanizaki et al., 2015). Zircon U-Pb crystallization age (1783±17 Ma) of a basaltic rock dated in this paper is similar to the age of rhyolites of the same formation, and this bimodal volcanism is coeval to the anorogenic magmatism of the Pedra Branca Suite (1.77 Ga; Pimentel and Botelho, 2001). The expressive volcano-plutonic magmatism generated during the early stages of development of the Araí intracontinental rift indicates the formation of a Large Igneous Province (LIP) in response to the action of mantellic plume in the regions.

Basaltic rocks from the Arraias Formation show negative high-field-strength elements anomalies (e.g. Nb, Ta and Ti). Such characteristics indicate the involvement of the lithosphere with the magmas that produced these rocks (Fan et al., 2013; Farmer, 2013; Jalowitzki et al., 2017; Li et al., 2008; Li and Chen, 2014; Wang et al., 2011; Xia et al., 2013b; Xu et al., 2017). This is because intracontinental rift basaltic rocks are associated with the asthenospheric mantle (Farmer, 2013; Xia et al., 2013) since in modern rifts lithosphere extension processes generally occur in response to the action of mantle plumes installed in the lithosphere base (Allen and Allen, 2005; Buck, 2004, 1991; Buck et al., 1999; Lavecchia et al., 2017; Piranjo and Santosh, 2015; Ruppel, 1995). However, the occurrence of basalts with the composition of the subcontinental lithospheric mantle (SCLM), sometimes metasomatized by subduction-related fluid and/or melts (Xu et al., 2017), suggests that these rocks may be subjected to different degrees of contamination during the extent of the lithosphere, especially with crustal rocks (Dusel-Bacon et al., 2004; Farmer, 2013; Pirajno and Santosh, 2014; Wilson, 1989; Xia et al., 2013; Xia and Li, 2018; Xu et al., 2017).

Nd versus crystallization age diagram shows that these rocks evolved with participation of sialic crust represented here by paleoproterozoic granites of the Aurumina Suite (Cuadros et al., 2017a) (Fig. 16). Nb/La ratios can be used as an index of crustal contamination (Kieffer et al., 2004). Uncontaminated rocks have Nb/La> 1 ratios such as those of OIB type basalts (Nb/La = ~1.3) (Sun and McDonough, 1989), while contaminated rocks exhibit Nb/La < 1 (Kieffer et al., 2004). Basaltic rocks from the Arraias Formation present low Nb/La (0.25-0.46) ratios (Tab. 3), close to continental crust ratios (Nb/La = ~0.40) (Rudnick and Gao, 2013).

In the Hf-Th-Ta diagram of Wood (1980) (Fig. 17) the basaltic rocks plot close to the continental crust average showing the importance of crustal contamination in these rocks (Pearce, 1996). Such contamination may have been responsible for enrichment in fluid-mobile elements (Wang et al., 2016) and led these rocks to occupy the continental arc basalt field similar to the rocks that evolved in the subduction setting (Dusel-Bacon et al., 2004, Pearce, 1996, Wang et al., 2016, Xia et al., 2013). In Zr versus Zr/Y (Pearce and Nory, 1979) and Ta/Hf versus Th/Hf (Wang et al., 2011) diagrams these rocks exhibit affinities with within-plate basalts (Fig. 18), and continental extensional zone/initial rift basalts (Fig. 19). The plotting of these rocks in the diagram $^{87}Sr/^{86}Sr_{(1783\ Ma)}$ versus $\varepsilon_{Nd\ (1783\ Ma)}$ (Fig. 20) close to the low Nb plume–related paleoprotezoic basalts (LN) from Xionger Group in North China Craton (Xia et al., 2013) suggests the involvement of the lithosphere in the origin of the basaltic rocks from the Arraias Formation during of the development of the Araí intracontinental rift in the Paleoproterozoic (Fan et al., 2013; Farmer, 2013; Xia et al., 2013; Xu et al., 2017).

Acknowledgements

The authors are thankful to the Institute of Geosciences and the Graduate Program in Geology of the Universidade de Brasília (IGD-UnB) for the infrastructure made available. This research had financial support from the Brazilian Conselho Nacional de Desenvolvimento Científico e Tecnológico (CNPq-Project n°443603/2014-6). Also, the authors acknowledge the reviewers for their comments which were very helpful for improving the final version of this paper.

REFERENCES

Alkmim, F.F., Martins-Neto, M.A., 2012. Proterozoic first-order sedimentary sequences of the São Francisco craton, eastern Brazil. Marine and Petroleum Geology 33, 127–139. https://doi.org/10.1016/j.marpetgeo.2011.08.011

Alkmim, F.F., Brito Neves, B.B., Alves, J.A.C., 1993. Arcabouço tectônico do Cráton do São Francisco - uma revisão. In: Dominguez, J.M.L., Misi, A. (Eds.), O Cráton do São Francisco. Sociedade Brasileira de Geologia, Salvador, 45–62

Allen, P.A., Allen J.R., 2005. Basins analysis: principles and applications. Oxford, Blackwell Scientific Publications Ltda, 560 p

Almeida, F.F.M., Hasui, Y., Brito Neves, B.B., Fuck, R.A., 1981. Brazilian structuralprovinces: an introduction. Earth-Science Reviews 17 (1), 1–29

Alvarenga, C.J.S., Botelho N.F., Dardenne M.A., Lima O.N.B., Machado M.A., 2007. Programa Levantamentos Geológicos Básicos do Brasil; Mapa Geológico da Folha Cavalcante (SD.23-V-C-V), escala: 1.100.000. Nota Explicativa Integrada com das folhas Monte Alegre de Goiás (SD.23-V-C-III), Cavalcante (SD.23-V-C-V) e Nova Roma (SD.23-V-C-VI). Goiás, UNB/CPRM, 67p

Bailey, R.A., 2004. Eruptive history and chemical evolution of the precaldera and postcaldera basalt-dacite sequences, Long Valley, California: implications for magma sources, current magmatic unrest, and future volcanism. US Geol. Surv. Prof. Pap. 1692, 76 pp.

Batata, M.E.F., Leite, J.A.D., Sousa, M.Z.A. de., 2008. Petrografia e geoquímica das rochas vulcânicas do Grupo Roosevelt, província ígnea Teles Pires, SW do Cráton Amazônico. Rev. Bras. Geociências 38, 36–53. https://doi.org/10.25249/0375-7536.20083813653

Bell, K., Lavecchia, G., Rosatelli, G., 2013. Cenozoic Italian magmatism - Isotope constraints for possible plume-related activity. J. South Am. Earth Sci. 41, 22–40. https://doi.org/10.1016/j.jsames.2012.10.005

Bell, K., Lavecchia, G., Stoppa, F., 2005. Reasoning and beliefs about Italian geodynamics. Boll. della Soc. Geol. Ital. Suppl. 5, 119–127.

Bosworth, W., Huchon, P., McClay, K., 2005. The Red Sea and Gulf of Aden Basins. J. African Earth Sci. 43, 334–378. https://doi.org/10.1016/j.jafrearsci.2005.07.020

Brito Neves, B.B., Fuck, R.A., Pimentel, M.M., 2014. The Brasiliano collage in South America: a review. Brazilian J. Geol. 44, 493–518.https://doi.org/10.5327/Z2317-4889201400030010

Brito Neves, B.B., 2011. The Paleproterozoic in the South American Continent: diversity in the geological time. Journal of South American Earth Sciences 32, 1–20. https://doi.org/10.1016/j.jsames.2011.02.004

Brito Neves, B.B., Sá, J.M., Nilson, A.A., Botelho, N.F., 1995. A Tafrogênese Estateriana nos Blocos Paleoproterozóicos da América do Sul e Processos Subsequentes. Rev. Geonomos. https://doi.org/10.18285/geonomos.v3i2.205

Buck, W.R., 2017. The role of magmatic loads and rift jumps in generating seaward dipping reflectors on volcanic rifted margins. Earth Planet. Sci. Lett. 466, 62–69. https://doi.org/10.1016/j.epsl.2017.02.041

Buck, W.R., Lavier, L., Poliakov, A.N.B., 1999. How to make a rift wide. Philos. Trans. 357, 671–

693. https://doi.org/10.1098/rsta.1999.0348

Bühn, B., Pimentel, M.M., Matteini, M., Dantas, E.L., 2009. High spatial resolution analysis of Pb and U isotopes for geochronology by laser ablation multi-collector inductively coupled plasma mass spectrometry (LA-MC-ICP-MS). An. Acad. Bras. Cienc. 81, 99–114

Caricchi, L., Blundy, J., 2015. The temporal evolution of chemical and physical properties of magmatic systems. Geol. Soc. London, Spec. Publ. 422, 1–15. https://doi.org/10.1144/SP422.11

Chemale, F., Dussin, I.A., Alkmim, F.F., Martins, M.S., Queiroga, G., Armstrong, R., Santos, M.N., 2012. Unravelling a Proterozoic basin history through detrital zircon geochronology: The case of the Espinhaço Supergroup, Minas Gerais, Brazil. Gondwana Res. 22, 200–206. https://doi.org/10.1016/j.gr.2011.08.016

Cordeiro, P.F. de O., Oliveira, C.G. de, 2017. The Goiás Massif: Implications for a pre-Columbia 2.2–2.0 Ga continent-wide amalgamation cycle in central Brazil. Precambrian Res. 298, 403–420. https://doi.org/10.1016/j.precamres.2017.06.021

Corfu, F., Hanchar, J.M., Hoskin, P.W.O., Kinny, P., 2003. Atlas of Zircon Textures. Reviews in Mineralogy and Geochemistry. 53 (1), 469–500. doi: https://doi.org/10.2113/0530469

Corti, G., 2009. Continental rift evolution: From rift initiation to incipient break-up in the Main Ethiopian Rift, East Africa. Earth-Science Rev. 96, 1–53. https://doi.org/10.1016/j.earscirev.2009.06.005

Cuadros, F.A., Botelho, N.F., Fuck, R.A., Dantas, E.L., 2017a. The peraluminous Aurumina Granite Suite in central Brazil: An example of mantle-continental crust interaction in a Paleoproterozoic cordilleran hinterland setting? Precambrian Res. 299, 75–100. https://doi.org/10.1016/j.precamres.2017.07.029

Cuadros, F.A., Botelho, N.F., Fuck, R.A., Dantas, E.L., 2017b. The Ticunzal Formation in central Brazil: Record of Rhyacian sedimentation and metamorphism in the western border of the São Francisco Craton. J. South Am. Earth Sci. 79, 307–325. https://doi.org/10.1016/j.jsames.2017.08.014

Danderfer Filho, A., Lana, C.C., Nalini Júnior, H.A., Costa, A.F.O., 2015. Constraints on the Statherian evolution of the intraplate rifting in a Paleo-Mesoproterozoic paleocontinent: New stratigraphic and geochronology record from the eastern São Francisco craton. Gondwana Res. 28, 668–688. https://doi.org/10.1016/j.gr.2014.06.012

Dardenne, M.A., 2000. The Brasília Fold Belt. In: Cordani U.G., Milani E, J., Thomaz Filho A., Campos D.A. (eds.), Tectonic Evolution of South América. 31st International Geological Congress. Rio de Janeiro, 231-263

Deer, R.A., Howie ,W.A., Zussman, J., 1966. Introduction to The Rock-Forming Minerals Longmans, London. 528 p

De la Roche, H., Leterrier, J., Grandclaude, P., Marchal, M., 1980. A classification of volcanic and plutonic rocks using R1R2-diagram and major-element analyses - Its relationships with current nomenclature. Chem. Geol. 29, 183–210. https://doi.org/10.1016/0009-2541(80)90020-0

Dusel-Bacon, C., Wooden, J.L., Hopkins, M.J., 2004. U-Pb zircon and geochemical evidence for bimodal mid-Paleozoic magmatism and syngenetic base-metal mineralization in the Yukon-Tanana terrane, Alaska. Bull. Geol. Soc. Am. 116, 989–1015.

https://doi.org/10.1130/B25342.1

Fan, H., Zhu, W., Li, Z., Zhong, H., Bai, Z., He, D., 2013. Lithos Ca . 1 . 5 Ga ma fi c magmatism in South China during the break-up of the supercontinent Nuna / Columbia : The Zhuqing Fe – Ti – V oxide ore-bearing ma fi c intrusions in western Yangtze Block. LITHOS 168–169, 85–98. https://doi.org/10.1016/j.lithos.2013.02.004

Farmer, G.L., 2013. Continental Basaltic Rocks, 2nd ed, Treatise on Geochemistry, 75–110 Second Edition. Elsevier Ltd. https://doi.org/10.1016/B978-0-08-095975-7.00303-X

Fram, M.S., Lesher, C.E., 1993. Geochemical constraints on mantle melting during creation of / the North Atlantic basin. Nature. 363, 712-715. DOI 10.1038363712a0

Fuck, R.A., Dantas, E.L., Pimentel, M.M., Botelho, N.F., Armstrong, R., Laux, J.H., Junges, S.L., Soares, J.E., Praxedes, I.F., 2014. Paleoproterozoic crust-formation and reworking events in the Tocantins Province, central Brazil: A contribution for Atlantica supercontinent reconstruction. Precambrian Res. 244, 53–74. https://doi.org/10.1016/j.precamres.2013.12.003

Gioia, S.M.C.L., Pimentel, M.M., 2000. The Sm-Nd isotopic method in the Geochronology Laboratory of the University of Brasilia. An. Acad. Bras. Cienc. 72, 218–245

Grove, T.L., 2000. Origin of magmas. In: Sigurdsson H (ed.) Encyclopedia of Volcanoes, San Diego, CA: Academic Press,133–147

Guadagnin, F., Chemale, F., Magalhães, A.J.C., Santana, A., Dussin, I., Takehara, L., 2015. Age constraints on crystal-tuff from the Espinhaço Supergroup - Insight into the Paleoproterozoic to Mesoproterozoic intracratonic basin cycles of the Congo-São Francisco Craton. Gondwana Res. 27, 363–376. https://doi.org/10.1016/j.gr.2013.10.009

He, X.F., Santosh, M., 2014. Crustal recycling through intraplate magmatism: Evidence from the Trans-North China Orogen. J. Asian Earth Sci. 95, 147–163. https://doi.org/10.1016/j.jseaes.2014.02.011

Irvine, T.N., Baragar, W.R.A., 1971. A Guide to the Chemical Classification of the Common Volcanic Rocks. Canadian Journal of Earth Science, 8, 523-548.

Jackson, S.E., Pearson, N.J., Griffin, W.L., Belousova, E.A., 2004. The application of laser ablation-inductively coupled plasma-mass spectrometry to in situ U-Pb zircon geochronology. Chem. Geol. 211, 47–69. https://doi.org/10.1016/j.chemgeo.2004.06.017

Jia, X., Wang, X., Yang, W., 2017. Petrogenesis and geodynamic implications of the early Paleozoic potassic and ultrapotassic rocks in the South China Block. J. Asian Earth Sci. 135, 80–94. https://doi.org/10.1016/j.jseaes.2016.12.013

Kieffer, B., Arndt, N., Bastien, F., Bosch, D., Pecher, A., Yirgu, G., Ayalew, D., Weis, D., Jerram, D.A., Keller, F., Meugniot, C., 2004. Flood and Shield Basalts from Ethiopia : Magmas from the African Superswell 45, 793–834. https://doi.org/10.1093/petrology/egg112

Li, Y.Q., Ma, C.Q., Robinson, P.T., 2016. Petrology and geochemistry of Cenozoic intra-plate basalts in east-central China: Constraints on recycling of an oceanic slab in the source region. Lithos 262, 27–43. https://doi.org/10.1016/j.lithos.2016.06.012

Ludwig, K.R. 2012. Isoplot. A Geochronological Toolkit for Microsoft Excel. Ver. 3.75. Berkeley Geochronology Center.

Martins-Ferreira, M.A.C., Chemale, F., Dias, A.N.C., Campos, J.E.G., 2018. Proterozoic

intracontinental basin succession in the western margin of the São Francisco Craton: Constraints from detrital zircon geochronology. J. South Am. Earth Sci. 81, 165–176. https://doi.org/10.1016/j.jsames.2017.11.018

Mayborn, K.R., Lesher, C.E., 2004. Paleoproterozoic mafic dyke swarms of northeast Laurentia: products of plumes orambientmantle? Earth and Planetary Science Letters. 225, 305–317

Morimoto, N. (1988) Nomenclature of Pyroxenes. Mineralogy and Petrology, 39, 55-76. http://dx.doi.org/10.1007/BF01226262

Nakamura, N., 1974. Determination of REE, Ba, Fe, Mg, Na and K in Carbonaceous and Ordinary Chondrites. Geochimica et Cosmochimica Acta, 38, 757-775. http://dx.doi.org/10.1016/0016-7037 (74)90149-5

Niu, Y., O'Hara, M.J., 2003. Origin of ocean island basalts: A new perspective from petrology, geochemistry, and mineral physics considerations. J. Geophys. Res. Solid Earth 108. https://doi.org/10.1029/2002JB002048

Oliveira, F.V., 2015. Chronus: um novo suplemento para a redução de dados U-Pb obtidos por LA-MC-ICPMS. Unpublished M.Sc thesis, Universidade de Brasília, Brasília, Distrito Federal, Brazil

Pearce, J.A., 2008. Geochemical fingerprinting of oceanic basalts with applications to ophiolite classification and the search for Archean oceanic crust. Lithos 100, 14–48. https://doi.org/10.1016/j.lithos.2007.06.016

Pearce, J.A., 1996. A User's Guide to Basalt Discrimination Diagrams. In: Wyman, D.A., Ed., Trace Element Geochemistry of Volcanic Rocks: Applications for Massive Sulphide Exploration, Geological Association of Canada, Short Course Notes, Vol. 12, 79-113

Pearce, J.A., Norry, M.J., 1979. Petrogenetic Implications of Ti, Zr, Y, and Nb Variation in Volcanic Rocks. Contributions to Mineralogy and Petrology, 69, 33-47. http://dx.doi.org/10.1007/BF00375192

Pimentel, M.M., 2016. The tectonic evolution of the Neoproterozoic Brasília Belt, central Brazil: a geochronological and isotopic approach. Brazilian J. Geol. 46, 67–82. https://doi.org/10.1590/2317-4889201620150004

Pimentel, M.M., Jost, H., Fuck, R.A. 2004. O embasamento da Faixa Brasília e o Arco Magmático de Goiás. In: Mantesso-Neto, V., Bartorelli, A., Carneiro, C.D.R., Brito-Neves, B.B. (Eds.). Geologia do continente Sul-Americano: evolução da obra de Fernando Flávio Marques de Almeida. Ed. Beca. 355–368

Pimentel, M. M., Botelho N. F., 2001. Sr and Nd isotopic characteristics of 1,77-1,58 Ga rift related granites and volcanics of the Goiás province, Central Brazil. Anais da Academia Brasileira de Ciências, 73: 263–276

Pirajno, F., Santosh, M., 2015. Mantle plumes, supercontinents, intracontinental rifting and mineral systems. Precambrian Res. 259, 243–261. https://doi.org/10.1016/j.precamres.2014.12.016

Rollinson, H.R., 1993. Using Geochemical Data: Evaluation, Presentation, Interpretation. Longman Scientific and Technical, England, 352 p

Rubatto, D., 2002. Zircon trace element geochemistry: partitioning with garnet and the link between U–Pb ages and metamorphism. Chemical Geology. 184 (2002), 123-138

Rudnick, R.L., Gao, S., 2013. Composition of the Continental Crust, 2nd ed, Treatise on Geochemistry: Second Edition. Elsevier Ltd. https://doi.org/10.1016/B978-0-08-095975-7.00301-6

Ruppel, C., 1995. Extensional processes in continental lithosphere. J. Geophys. Res. Solid Earth 100, 24187–24215. https://doi.org/10.1029/95JB02955

Sun, S. -s., McDonough, W.F., 1989. Chemical and isotopic systematics of oceanic basalts: implications for mantle composition and processes. Geol. Soc. London, Spec. Publ. 42, 313–345. https://doi.org/10.1144/GSL.SP.1989.042.01.19

Tanizaki, M.L.N., Campos, J.E.G., Dardenne, M.A., 2015. Estratigrafia do Grupo Araí: registro de rifteamento paleoproterozoico no Brasil Central. Brazilian J. Geol. 45, 95–108. https://doi.org/10.1590/23174889201500010007

Valeriano, C.M., Dardenne, M.A., Fonseca, M.A., Simões, L.S.A., Seer, H.J., 2004.A evoluc¸ ão tectônica da Faixa Brasília. In: Mantesso Neto, V., Bartorelli, A.,Carneiro, C.D.R., Brito Neves, B.B. (Org.), Geologia do Continente Sul-Americano– Evolução da obra de Fernando Flávio Marques de Almeida. São Paulo, Beca. 575–592

Xia, L., Li, X., 2019. Basalt geochemistry as a diagnostic indicator of tectonic setting. Gondwana Res. 65, 43–67. https://doi.org/10.1016/j.gr.2018.08.006

Xia, L., Xia, Z., Xu, X., Li, X., Ma, Z., 2013b. Late Paleoproterozoic rift-related magmatic rocks in the North China Craton: Geological records of rifting in the Columbia supercontinent. Earth-Science Rev. 125, 69–86. https://doi.org/10.1016/j.earscirev.2013.06.004

Xu, Z., Zheng, Y.F., Zhao, Z.F., 2017. The origin of Cenozoic continental basalts in east-central China: Constrained by linking Pb isotopes to other geochemical variables. Lithos 268–271, 302–319. https://doi.org/10.1016/j.lithos.2016.11.006

Wang, X.C., Wilde, S.A., Xu, B., Pang, C.J., 2016. Origin of arc-like continental basalts: Implications for deep-Earth fluid cycling and tectonic discrimination. Lithos 261, 5–45. https://doi.org/10.1016/j.lithos.2015.12.014

Wang, Y., Zhao, Z., Zheng, Y., Zhang, J., 2011. Lithos Geochemical constraints on the nature of mantle source for Cenozoic continental basalts in east-central China. LITHOS 125, 940–955. https://doi.org/10.1016/j.lithos.2011.05.007

Wilson, M., 1995. Magmatic differentiation. Geol.Soc. London, Mem. 16, 205–218. https://doi.org/10.1144/GSL.MEM.1995.016.01.21

Wilson, M., 1989. Igneous petrology. A global tectonic approach, Unwin Hyman. Boston. 466 p

Winchester, J.A., Floyd, P.A., 1977. Geochemical Discrimination of Different Magma Series and Their Differentiation Product Using Immobile Elements. Chemical Geology, 20, 325-343. http://dx.doi.org/10.1016/0009-2541(77)90057-2

Wood, D.A., 1980. The application of a Th{single bond}Hf{single bond}Ta diagram to problems of tectonomagmatic classification and to establishing the nature of crustal contamination of basaltic lavas of the British Tertiary Volcanic Province. Earth Planet. Sci. Lett. 50, 11–30. https://doi.org/10.1016/0012-821X(80)90116-8

Zhang, Z., Mao, J., Saunders, A.D., Ai, Y., Li, Y., Zhao, L., 2009. Petrogenetic modeling of three mafic-ultramafic layered intrusions in the Emeishan large igneous province, SW China, based on isotopic and bulk chemical constraints. Lithos 113, 369–392.

https://doi.org/10.1016/j.lithos.2009.04.023

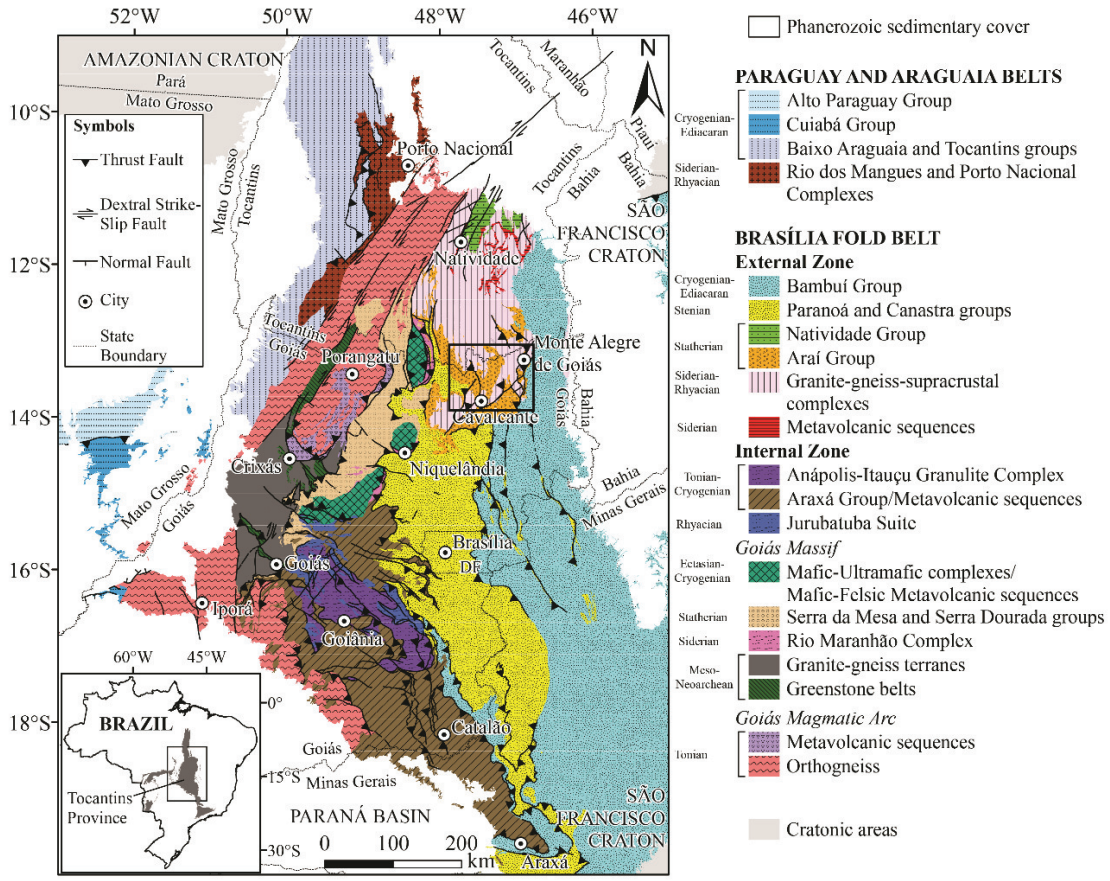

Figure 1. Geological map of the Brasilia Belt, showing the location of the study area (black rectangle), after Pimentel et al., (2004) in Cuadros et al., (2017).

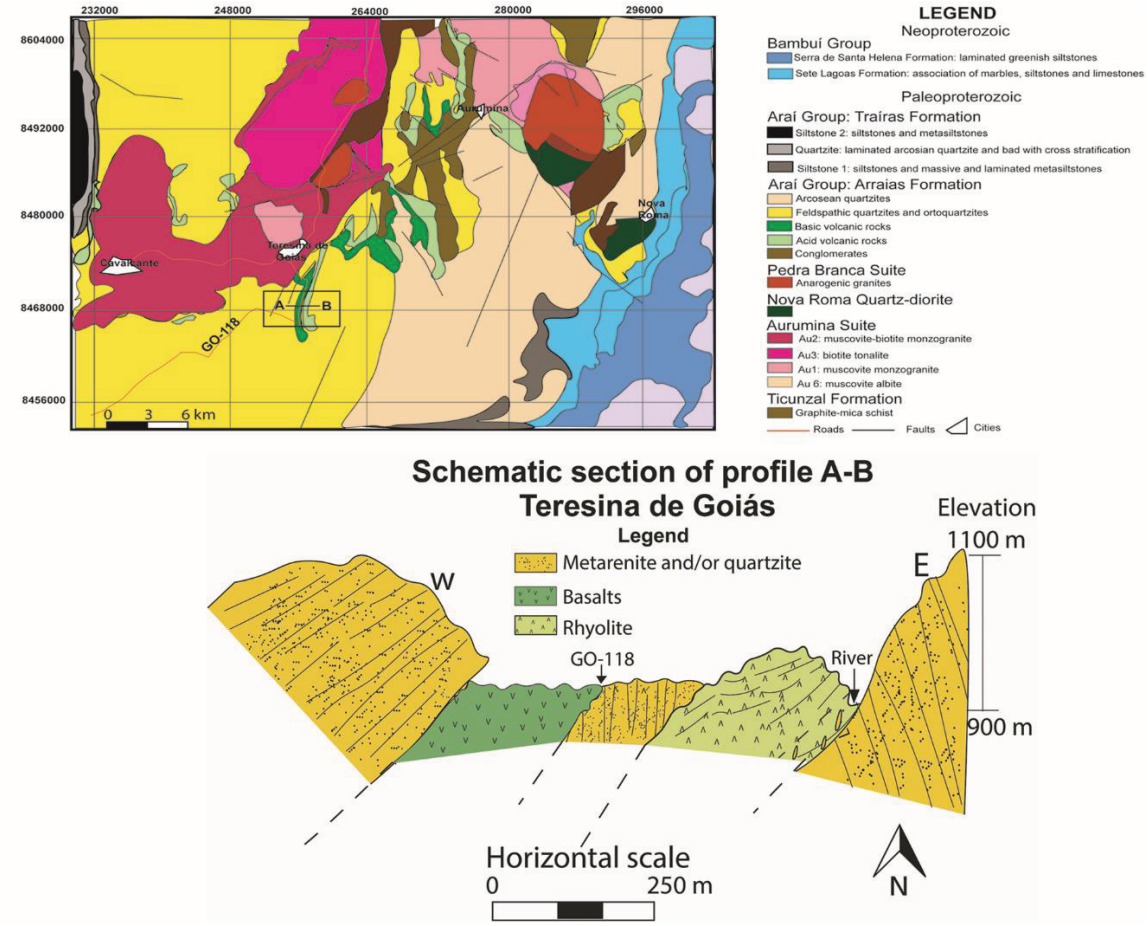

Figure 2. Geological map of the study area showing discontinuous distribution of the volcanic rocks from the Arraias Formation, Araí Group (after Alvarenga et al., 2007) and schematic section of profile A-B showing interbedding of basaltic and metasedimentary rocks.

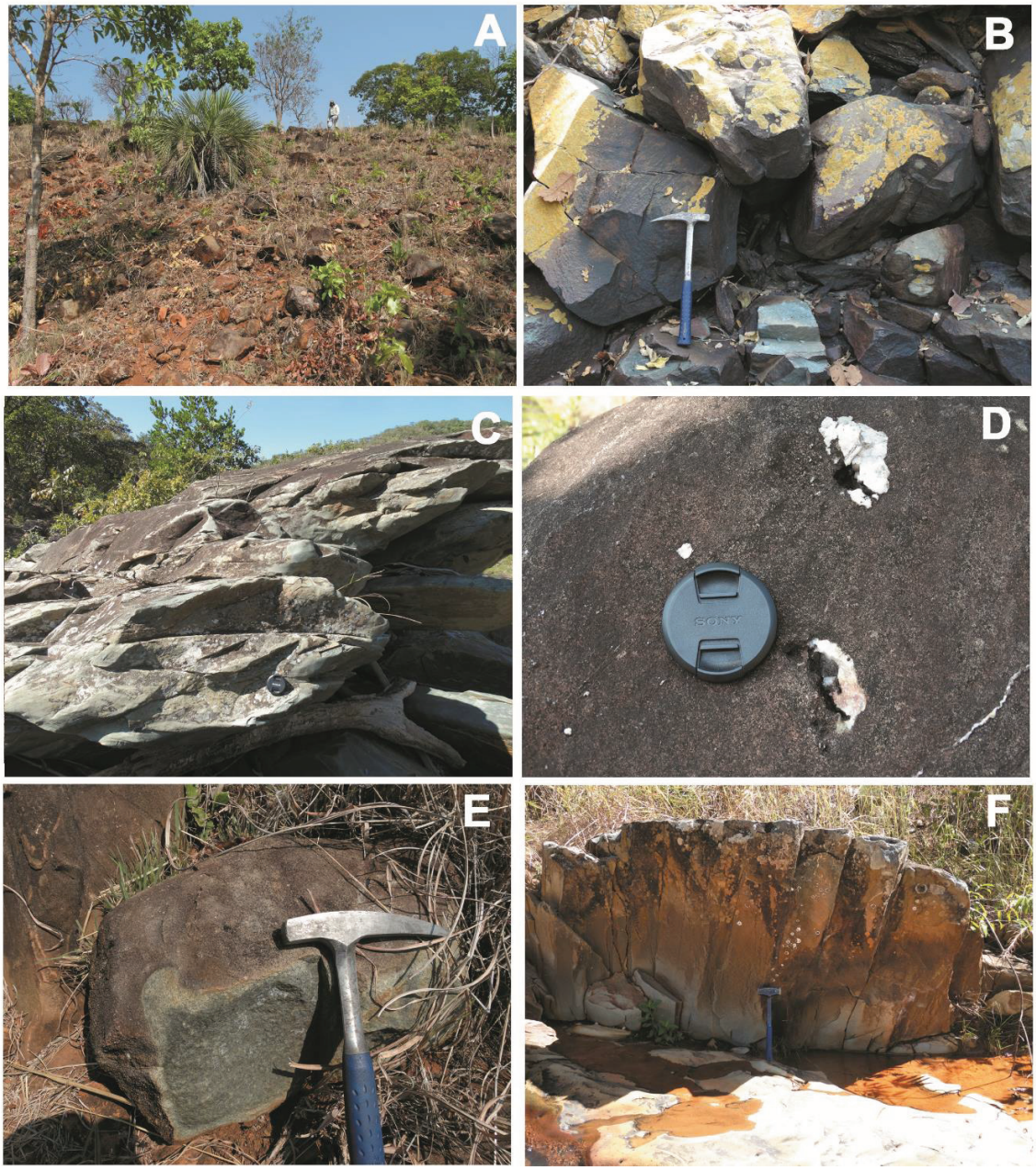

Figure 3. Outcrops of the basaltic rocks from the Arraias Formation [A-F]. Basaltic rocks exhibit fractures [B] with developed foliation [C], textural gradation marked by amygdaloidal structure in top [D] and sub-phaneritic texture at the base [E] and centimetric columnar disjunctions [F].

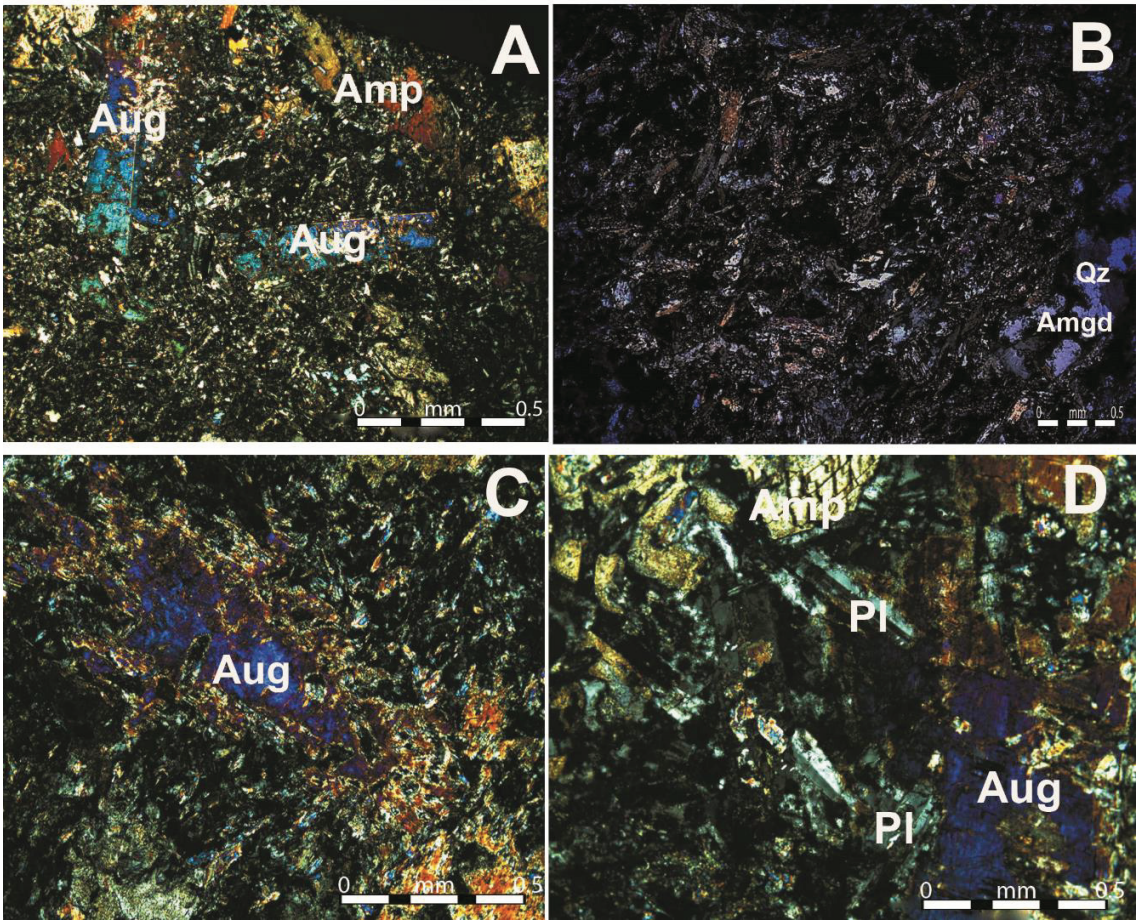

Figure 4. Photomicrographs of basaltic rocks of the Arraias Formation. Textural aspects of basic rocks, exhibiting augite phenocrysts immersed in a very fine granular matrix [A]. Amygdaloidal structure [B]. Augite exhibit corrosive gulfs [C]. Subophitic texture, represented by the partial inclusions of plagioclase in the crystals of augite [D]. Augite (Aug); Plagioclase (Pl); amphibole (Amp); Quartz (Qz); Amgd (amygdale).

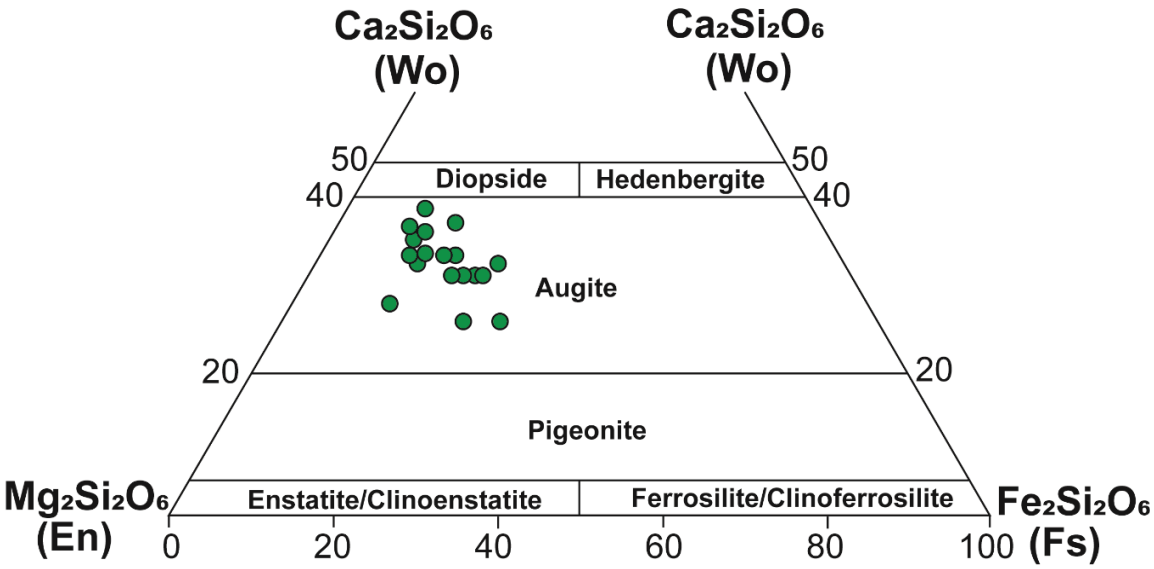

Figure 5. Pyroxene mineral chemistry. Plot of Ca-Mg-Fe pyroxenes in the Wo-En-Fs ternary diagram (after Morimoto et al. 1988) of basaltic rocks in the Arraias Formation.

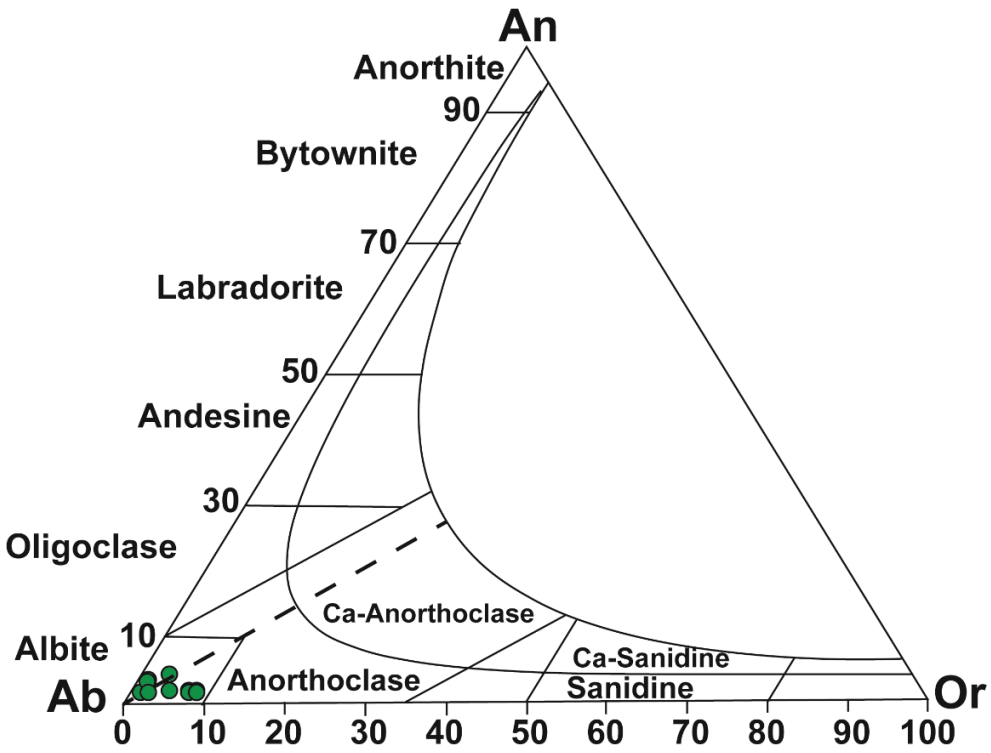

Figure 6. Feldspar mineral chemistry. (a) Anorthite (An)-Albite (Ab)-Orthoclase (Or) feldspar classification diagram (after Deer et al., 1996) of basaltic rocks in the Arraias Formation.

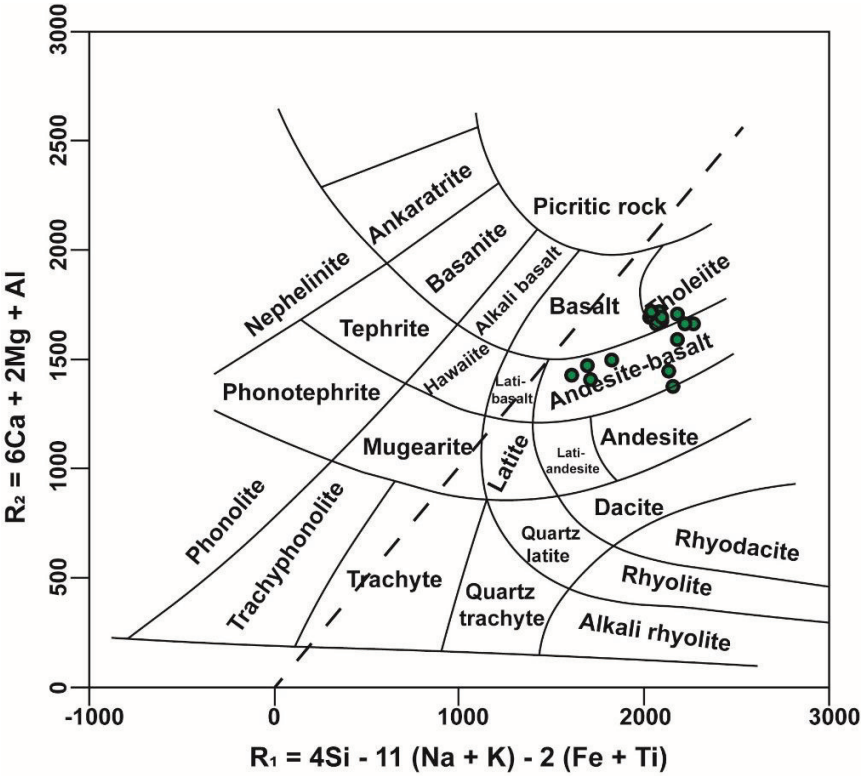

Figure 7. R1 versus R2 classification diagram (De la Roche et al., 1980), applied to the basaltic rocks from the Arraias Formation. The 45°degree dashed line marks the line of critical silica saturation (Bell et al., 2013).

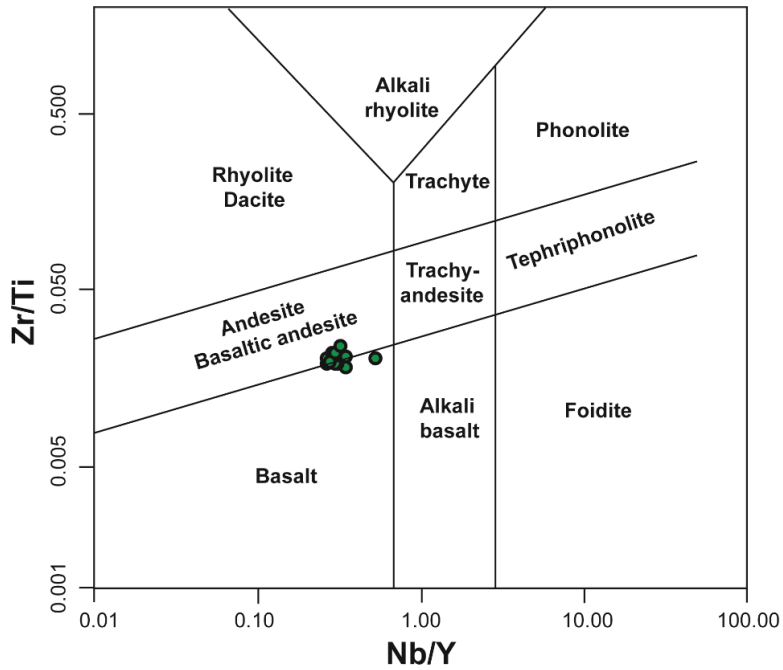

Figure 8. Nb/Y versus Zr/Ti classification diagram (Winchester & Floyd, 1977 modified by Pearce, 1996).

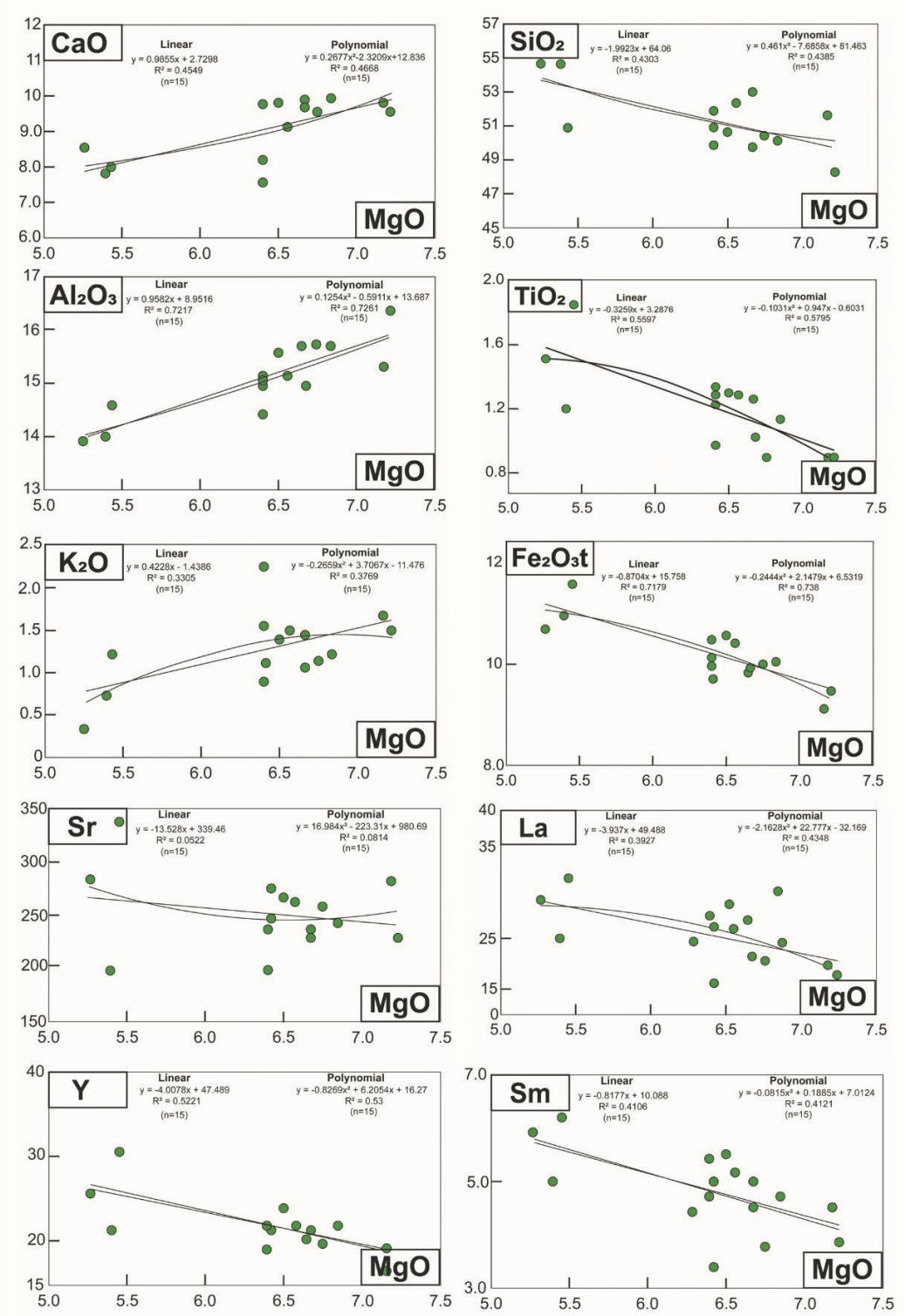

Figure 9. Fenner variation diagrams for major (wt.%) and trace elements (ppm) of basaltic rocks in the Arraias Formation. Equations and respective squares of the Pearson's correlation coefficients (R^2) are indicated.

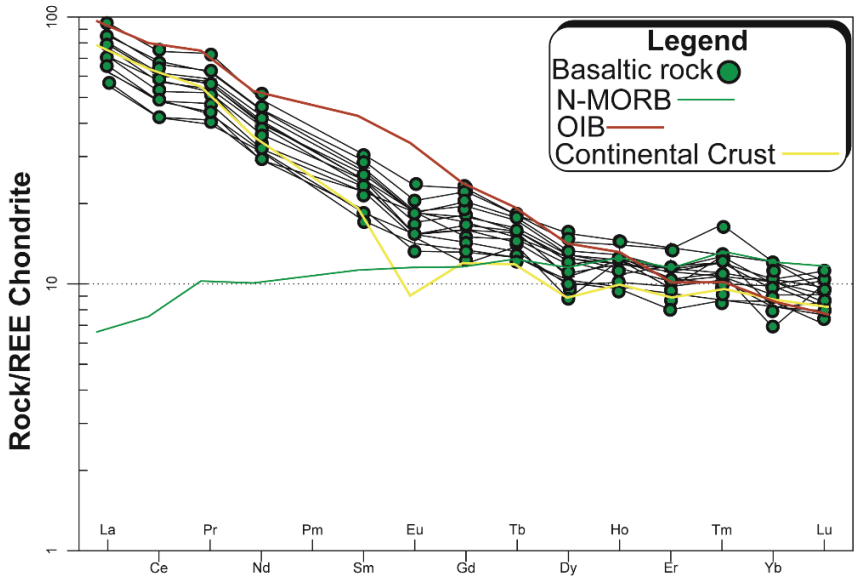

Figure 10. Chondrite-normalized REE diagram (Nakamura,1974) for basaltic rocks of the Arraias Formation. Data for Oceanic Island Basalt and Normal Mid-Oceanic Basalt Ridge (N-MORB) from Sun and MacDonough (1989) and Continental Crust from Rudnick and Gao (2013).

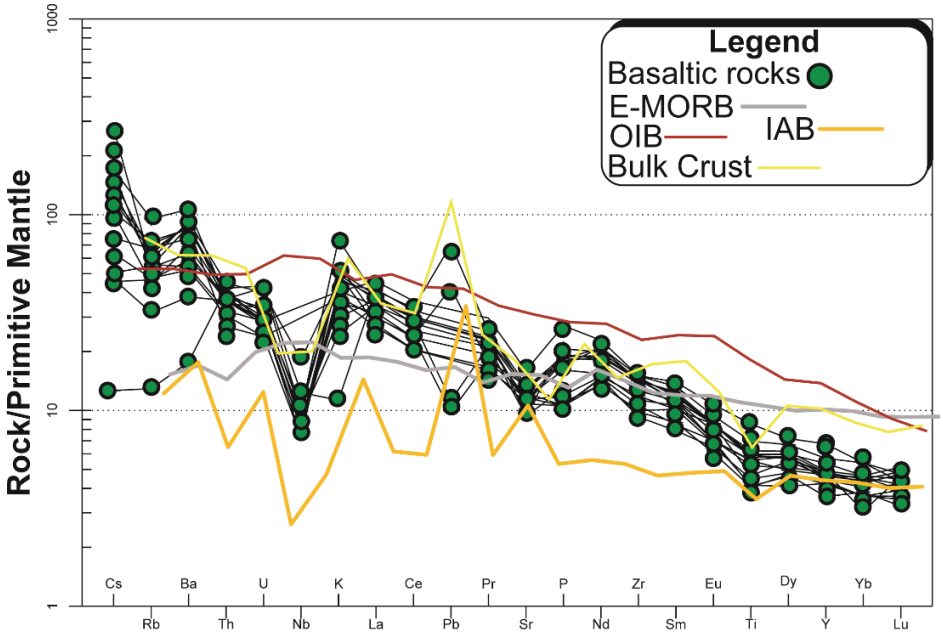

Figure 11. Primitive mantle-normalized multielementar diagram for basaltic rocks of the Arraias Formation. Normalizing values are from Sun & MacDonough (1989). Data for Oceanic Island Basalt (OIB) and Enriched Mid-Oceanic Basalt Ridge (E-MORB) from Sun and MacDonough (1989) and Bulk Crust from Rudnick and Gao (2013).

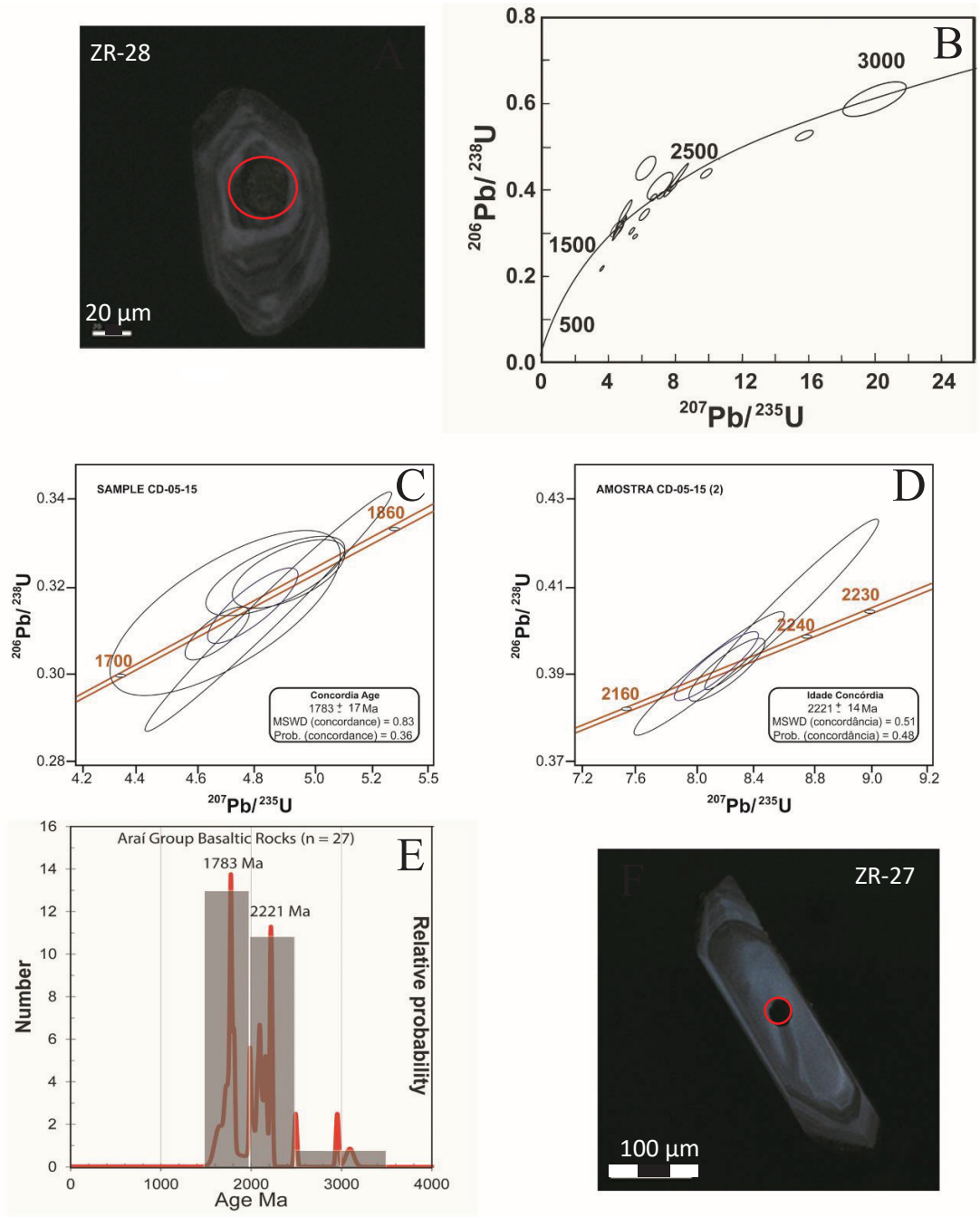

Figure 12. LA-ICP-MS U-Pb zircon data (Tab.4) of the sample CD-05-15 (B-D) and CL images of representative zircon crystals (A and F). The ages shown in the histograms correspond to $^{207}Pb/^{206}Pb$ ages (E).

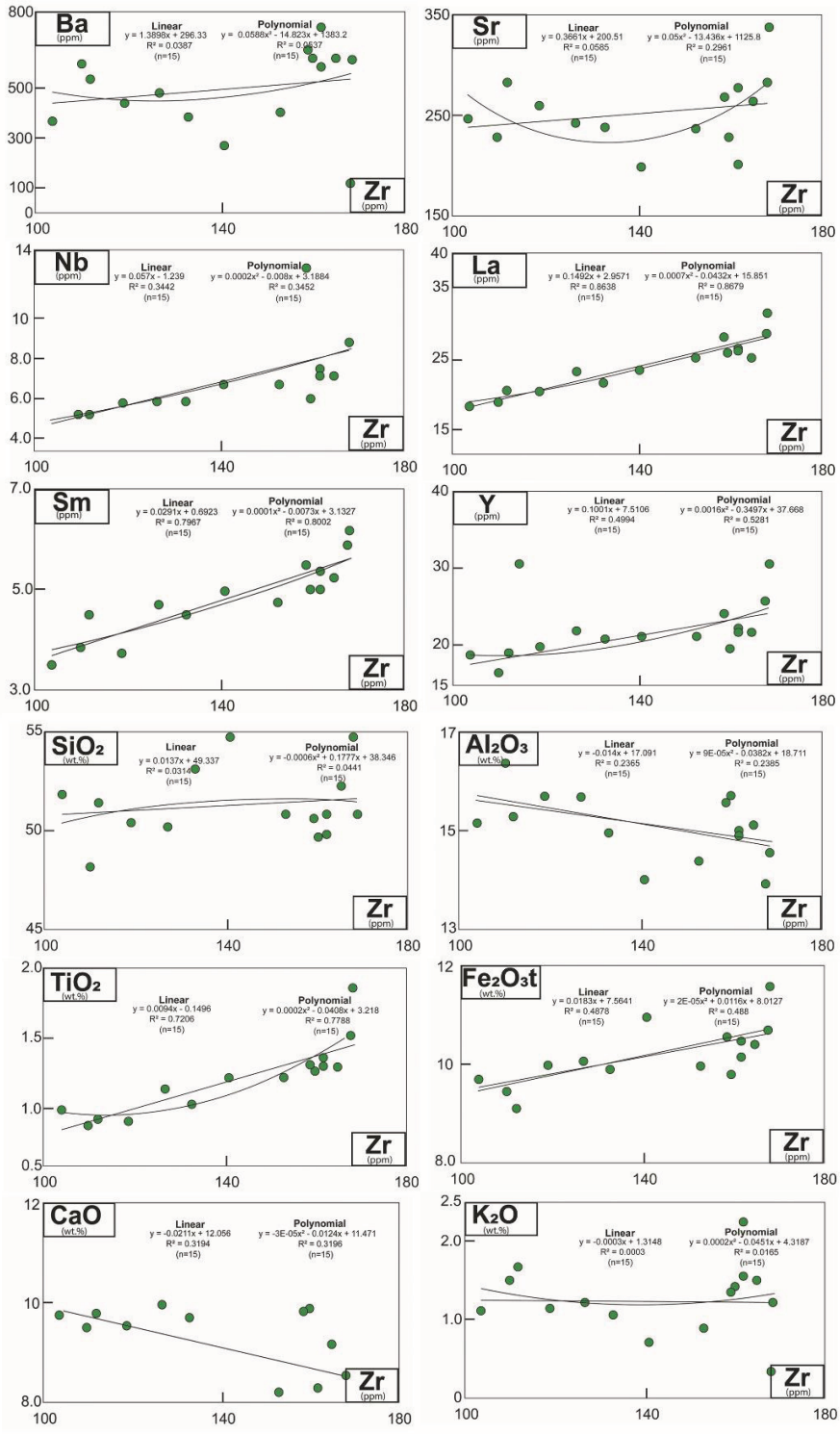

Figure 13. Zr versus Major (wt.%) and trace elements (ppm) diagrams to evaluate the element mobility during alteration.

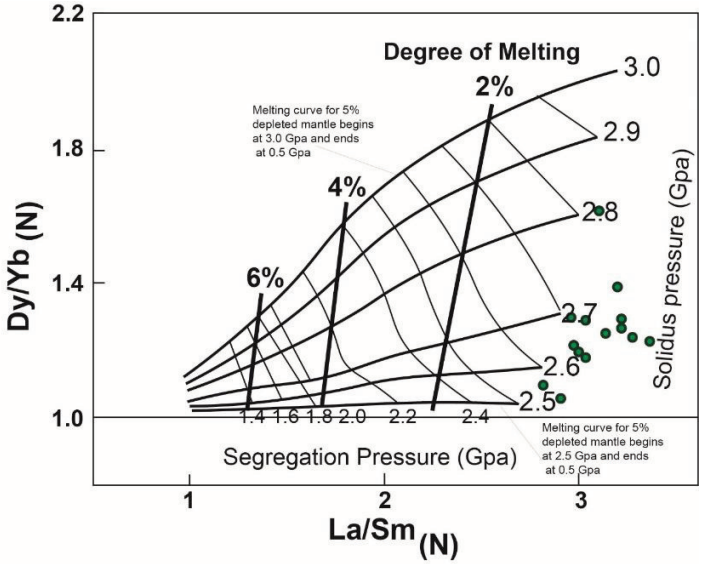

Figure 14. Chondrite-normalized $La/Sm_{(N)}$ and $Dy/Yb_{(N)}$ ratios for mantle melting models using the algorithm for primitive mantle depleted. Model curves, for melting starting at 3.0, 2.9, 2.8, 2.7, 2.6, and 2.5 GPa and ending at 0.5 GPa, define a melting grid, where solid sub-vertical lines contour constant mean melt fraction (after Mayborn and Lesher, 2004 in Srivastava and Gautam, 2014).

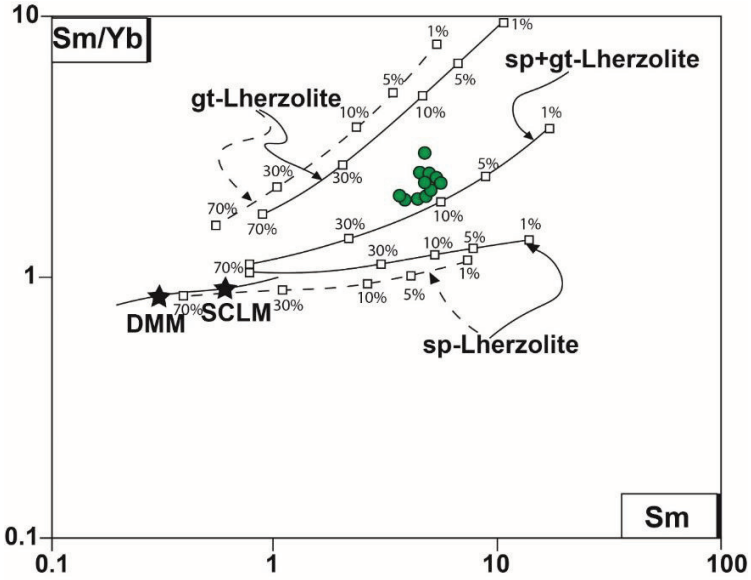

Figure 15. Sm/Yb versus Sm diagram (Li and Chen, 2014) for modeling of mantle melting with different starting materials (garnet lherzolite, garnet-spinel lherzolite and spinel lherzolite) are shown, based on the non-batch melting equations of Shaw (1970). The dashed and solid lines are the melting trends for depleted mantle (DM) and enriched subcontinental lithospheric mantle (SCLM) (Li and Chen, 2014).

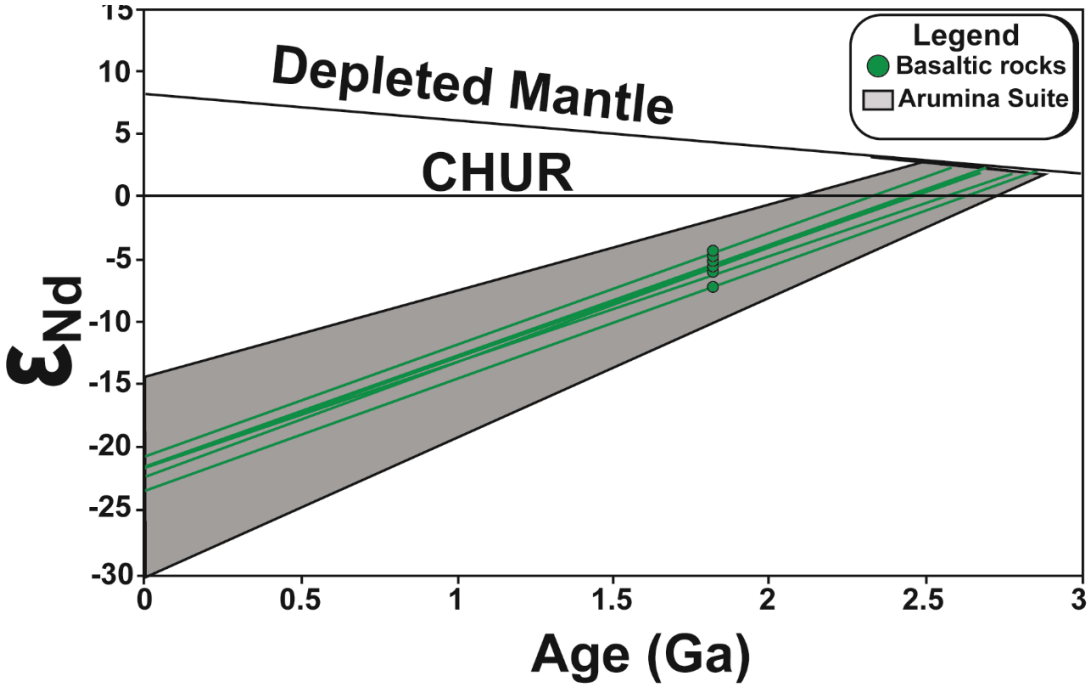

Figure 16. εNd versus age plot of the analyzed samples. Depleted mantle (DM) curve according DePaolo (1981). Gray area corresponds granites of the Aurumina Suite (Cuadros et al. 2017).

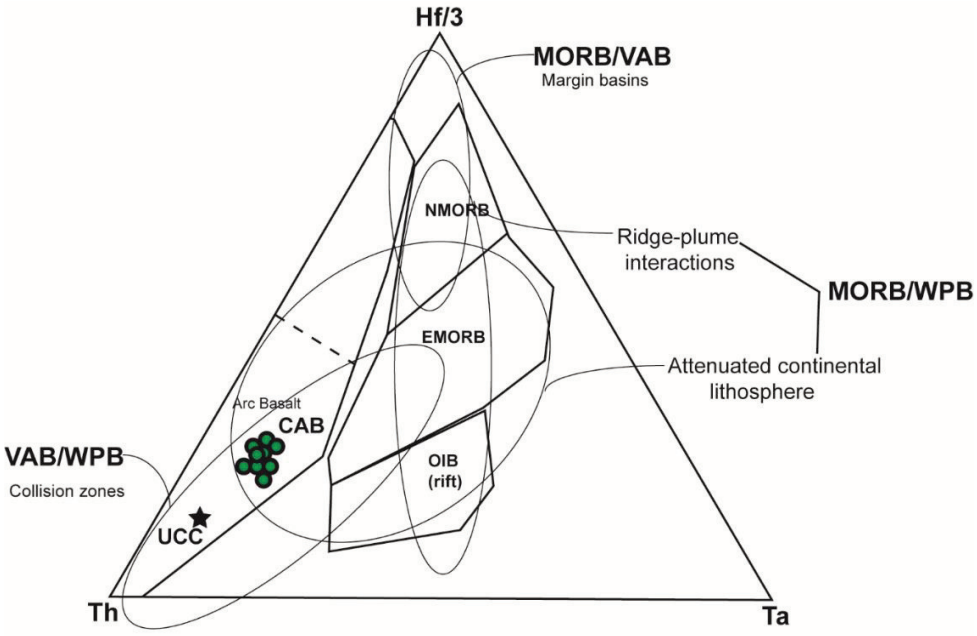

Figure 17. Hf-Th-Ta diagram of tectonic setting of Wood (1980) of basaltic rocks Arraias Formation showing the elliptic contours with 10% probability for magmas and transitional environments of Pearce (1996) and the average composition of the Uper Continental Crust (UCC) extracted from McLennan (2001). Oceanic Island Basalt (OIB), Normal Mid-Oceanic Ridge Basalt (N-MORB), Enriched Mid-Oceanic Ridge Basalt (N-MORB), within-plate Basalt (WPB) and Continental Arc Basalt (CAB).

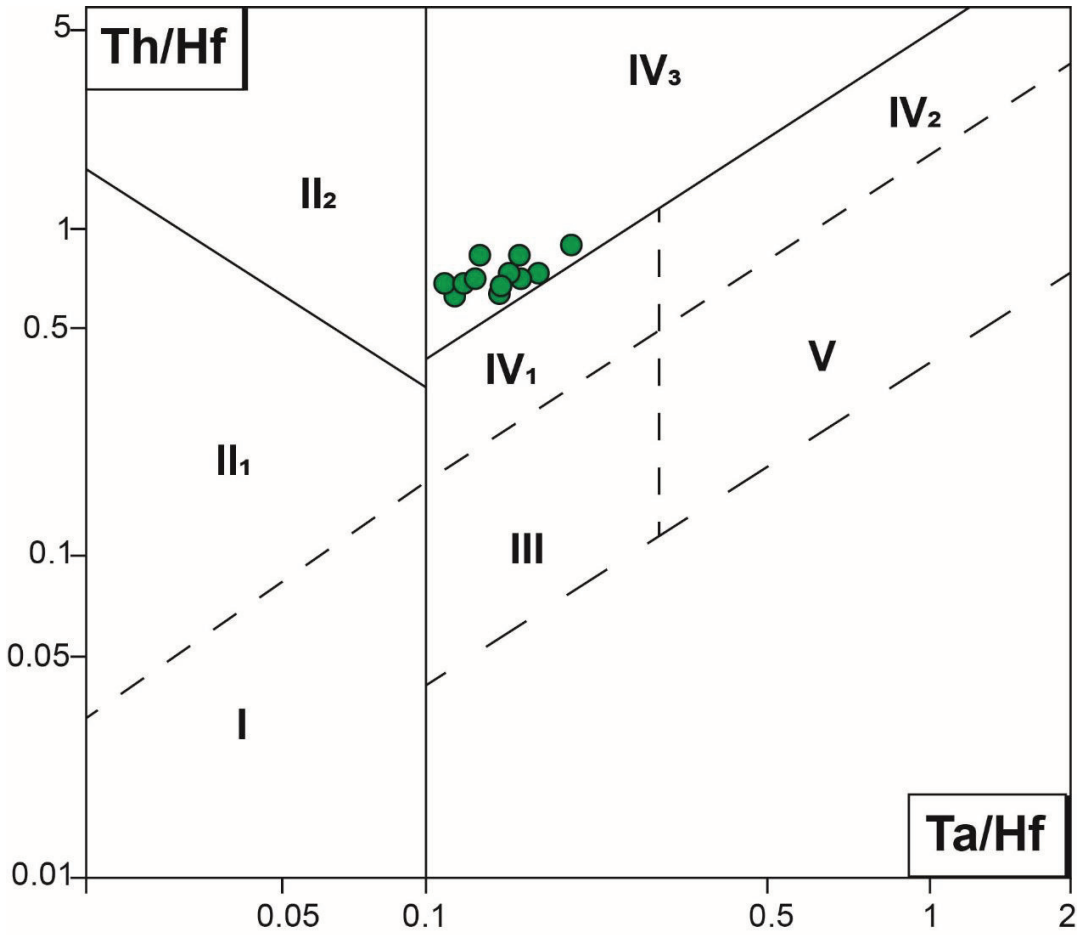

Figure 18. Th/Hf–Ta/Hf diagram (Wang et al., 2001 in Fu et al., 2010) of tectonic setting of basaltic rocks Arraias Formation. I: Plate divergent margin MORB; II: Plate convergent margin basalts (II1: ocean island-arc basalts; II2: Continental margin island-arc+continental margin volcanic-arc basalts); III: Oceanic within-plate basalts (oceanic island+sea mountain basalt+T-MORB+E-MORB); IV: Continental withinplate basalts (IV1: Intracontinental rift+continental margin rift tholeiites IV2: Intracontinental rift alkali basalts IV3: Continental extensional zone/initial rift basalts); V: Mantle plume basalts.

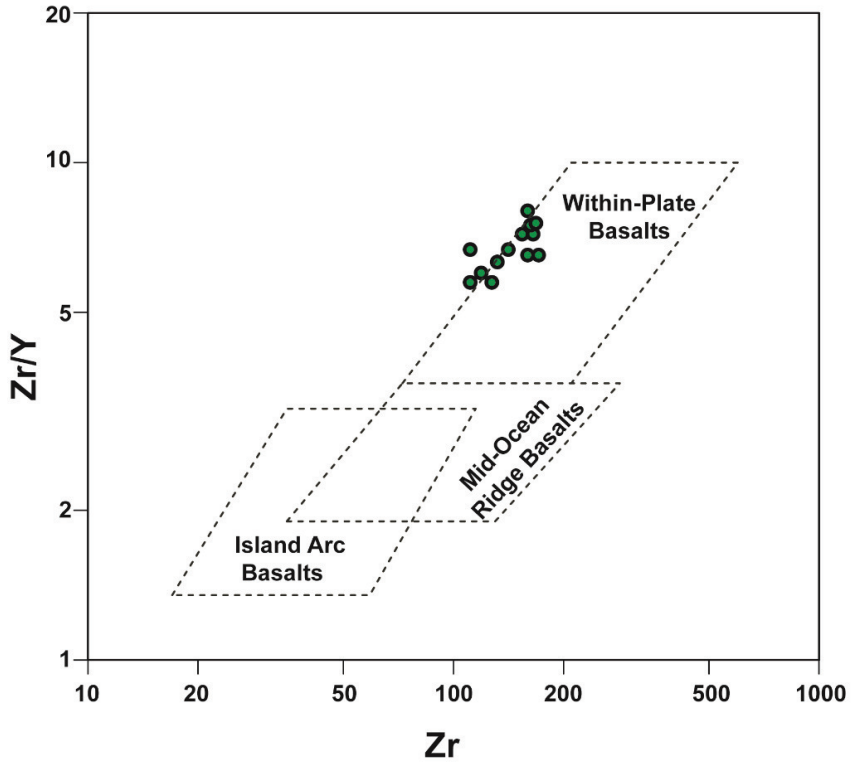

Figure 19. Zr versus Zr/Y discriminant diagram Pearce and Nory (1979) for tectonic setting of applied to the basaltic rocks Arraias Formation.

.

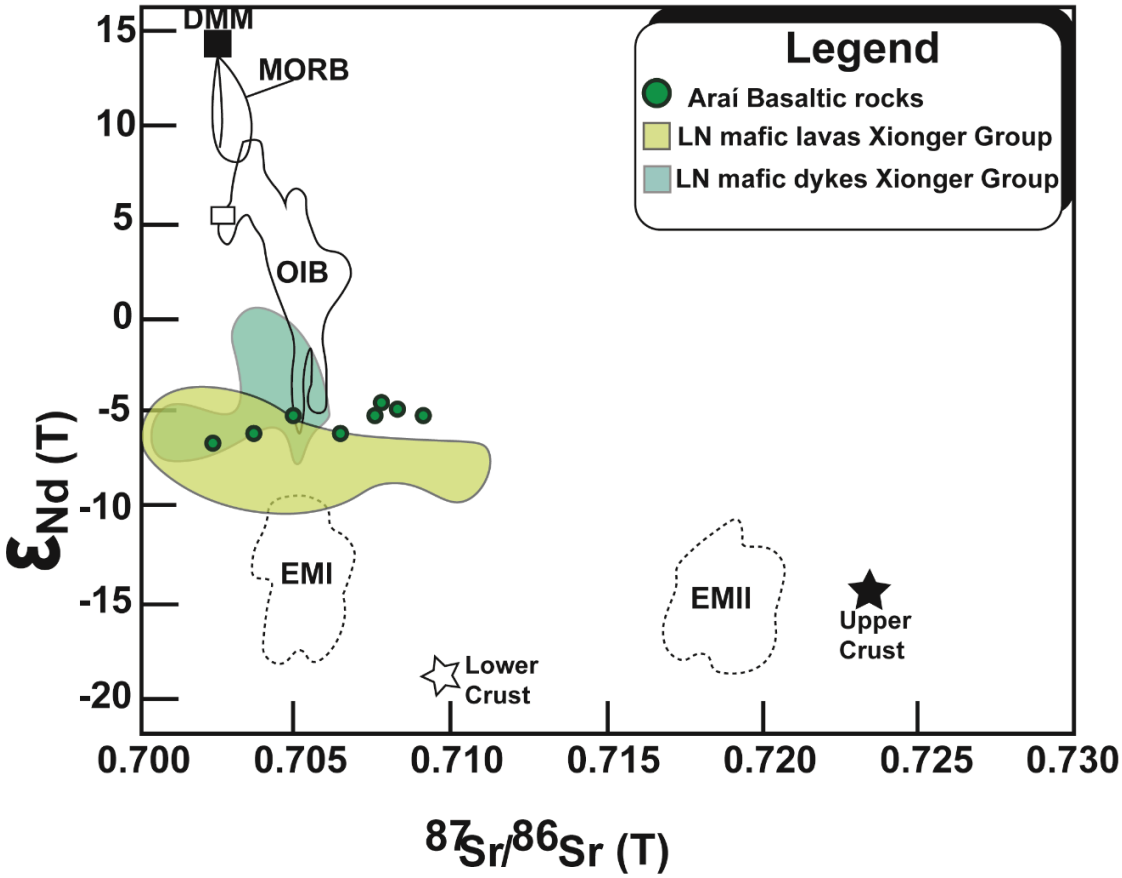

Figure 20. $^{87}Sr/^{86}Sr_{(1783)}$ vs. $\varepsilon Nd_{(1783)}$ diagram for the basaltic rocks from Arraias Formation with the fields of the low Nb basaltic rocks (lava and dykes) of the Xionger Group in the North China Craton (Xia et al. 2013). Data for OIB, MORB, DMM, EMI and EMII are from Zindler and Hart (1986) and Hart et al. (1992). Values of the Crust from Rudnick and Gao (2013).

Table 2. Analysis and formulae of representative pyroxenes of basaltic rocks from the Arraias Formation. R: rim analysis. C: core analysis.

Sample	28_3[1] **C**	28_3[1] **R**	28_5[2]	28_10[2]	29_9[1] **C**	29_9[1] **R**	29_7[2]	29_6[2]	05_1[2]	05_9[1] **C**	05_9[1] **R**	05_6[1] **C**	05_6[1] **R**	05_7[1] **C**	05_7[1] **R**	05_2[2]	65_1[2]
SiO_2	51.52	51.77	51.85	52.33	52.26	52.32	51.60	52.56	52.34	58.36	54.09	53.50	52.28	53.11	52.55	53.85	55.63
TiO_2	0.65	0.46	0.45	0.62	0.23	0.72	0.47	0.88	0.75	0.07	0.27	0.42	0.78	0.79	1.04	0.64	0.11
Al_2O_3	1.89	1.74	1.21	1.71	1.95	1.87	1.74	0.00	1.56	0.70	0.00	1.25	1.29	1.32	1.37	0.00	1.09
FeO	8.79	8.50	9.65	8.84	8.83	8.70	9.12	7.44	12.78	6.82	9.50	11.37	14.21	11.79	13.55	12.53	15.28
MnO	0.25	0.27	0.34	0.40	0.17	0.15	0.46	0.20	0.17	0.09	0.27	0.30	0.21	0.32	0.10	0.17	0.26
MgO	17.44	17.30	15.95	15.04	17.92	17.54	15.60	17.11	15.69	19.54	17.17	17.22	14.71	16.60	14.42	16.13	14.55
CaO	18.06	19.13	18.78	19.60	17.61	18.14	19.64	19.63	16.38	14.21	18.24	16.75	17.10	16.89	17.06	16.78	12.31
Na_2O	0.23	0.19	0.80	0.44	0.20	0.17	0.64	0.17	0.32	0.08	0.21	0.16	0.29	0.22	0.28	0.24	0.11
Cr_2O_3	0.37	0.40	0.10	0.23	0.26	0.17	0.19	0.84	0.00	0.13	0.06	0.00	0.00	0.07	0.07	0.04	0.06
V_2O_3	0.10	0.07	0.07	0.08	0.03	0.06	0.08	0.07	0.06	0.05	0.13	0.13	0.13	0.13	0.11	0.13	0.00
NiO_2	0.02	0.00	0.09	0.00	0.06	0.00	0.06	0.00	0.00	0.10	0.00	0.04	0.03	0.07	0.03	0.02	0.02
Total	99.30	99.84	99.29	99.29	99.51	99.84	99.60	98.92	100.05	100.14	99.93	101.13	101.02	101.31	100.57	100.53	99.40
Si	1.909	1.908	1.927	1.955	1.927	1.928	1.914	1.961	1.953	2.127	2.000	1.961	1.948	1.951	1.967	2.002	2.117
Al	0.082	0.076	0.053	0.045	0.073	0.072	0.076	0.000	0.047	0.000	0.000	0.039	0.052	0.049	0.033	0.000	0.000
Fe^{3+}	0.090	0.016	0.020	0.000	0.000	0.000	0.010	0.014	0.000	0.000	0.000	0.000	0.000	0.000	0.000	0.000	0.000
SumT	1.991	1.984	1.980	2.000	2.000	2.000	1.990	1.961	2.000	2.127	2.000	2.000	2.000	2.000	2.000	2.002	2.117
Cations based on 6 oxygen																	
Al	0.000	0.000	0.000	0.030	0.011	0.009	0.000	0.000	0.022	0.030	0.000	0.015	0.004	0.009	0.028	0.000	0.049
Fe^{3+}	0.058	0.067	0.101	0.003	0.055	0.029	0.098	0.000	0.003	0.000	0.000	0.008	0.022	0.000	0.000	0.000	0.000
Ti	0.018	0.013	0.130	0.017	0.006	0.020	0.013	0.025	0.021	0.002	0.007	0.012	0.022	0.022	0.029	0.018	0.003
Cr	0.011	0.012	0.003	0.007	0.008	0.005	0.006	0.025	0.000	0.004	0.002	0.000	0.000	0.002	0.002	0.001	0.002

V	0.003	0.002	0.003	0.003	0.001	0.002	0.002	0.002	0.002	0.002	0.004	0.004	0.004	0.004	0.003	0.004	0.000
Ni	0.001	0.000	0.003	0.000	0.002	0.000	0.002	0.000	0.000	0.003	0.000	0.001	0.001	0.002	0.001	0.001	0.000
Mg	0.910	0.907	0.879	0.838	0.917	0.936	0.863	0.948	0.873	0.960	0.947	0.941	0.817	0.909	0.805	0.894	0.825
Fe^{2+}	0.000	0.000	0.000	0.102	0.000	0.000	0.017	0.000	0.079	0.000	0.040	0.019	0.133	0.047	0.132	0.082	0.121
Sum M1	1.000	1.000	1.000	1.000	1.000	1.000	1.000	1.000	1.000	1.000	1.000	1.000	1.000	1.000	1.000	1.000	1.000
Mg	0.053	0.044	0.005	0.000	0.068	0.028	0.000	0.003	0.000	0.102	0.000	0.000	0.000	0.000	0.000	0.000	0.000
Fe^{2+}	0.205	0.179	0.179	0.171	0.217	0.239	0.159	0.218	0.317	0.208	0.253	0.321	0.290	0.310	0.292	0.307	0.366
Mn	0.008	0.008	0.011	0.013	0.005	0.005	0.014	0.006	0.005	0.003	0.009	0.009	0.007	0.010	0.003	0.005	0.008
Ca	0.717	0.755	0.748	0.784	0.696	0.716	0.781	0.785	0.655	0.555	0.723	0.658	0.682	0.665	0.684	0.668	0.502
Na	0.016	0.014	0.058	0.032	0.014	0.012	0.046	0.013	0.023	0.006	0.015	0.011	0.021	0.016	0.020	0.017	0.008
Sum M2	1.000	1.000	1.000	1.000	1.000	1.000	1.000	1.025	1.000	1.000	1.000	1.000	1.000	1.000	1.000	0.998	0.883

Table 3. Analysis of the representative feldspar of basaltic rocks From the Arraias Formation.

Sample	41_3	41_5	29_8	28_5	28_8	39_9	05_3	05_4
SiO_2	62.5	62.6	65.9	64.4	66.0	67.6	68.0	66.7
TiO_2	0.1	0.1	0.0	0.0	0.0	0.0	0.0	0.0
Al_2O_3	19.0	21.6	19.3	19.1	19.6	18.8	19.1	19.4
FeO	4.6	1.8	1.8	3.2	1.5	1.0	0.2	1.8
MnO	0.1	0.1	0.2	0.1	0.1	0.0	0.1	0.0
MgO	2.3	1.2	0.9	1.8	0.7	0.6	0.1	1.0
CaO	0.3	0.7	0.6	0.2	0.7	0.2	0.5	0.4
Na_2O	9.9	8.4	10.5	10.6	11.2	11.5	12.1	10.9
K_2O	0.2	2.7	0.3	0.1	0.1	0.1	0.1	0.2
Total	99.0	99.1	99.3	99.4	99.7	99.8	100.0	100.3
Si	2.8	2.8	2.9	2.9	2.9	3.0	3.0	2.9
Al	1.0	1.2	1.0	1.0	1.0	1.0	1.0	1.0
Ti	0.0	0.0	0.0	0.0	0.0	0.0	0.0	0.0
Ca	0.0	0.0	0.0	0.0	0.0	0.0	0.0	0.0
Na	0.9	0.7	0.9	0.9	1.0	1.0	1.0	0.9
K	0.0	0.2	0.0	0.0	0.0	0.0	0.0	0.0
% An	1.8	3.6	2.8	1.0	3.3	0.9	2.1	1.8
% Ab	97.0	79.4	95.7	98.4	96.2	98.4	97.5	97.3
% Or	1.2	17.0	1.5	0.6	0.5	0.7	0.4	1.0

Table 4. Whole-rock major (wt.%) and trace element (ppm) compositions for the Basaltic Rocks from the Arraias Formation, Araí Group.

Sample	CD-29A-16	05-III-034	05-IV-077	CD-05-15	CD-50-17	CD-28-16	CD-46-17	CD-29B-6	CD-65-17	CD-41-17	CD-39-17	CD-40-17	CD-45-17	K-20	01-III-27
SiO_2	48.20	51.50	50.16	50.40	53.10	49.72	52.30	50.60	49.80	50.80	50.80	54.70	54.80	51.84	50.78
TiO_2	0.88	0.90	1.13	0.89	1.01	1.25	1.28	1.30	1.28	1.21	1.35	1.20	1.51	0.97	1.85
Al_2O_3	16.35	15.29	15.71	15.70	14.95	15.70	15.10	15.55	14.95	14.40	15.00	14.00	13.90	15.15	14.58
Fe_2O_{3T}	9.45	9.11	10.06	9.97	9.91	9.83	10.40	10.55	10.15	9.96	10.45	10.95	10.70	9.69	11.57
MnO	0.13	0.13	0.13	0.15	0.15	0.15	0.15	0.15	0.15	0.18	0.16	0.15	0.16	0.13	0.16
MgO	7.22	7.17	6.84	6.75	6.67	6.66	6.56	6.50	6.40	6.40	6.40	5.39	5.26	6.41	5.44
CaO	9.53	9.81	9.98	9.57	9.71	9.89	9.16	9.85	7.58	8.20	8.24	7.83	8.52	9.76	7.99
Na_2O	1.58	1.72	1.96	2.13	2.21	1.81	1.87	1.87	2.53	3.37	2.54	2.85	3.19	1.87	2.96
K_2O	1.50	1.67	1.23	1.15	1.07	1.43	1.50	1.37	2.25	0.90	1.55	0.74	0.34	1.12	1.22
P_2O_5	0.23	0.24	0.35	0.23	0.26	0.39	0.42	0.40	0.41	0.40	0.45	0.28	0.37	0.23	0.59
LOI	3.28	2.20	2.20	2.37	2.44	2.43	2.87	2.91	2.56	2.47	2.67	2.45	2.44	2.60	2.50
Total	98.35	99.74	99.75	99.31	101.48	99.26	101.61	101.05	98.06	98.29	99.61	100.54	101.19	99.77	99.64
Mg#-number	61.71	63.4	59.94	59.84	59.7	59.86	58.13	57.55	58.12	58.58	57.41	52	51.97	59.28	59.85
V	170	175	171	184	201	177	200	203	193	193	203	217	258	167	200
Cr	220	-	-	250	190	240	190	250	180	180	180	90	40	-	-
Ni	-	46	68	140	-	140	-	125	-	-	-	-	-	68	59
Sc	-	-	-	27	-	26	-	29	-	-	-	-	-	28	24
Rb	45	43	29	34	35	40	41	37	61	30	47	20	8	30	35
Sr	228	283	244	260	238	229	264	268	277	237	201	198	284	245	338
Y	17	19	22	20	21	20	22	24	22	21	22	21	26	19	31
Zr	110	112	127	119	133	160	165	159	162	153	162	141	168	104	169

Nb	5	5	6	6	6	6	7	13	7	7	8	7	9	-	-
Cs	1	1	1	1	2	1	1	1	1	0	1	0	0	1	0
Ba	594	529	480	442	378	624	619	647	745	410	591	266	124	365	610
La	18.9	20.6	23.5	20.5	21.7	26.0	25.1	28.1	26.1	25.3	26.5	23.5	28.6	18.3	31.4
Ce	36.4	41.8	50.1	42.3	41.9	52.6	52.6	59.1	52.1	49.4	53.5	45.5	57.5	36.3	64.3
Pr	4.6	4.9	5.9	4.9	5.3	6.3	6.3	7.0	6.4	6.0	6.6	5.8	7.0	4.4	8.2
Nd	18.4	18.3	20.9	19.9	20.2	25.4	25.0	28.2	25.8	24.6	26.9	22.9	28.4	19.7	30.9
Sm	3.9	4.5	4.7	3.8	4.5	5.0	5.2	5.5	5.0	4.8	5.4	5.0	5.9	3.5	6.2
Eu	1.0	1.2	1.2	1.2	1.4	1.4	1.4	1.4	1.3	1.2	1.4	1.2	1.6	1.1	1.8
Gd	3.6	3.3	4.4	4.0	4.1	4.7	4.9	5.4	5.0	4.6	5.6	4.4	6.1	3.7	6.3
Tb	0.6	0.7	0.7	0.6	0.7	0.7	0.8	0.8	0.7	0.7	0.8	0.7	0.9	0.6	0.9
Dy	3.5	3.0	3.8	3.4	4.1	4.3	4.4	4.4	4.2	4.3	4.6	3.7	4.9	3.5	5.3
Ho	0.7	0.9	0.8	0.7	0.9	0.8	0.9	0.8	0.8	0.8	0.9	0.9	1.0	-	-
Er	1.8	2.2	2.6	2.2	2.4	2.3	2.6	2.5	2.6	2.5	2.6	2.3	3.0	-	-
Tm	0.3	0.4	0.3	0.3	0.3	0.3	0.4	0.4	0.4	0.3	0.4	0.3	0.5	-	-
Yb	1.9	1.8	1.5	1.8	2.2	2.0	2.2	2.3	2.1	2.2	2.3	2.3	2.7	1.8	2.7
Lu	0.2	0.3	0.3	0.3	0.3	0.3	0.4	0.4	0.4	0.3	0.3	0.3	0.4	0.3	0.3
Hf	2.8	3.0	3.3	3.1	3.2	3.6	4.3	4.2	4.3	3.9	4.4	3.5	4.1	2.9	4.2
Ta	0.4	0.6	0.5	0.4	0.5	0.4	0.6	0.7	0.5	0.5	0.6	0.6	0.6	0.5	0.5
Pb	-	0.7	0.8	3.0	-	-	-	5.0	-	-	-	-	-	-	-
Th	2.3	3.2	3.1	3.1	2.7	3.0	3.2	3.8	3.2	3.3	3.4	3.1	3.6	2.6	3.4
U	0.5	0.6	0.6	0.6	0.6	0.7	0.7	0.8	0.9	0.6	0.7	0.6	0.9	0.5	0.6
Eu/Eu*	0.82	0.88	0.79	0.93	1.00	0.89	0.85	0.80	0.80	0.77	0.79	0.76	0.80	0.92	0.88
$La/Yb_{(CN)}$	6.69	7.65	10.41	7.62	6.72	8.69	7.63	8.21	8.31	7.55	7.74	6.98	7.19	6.76	7.89

$La/Sm_{(CN)}$	3.02	2.82	3.09	3.37	2.98	3.21	2.96	3.14	3.23	3.28	3.04	2.91	3	-	-
$Dy/Yb_{(CN)}$	1.17	1.08	1.6	1.21	1.2	1.38	1.28	1.24	1.27	1.22	1.28	1.04	1.19	1.17	1.08
Zr/Y	6.67	5.8	5.77	6.01	6.33	8	7.53	6.52	7.36	7.22	7.26	6.62	6.49	5.46	5.49
Nb/La	0.28	0.25	0.25	0.28	0.27	0.23	0.28	0.46	0.27	0.26	0.28	0.28	0.31	-	-

Note: Mg#=100∗molar MgO/(Mg+FeO_T), assuming FeO_T=0.9∗Fe_2O_3, LOI=loss on ignition; Eu/Eu* calculated as $Eu/Eu^*=Eu_N/(Sm_N*Gd_N)^{1/2}$;CN: Chondrite normalization Nakamura (1974).

Table 5. Results in situ U-Pb isotope analysis (LA-ICP-MS) of zircon of the basaltic rock from the Arraias Formation.

Grain n°	Th/U	$^{207}Pb/^{206}Pb$	2 σ (abs)	$^{207}Pb/^{235}U$	1 σ (%)	$^{206}Pb/^{238}U$	1 σ (%)	Rho	$^{207}Pb/^{206}Pb$	2 σ abs	$^{207}Pb/^{235}U$	1 σ (%)	$^{206}Pb/^{238}U$	1 σ (%)	% Disc
ZR29	0.834	0.109	0.001	4.902	1.60	0.325	0.98	0.62	1789	44	1803	27	1815	31	-1.46
ZR08	0.576	0.111	0.001	4.826	3.56	0.316	3.50	0.98	1813	19	1789	59	1769	108	2.40
ZR21	0.788	0.108	0.001	4.800	1.54	0.323	1.13	0.73	1762	36	1785	26	1805	35	-2.46
ZR28	0.389	0.109	0.001	4.723	1.22	0.313	0.87	0.71	1788	28	1771	20	1757	27	1.72
ZR22	0.674	0.108	0.003	4.690	3.44	0.316	2.41	0.70	1763	87	1765	57	1768	74	-0.29
ZR04	0.770	0.109	0.000	4.624	1.40	0.309	1.27	0.91	1775	17	1754	23	1736	39	2.19
ZR15	0.424	0.139	0.001	8.287	3.02	0.433	2.97	0.98	2211	16	2263	54	2321	115	-4.99
ZR23	0.434	0.140	0.001	7.959	1.32	0.412	1.05	0.79	2227	25	2226	24	2225	39	0.09
ZR26	0.259	0.140	0.001	7.898	2.31	0.410	2.18	0.94	2222	23	2219	41	2217	82	0.23
ZR06	0.444	0.236	0.007	19.899	3.85	0.612	2.63	0.68	3093	88	3086	73	3076	128	0.55
ZR07	0.323	0.216	0.002	15.754	1.36	0.528	0.92	0.67	2954	30	2862	26	2734	41	7.45
ZR02	0.301	0.163	0.001	9.954	1.39	0.442	1.00	0.72	2492	30	2431	25	2358	39	5.36
ZR09	0.229	0.130	0.004	7.476	4.13	0.416	3.06	0.74	2103	95	2170	73	2242	115	-6.58
ZR27	0.452	0.135	0.001	7.272	1.16	0.392	0.84	0.73	2160	24	2145	21	2130	31	1.35
ZR19	0.221	0.128	0.001	6.833	1.17	0.387	0.84	0.72	2071	25	2090	21	2109	30	-1.81
ZR20	0.864	0.102	0.003	6.381	3.82	0.454	2.48	0.65	1660	105	2030	66	2413	99	-45.4
ZR10	0.362	0.131	0.001	6.295	1.94	0.348	1.56	0.80	2115	38	2018	34	1924	52	8.99
ZR18	0.708	0.140	0.001	5.749	1.01	0.298	0.70	0.69	2226	22	1939	17	1682	21	24.43
ZR25	0.313	0.130	0.001	5.554	1.23	0.310	1.03	0.83	2095	20	1909	21	1743	31	16.80
ZR16	0.679	0.105	0.001	5.174	3.07	0.356	2.88	0.94	1720	37	1848	52	1964	97	-14.1
ZR17	1.017	0.108	0.001	5.082	1.08	0.340	0.81	0.75	1771	22	1833	18	1888	26	-6.57
ZR24	0.214	0.122	0.001	3.788	1.31	0.225	1.14	0.87	1987	18	1590	21	1308	27	34.15

Table 6. Whole-rock $^{87}Sr/^{86}Sr$ isotopic ratios for basaltic rocks from the Arraias Formation

Sample	Rb(ppm)[1]	Sr(ppm)[1]	$^{87}Sr/^{86}Sr^{*}_{(0)}$	2(σ)	$^{87}Sr/^{86}Sr_{(i)}$[(2)]
D-29A	44.40	228.00	0.716860	0.000021	0.702400
CD-05	34.10	260.00	0.71612	0.000002	0.706382
CD-50	35.40	238.00	0.71589	0.000024	0.704846
CD-28	40.00	229.00	0.716560	0.000034	0.703590
CD-29B	37.30	268.00	0.717820	0.000021	0.707484
CD-41	29.50	237.00	0.717010	0.000019	0.707767
CD-40	20.10	198.00	0.71583	0.000020	0.708293
CD-45	28.20	284.00	0.714830	0.000019	0.707458

Note: [1]Rb and Sr from the table 3 were used in calculation of isotopic ratios. [2]Initial $^{87}Sr/^{86}Sr$ isotopic ratios were calculated using age of sample CD-05-15 (1783 Ma).

Table 7. Whole-rock Sm/Nd isotopic data for basaltic rocks from the Arraias Formation.

Sample	Sm (ppm)	Nd (ppm)	$^{147}Sm/^{144}Nd$	$^{143}Nd/^{144}Nd$	2(σ)	$^{143}Nd/^{144}Nd_{(T)}$	$\varepsilon Nd_{(0)}$	$\varepsilon Nd_{(T)}$	T_{DM} (Ga)
D-29A	3.96	19.96	0.12002	0.511403	0.000012	0.509995	-24.09	-6.58	2.6
CD-05	5.35	25.41	0.12737	0.511513	0.000019	0.510019	-21.91	-6.11	2.7
CD-50	4.50	22.16	0.12277	0.511507	0.000012	0.510067	-22.06	-5.17	2.5
CD-28	5.57	21.93	0.12604	0.511497	0.000012	0.510019	-22.26	-6.12	2.7
CD-46	5.50	27.95	0.11893	0.511495	0.000012	0.510100	-22.30	-4.52	2.5
CD-29B	5.59	28.29	0.11940	0.511468	0.000012	0.510068	-22.82	-5.16	2.5
CD-65	5.57	28.27	0.11912	0.511498	0.000012	0.510101	-22.24	-4.51	2.50
CD-41	5.42	27.53	0.11892	0.511498	0.000007	0.510103	-22.24	-4.46	2.4
CD-40	4.95	24.61	0.12160	0.511514	0.000012	0.510088	-21.93	-4.77	2.5
CD-45	6.00	31.34	0.12148	0.511507	0.000012	0.510082	-22.06	-4.87	2.5

Note: Chondrite uniform reservoir (CHUR) values (147Sm/144Nd=0.1967, 143Nd/144Nd=0.512638) are used for the calculation. λSm=6.54×10−12 year−1 (Lugmair and Harti, 1978). The $(^{143}Nd/^{144}Nd)_i$ and $\varepsilon Nd_{(T)}$ were calculated using the age of 1783 Ma. TDM values were calculated according to the two-stage model as presented by Liew and Hofmann (1988).

Capítulo V – Considerações Finais

As rochas vulcânicas da Formação Arraias estão distribuídas de forma irregular na porção basal do Grupo Araí, ocorrendo intercaladas com espessas camadas de rochas metassedimentares (quartzito, metarenito, metassiltito, metaconglomerado), da mesma formação, ou em contato tectônico com os granitos anarogênicos da Província Estanífera da Suíte Pedra Branca. Em outros pontos, essas rochas estão assentadas diretamente sobre o embasamento do Grupo Araí, representado pelos quartzitos, gnaisses, conglomerados e xistos grafitosos da Formação Ticunzal e dos granitos peraluminosos da Suíte Aurumina.

Na preservação de suas texturas originais permitiu-se reconhecer os dois tipos de depósitos: piroclásticos e efusivos. Essa preservação pode ser reflexo das altas temperaturas no momento da formação desses depósitos e/ou da deposição dos espessos pacotes sedimentares que recobriram as sequências vulcânicas.

A análise petrográfica possibilitou reunir as rochas vulcânicas da Formação Arraias em depósitos vulcânicos distintos: efusivos e piroclásticos.

Os depósitos efusivos possuem uma heterogeneidade composicional, formada, essencialmente, por rochas máficas e félsicas, produzidas por derrames de lavas, com importantes variações texturais, de composição bimodal (basalto-riolito). Os litotipos ácidos são leucocráticos a mesocráticos, cujas cores variam de cor-de-rosa até vermelho-acastanhado a vermelho-acinzentado. Exibem arranjo textural porfirítico a glomoroporfirítico, ressaltados por fenocristais de quartzo, álcali-feldspato e plagioclásio, imersos em uma matriz de granulação fina a afanítica. Os feldspatos se mostram parcialmente serecitizados e/ou saussuritizados. Na matriz dessas rochas ocorrem proporções variadas de quartzo, feldspatos, muscovita, biotita, anfibólio, apatita, magnetita, zircão, além de epídoto e carbonato.

As rochas básicas são melanocráticas, com coloração variando de verde musgo a cinza esverdeado, porfiríticas, ressaltado pela presença de fenocristais de plagioclásio, piroxênio e anfibólio, imersos em matriz afanítica a microcristalina. Os fenocristais de piroxênio exibem bordas uralitizadas, enquanto que plagioclásio se mostra parcialmente saussuritizados e anfibólio cloritizado. Ocasionalmente formam texturas ofíticas a subofíticas, e hospedam vesículas preenchidas por zeolita, carbonato e quartzo. Em geral, a

matriz é formada por agregados clinopiroxênio, plagioclásio e anfibólio, tendo como minerais acessórios quartzo, titanita, epídoto, clorita e opacos.

Os depósitos de fluxos piroclásticos são composição ácida, constituídos por depósitos igimbríticos compostos por litoclastos angulosos (quartzito, granito e riolito), cujos tamanhos variam de bloco a lapilli, imersos em uma matriz cinerítica. Apresentam, ainda, fragmentos de púmices angulosos a densamente estirados (*fiammes*) e regiões de liberações de gases (*pipes*). Nesses depósitos, os cristaloclastos e os fenocristais de quartzo e feldspatos exibem, geralmente, aspectos quebradiços e fraturados. Textura do tipo parataxítica são observadas, as quais geram uma foliação planar com indicações de reomorfismo.

Os dados geoquímicos mostraram que as rochas vulcânicas da Formação Arraias têm uma composição bimodal, constituídas por basalto, basalto andesítico, dacito, riodacito, riolito e álcali-riolito, essencialmente subalcalinas.

As rochas efusivas félsicas são ácidas (66,10% a 76,60% de SiO_2), possuindo afinidades com as rochas das séries alcalinas e subalcalinas, e são classificadas como dacito, riolito, álcali riolito e traquito peraluminosos. Em diagrama normalizado pelo condrito, essas rochas são enriquecidas em ETR_{Leves} em relação aos $ETR_{Pesados}$, com as suas expressivas anomalias negativas de Eu, indicando um importante fracionamento dos feldspatos. Para ambiência tectônica, no diagrama Rb *versus* Y+Nb, o conjunto de rochas vulcânicas ácidas do Grupo Araí exibem afinidades com àquelas geradas em ambiente intraplaca (anarogênico).

O vulcanismo máfico, por sua vez, é composto por rochas básicas afaníticas (49,72% a 54,70% de SiO_2), classificadas como basalto, basalto alcalino, basalto andesítico e traquibasalto. No diagrama para ETRs normalizado pelo condrito, exibem um forte enriquecimento de ETR_{Leves} em relação aos $ETR_{Pesados}$, com anomalias pouco pronunciadas de Eu. Quando normalizadas pelo manto primitivo, essas rochas exibem anomalias positivas de Ba, Pb, Nd, e anomalias negativas de Rb, Nb, Sr e Ti. Os baixos valores de $\varepsilon Nd(T)$, variando de -6,78 a -4,89, para uma idade de cristalização de 1.78 Ga, reforçam a importância da contaminação dos magmas responsáveis pela geração dos basaltos com as rochas da crosta continental, comum em regiões de crosta continental atenuada, como é caso do Rifte Intracontinental Araí.

Referências Bibliográficas

Alkmim, F.F., Martins-Neto, M.A., 2012. Proterozoic first-order sedimentary sequences of the São Francisco craton, eastern Brazil. Marine and Petroleum Geology 33, 127–139. https://doi.org/10.1016/j.marpetgeo.2011.08.011

Alkmim, F.F., Brito Neves, B.B., Alves, J.A.C., 1993. Arcabouço tectônico do Cráton do São Francisco - uma revisão. In: Dominguez, J.M.L., Misi, A. (Eds.), O Cráton do São Francisco. Sociedade Brasileira de Geologia, Salvador, 45–62

Allen, P.A., Allen J.R., 2005. Basins analysis: principles and applications. Oxford, Blackwell Scientific Publications Ltda, 560p

Almeida, F.F.M., Hasui, Y., Brito Neves, B.B., Fuck, R.A., 1981. Brazilian structuralprovinces: an introduction. Earth-Science Reviews 17 (1), 1–29

Alvarenga, C.J.S., Botelho N.F., Dardenne M.A., Lima O.N.B., Machado M.A., 2007. Programa Levantamentos Geológicos Básicos do Brasil; Mapa Geológico da Folha Cavalcante (SD.23-V-C-V), escala: 1.100.000. Nota Explicativa Integrada com das folhas Monte Alegre de Goiás (SD.23-V-C-III), Cavalcante (SD.23-V-C-V) e Nova Roma (SD.23-V-C-VI). Goiás, UNB/CPRM, 67p

Bailey, R.A., 2004. Eruptive history and chemical evolution of the precaldera and postcaldera basalt-dacite sequences, Long Valley, California: implications for magma sources, current magmatic unrest, and future volcanism. US Geol. Surv. Prof. Pap. 1692, 76 pp.

Barbosa, O., Baptista M.B., Braun O.P.G, Dyer R.C., Costa J.C., 1969. Geologia e inventário dos recursos minerais do Projeto Brasília-Goiás. Rio de Janeiro, PROSPEC/ DNPM, 225 p.

Batata, M.E.F., Leite, J.A.D., Sousa, M.Z.A. de., 2008. Petrografia e geoquímica das rochas vulcânicas do Grupo Roosevelt, província ígnea Teles Pires, SW do Cráton Amazônico. Rev. Bras. Geociências 38, 36–53. https://doi.org/10.25249/0375-7536.20083813653

Bell, K., Lavecchia, G., Rosatelli, G., 2013. Cenozoic Italian magmatism - Isotope constraints for possible plume-related activity. J. South Am. Earth Sci. 41, 22–40. https://doi.org/10.1016/j.jsames.2012.10.005

Bell, K., Lavecchia, G., Stoppa, F., 2005. Reasoning and beliefs about Italian geodynamics. Boll. della Soc. Geol. Ital. Suppl. 5, 119–127.

Bizzi, L.A., Schobbenhaus, C., Vidotti, R.M., Gonçalves, J.H., 2003. Geologia Tectônicae Recursos Minerais do Brasil. CPRM Serviço Geológico do Brasil, Brasília, 674p.

Bosworth, W., Huchon, P., McClay, K., 2005. The Red Sea and Gulf of Aden Basins. J. African Earth Sci. 43, 334–378. https://doi.org/10.1016/j.jafrearsci.2005.07.020

Botelho, N.F., Alvarenga, C.J.S., Meneses, P.R., D'el-Rey Silva, L.J.H., 1995. Mapa Geológico da Região de Teresina de Goiás, GO. Universidade de Brasília, Brasília.

Botelho, N.F., Rossi G., 1988. Depósito de estanho da Pedra Branca, Nova Roma, Goiás. Principais Depósitos Minerais Brasileiros - Metais Básicos Não Ferrosos, Ouro e Alumínio. DNPM, Vol. 3, 267-285

Bott, M.H.P., 1995. Mechanism of rifting: geodynamic modelling of continental rift system In. Oslen

K.H (ed.). 1995. Continental Rifts: Evolution, Structure, Tectonics (Developments in Geotectonics). Amsterdam, Elsevier Science. 27-41

Brito Neves, B.B., Fuck, R.A., Pimentel, M.M., 2014. The Brasiliano collage in South America: a review. Brazilian J. Geol. 44, 493–518.https://doi.org/10.5327/Z2317-4889201400030010

Brito Neves, B.B., 2011. The Paleproterozoic in the South American Continent: diversity in the geological time. Journal of South American Earth Sciences 32, 1–20. https://doi.org/10.1016/j.jsames.2011.02.004

Brito Neves, B.B., Sá, J.M., Nilson, A.A., Botelho, N.F., 1995. A Tafrogênese Estateriana nos Blocos Paleoproterozóicos da América do Sul e Processos Subsequentes. Rev. Geonomos. https://doi.org/10.18285/geonomos.v3i2.205

Buck, W.R., 2017. The role of magmatic loads and rift jumps in generating seaward dipping reflectors on volcanic rifted margins. Earth Planet. Sci. Lett. 466, 62–69. https://doi.org/10.1016/j.epsl.2017.02.041

Buck, W.R., 2004. Rheology and deformation of the lithosphere at continental margins in Karner G et al. (eds), Columbia Univ. Press. https://doi.org/10.1177/004057368303900411

Buck, W.R., Lavier, L., Poliakov, A.N.B., 1999. How to make a rift wide. Philos. Trans. 357, 671–693. https://doi.org/10.1098/rsta.1999.0348

Bühn, B., Pimentel, M.M., Matteini, M., Dantas, E.L., 2009. High spatial resolution analysis of Pb and U isotopes for geochronology by laser ablation multi-collector inductively coupled plasma mass spectrometry (LA-MC-ICP-MS). An. Acad. Bras. Cienc. 81, 99–114.

Campos, J.E.G., Botelho, N.F., Alvarenga, C.J.S., Meneses, P.R., Moura, M.A., Dardenne, M.A., Nogueira, C., Souza, V.S., 2001. Mapa Geológico da Região de Arraias, TO. Universidade de Brasília, Brasília.

Caricchi, L., Blundy, J., 2015. The temporal evolution of chemical and physical properties of magmatic systems. Geol. Soc. London, Spec. Publ. 422, 1–15. https://doi.org/10.1144/SP422.11

Chemale, F., Dussin, I.A., Alkmim, F.F., Martins, M.S., Queiroga, G., Armstrong, R., Santos, M.N., 2012. Unravelling a Proterozoic basin history through detrital zircon geochronology: The case of the Espinhaço Supergroup, Minas Gerais, Brazil. Gondwana Res. 22, 200–206. https://doi.org/10.1016/j.gr.2011.08.016

Cordeiro, P.F. de O., Oliveira, C.G. de, 2017. The Goiás Massif: Implications for a pre-Columbia 2.2–2.0 Ga continent-wide amalgamation cycle in central Brazil. Precambrian Res. 298, 403–420. https://doi.org/10.1016/j.precamres.2017.06.021

Corfu, F., Hanchar, J.M., Hoskin, P.W.O., Kinny, P., 2003. Atlas of Zircon Textures. Reviews in Mineralogy and Geochemistry. 53 (1), 469–500. doi: https://doi.org/10.2113/0530469

Corti, G., 2009. Continental rift evolution: From rift initiation to incipient break-up in the Main Ethiopian Rift, East Africa. Earth-Science Rev. 96, 1–53. https://doi.org/10.1016/j.earscirev.2009.06.005

Cristóvão, C. A.M (Coord.)., 2017. Mapa do Estado de Goiás. Disponível em: <http://www.sieg.gov.br/siegmapas/mapa.php>. Acesso em: 25 jun.2019

Cuadros, F.A., Botelho, N.F., Fuck, R.A., Dantas, E.L., 2017a. The peraluminous Aurumina Granite Suite in central Brazil: An example of mantle-continental crust interaction in a Paleoproterozoic

cordilleran hinterland setting? Precambrian Res. 299, 75–100. https://doi.org/10.1016/j.precamres.2017.07.029

Cuadros, F.A., Botelho, N.F., Fuck, R.A., Dantas, E.L., 2017b. The Ticunzal Formation in central Brazil: Record of Rhyacian sedimentation and metamorphism in the western border of the São Francisco Craton. J. South Am. Earth Sci. 79, 307–325. https://doi.org/10.1016/j.jsames.2017.08.014

Daley, E.E., DePaolo, D.J., 1992. Isotopic evidence for lithospheric thinning during extension:Southeastern Great Basin. Geology 20 (2), 104–108. https://doi.org/10.1130/0091-7613(1992)020<0104:IEFLTD>2.3.CO;2

Danderfer Filho, A., Lana, C.C., Nalini Júnior, H.A., Costa, A.F.O., 2015. Constraints on the Statherian evolution of the intraplate rifting in a Paleo-Mesoproterozoic paleocontinent: New stratigraphic and geochronology record from the eastern São Francisco craton. Gondwana Res. 28, 668–688. https://doi.org/10.1016/j.gr.2014.06.012

Dardenne, M.A., 2000. The Brasília Fold Belt. In: Cordani U.G., Milani E, J., Thomaz Filho A., Campos D.A. (eds.), Tectonic Evolution of South América. 31st International Geological Congress. Rio de Janeiro, 231-263

De la Roche, H., Leterrier, J., Grandclaude, P., Marchal, M., 1980. A classification of volcanic and plutonic rocks using R1R2-diagram and major-element analyses - Its relationships with current nomenclature. Chem. Geol. 29, 183–210. https://doi.org/10.1016/0009-2541(80)90020-0

Deer, R.A., Howie ,W.A., Zussman, J., 1966. Introduction to The Rock-Forming Minerals Longmans, London. 528 p

Delgado, I.M., Souza, J.D., Silva, L.C., Silveira, Filho N.C., Santos R.A., Pedreira, A.J., Guimarães, J.T., Angelim, L.A.A., Vasconcelos, A.M., Gomes, I.P., Lacerda, Filho J.V., Valente, C.R., Perrotta, M.M., Heineck, C.A. 2003. Geotectônica do Escudo Atlântico. In: Bizzi L.A., Schobbenhaus C., Vidoti R.M., Gonçalves J.H. (eds.). Geologia, Tectônica e Recursos Minerais do Brasil, Texto, Mapa & SIG. Brasília, CPRM, Serviço Geológico do Brasil. 227-334.

Dusel-Bacon, C., Wooden, J.L., Hopkins, M.J., 2004. U-Pb zircon and geochemical evidence for bimodal mid-Paleozoic magmatism and syngenetic base-metal mineralization in the Yukon-Tanana terrane, Alaska. Bull. Geol. Soc. Am. 116, 989–1015. https://doi.org/10.1130/B25342.1

Dyer, R.C., 1970. Grupo Araí. Um Grupo de metamorfitos do Centro-Leste de Goiás. Revista da Escola de Minas de Ouro Preto, 28(2): 55-64.

Fan, H., Zhu, W., Li, Z., Zhong, H., Bai, Z., He, D., 2013. Lithos Ca . 1 . 5 Ga ma fi c magmatism in South China during the break-up of the supercontinent Nuna / Columbia : The Zhuqing Fe – Ti – V oxide ore-bearing ma fi c intrusions in western Yangtze Block. LITHOS 168–169, 85–98. https://doi.org/10.1016/j.lithos.2013.02.004

Farmer, G.L., 2013. Continental Basaltic Rocks, 2nd ed, Treatise on Geochemistry, 75–110 Second Edition. Elsevier Ltd. https://doi.org/10.1016/B978-0-08-095975-7.00303-X

Fram, M.S., Lesher, C.E., 1993. Geochemical constraints on mantle melting during creation of / the North Atlantic basin. Nature. 363, 712-715. DOI 10.1038363712a0

Friedmann, S.J., Burbank, D.W., 1995. Rift basins and supradetachment basins: Intracontinental extensional end-members. Basin Res. 7, 109–127. https://doi.org/10.1111/j.1365 2117.1995.tb00099.x

Fuck, R.A., Dantas, E.L., Pimentel, M.M., Botelho, N.F., Armstrong, R., Laux, J.H., Junges, S.L., Soares, J.E., Praxedes, I.F., 2014. Paleoproterozoic crust-formation and reworking events in the Tocantins Province, central Brazil: A contribution for Atlantica supercontinent reconstruction. Precambrian Res. 244, 53–74. https://doi.org/10.1016/j.precamres.2013.12.003

Fuck, R.A (coord.)., 2005. Projeto Nova Roma-Porto Real. Escala 1:50.000. Brasília, Instituto de Geociências, Universidade de Brasília.

Gioia, S.M.C.L., Pimentel, M.M., 2000. The Sm-Nd isotopic method in the Geochronology Laboratory of the University of Brasilia. An. Acad. Bras. Cienc. 72, 218–245

Grove, T.L., 2000. Origin of magmas. In: Sigurdsson H (ed.) Encyclopedia of Volcanoes, San Diego, CA: Academic Press,133–147

Guadagnin, F., Chemale, F., Magalhães, A.J.C., Santana, A., Dussin, I., Takehara, L., 2015. Age constraints on crystal-tuff from the Espinhaço Supergroup - Insight into the Paleoproterozoic to Mesoproterozoic intracratonic basin cycles of the Congo-São Francisco Craton. Gondwana Res. 27, 363–376. https://doi.org/10.1016/j.gr.2013.10.009

He, X.F., Santosh, M., 2014. Crustal recycling through intraplate magmatism: Evidence from the Trans-North China Orogen. J. Asian Earth Sci. 95, 147–163. https://doi.org/10.1016/j.jseaes.2014.02.011

Huismans, R.S., Beaumont, C., 2003. Symmetric and asymmetric lithospheric extension: Relative effects of frictional-plastic and viscous strain softening. J. Geophys. Res. Solid Earth 108, 1–22. https://doi.org/10.1029/2002JB002026

Irvine, T.N., Baragar, W.R.A., 1971. A Guide to the Chemical Classification of the Common Volcanic Rocks. Canadian Journal of Earth Science, 8, 523-548.

Jackson, S.E., Pearson, N.J., Griffin, W.L., Belousova, E.A., 2004. The application of laser ablation-inductively coupled plasma-mass spectrometry to in situ U-Pb zircon geochronology. Chem. Geol. 211, 47–69. https://doi.org/10.1016/j.chemgeo.2004.06.017

Jia, X., Wang, X., Yang, W., 2017. Petrogenesis and geodynamic implications of the early Paleozoic potassic and ultrapotassic rocks in the South China Block. J. Asian Earth Sci. 135, 80–94. https://doi.org/10.1016/j.jseaes.2016.12.013

Kearey, 2013. Global Tectonics, Journal of Chemical Information and Modeling. https://doi.org/10.1017/CBO9781107415324.004

Kieffer, B., Arndt, N., Bastien, F., Bosch, D., Pecher, A., Yirgu, G., Ayalew, D., Weis, D., Jerram, D.A., Keller, F., Meugniot, C., 2004. Flood and Shield Basalts from Ethiopia : Magmas from the African Superswell 45, 793–834. https://doi.org/10.1093/petrology/egg112

Leeman, W.P., Annen, C., Dufek, J., 2008. Snake River Plain – Yellowstone silicic volcanism: implications for magma genesis and magma fluxes. Geol. Soc. London, Spec. Publ. 304, 235–259. https://doi.org/10.1144/SP304.12

Li, Y.Q., Ma, C.Q., Robinson, P.T., 2016. Petrology and geochemistry of Cenozoic intra-plate basalts in east-central China: Constraints on recycling of an oceanic slab in the source region. Lithos 262, 27–43. https://doi.org/10.1016/j.lithos.2016.06.012

Ludwig, K.R. 2012. Isoplot. A Geochronological Toolkit for Microsoft Excel. Ver. 3.75. Berkeley Geochronology Center.

Ludwig, K.R., 2008. User's Manual for Isoplot 3.70. Berkeley Geochronol. Cent. Spec. Publ. 76.

Lugmair, G.W., Marti, K., 1978. Chemistry Department, B-O17, University of California at San Diego, La Jolla, CA 92093 (U.S.A.). Evolution (N. Y). 39, 349–357.

Marini, O. J., Botelho N. F., 1986. A província de granitos estaníferos de Goiás. Revista Brasileira de Geociências, 16:119-131

Marques, G.C., 2009. Geologia dos grupos Araí e Serra da Mesa e seu embasa-mento no sul de Tocantins. Universidade de Brasília, Brasília (MSc Dissertation),120p.

Martins-Ferreira, M.A.C., Chemale, F., Dias, A.N.C., Campos, J.E.G., 2018. Proterozoic intracontinental basin succession in the western margin of the São Francisco Craton: Constraints from detrital zircon geochronology. J. South Am. Earth Sci. 81, 165–176. https://doi.org/10.1016/j.jsames.2017.11.018

Mayborn, K.R., Lesher, C.E., 2004. Paleoproterozoic mafic dyke swarms of northeast Laurentia: products of plumes orambientmantle? Earth and Planetary Science Letters. 225, 305–317

Mazumder, R., Arima, M., 2009. Implication of Mafic Magmatism in an Intracontinental Rift Setting : A Case Study from the Paleoproterozoic Dhanjori Formation , Singhbhum Crustal Province , India 117, 455–466. https://doi.org/10.1086/599197

Menzies, M.A., Klemperer, S.L., Ebinger, C.J., Baker, J., 2002. Characteristics of volcanic rifted margins. Spec. Pap. 362 Volcan. Rift. Margins 362, 1–14. https://doi.org/10.1130/0-8137-2362-0.1

Morimoto, N., 1988. Nomenclature of Pyroxenes. Mineralogy and Petrology, 39, 55-76. http://dx.doi.org/10.1007/BF01226262

Nakamura, N., 1974. Determination of REE, Ba, Fe, Mg, Na and K in Carbonaceous and Ordinary Chondrites. Geochimica et Cosmochimica Acta, 38, 757-775. http://dx.doi.org/10.1016/0016-7037 (74)90149-5

Niu, Y., O'Hara, M.J., 2003. Origin of ocean island basalts: A new perspective from petrology, geochemistry, and mineral physics considerations. J. Geophys. Res. Solid Earth 108. https://doi.org/10.1029/2002JB002048

Olsen, K.H., 1995. Continental Rifts: Evolution, Structure, Tectonics (Developments in Geotectonics). Amsterdam, Elsevier Science, 490 p

Pearce, J.A., 2008. Geochemical fingerprinting of oceanic basalts with applications to ophiolite classification and the search for Archean oceanic crust. Lithos 100, 14–48. https://doi.org/10.1016/j.lithos.2007.06.016

Pearce, J.A., 1996. A User's Guide to Basalt Discrimination Diagrams. In: Wyman, D.A., Ed., Trace Element Geochemistry of Volcanic Rocks: Applications for Massive Sulphide Exploration, Geological Association of Canada, Short Course Notes, Vol. 12, 79-113

Pearce, J.A., Norry, M.J., 1979. Petrogenetic Implications of Ti, Zr, Y, and Nb Variation in Volcanic Rocks. Contributions to Mineralogy and Petrology, 69, 33-47. http://dx.doi.org/10.1007/BF00375192

Pimentel, M.M., 2016. The tectonic evolution of the Neoproterozoic Brasília Belt, central Brazil: a geochronological and isotopic approach. Brazilian J. Geol. 46, 67–82. https://doi.org/10.1590/2317-4889201620150004

Pimentel, M.M., Jost, H., Fuck, R.A. 2004. O embasamento da Faixa Brasília e o Arco Magmático de Goiás. In: Mantesso-Neto, V., Bartorelli, A., Carneiro, C.D.R., Brito-Neves, B.B. (Eds.). Geologia do continente Sul-Americano: evolução da obra de Fernando Flávio Marques de Almeida. Ed. Beca. 355–368

Pimentel, M. M., Botelho N. F., 2001. Sr and Nd isotopic characteristics of 1,77-1,58 Ga rift related granites and volcanics of the Goiás province, Central Brazil. Anais da Academia Brasileira de Ciências, 73: 263–276

Pimentel, M.M., Heaman L., Fuck R.A., Marini O.J., 1991. U-Pb Zircon Geochronology of Precambrian tin-bearing continental – type acid in central Brazil. Precambrian Research, 52, 321-335

Pirajno, F., Santosh, M., 2015. Mantle plumes, supercontinents, intracontinental rifting and mineral systems. Precambrian Res. 259, 243–261. https://doi.org/10.1016/j.precamres.2014.12.016

Ring, U., Livingstone, D., Stanley, H.M., Fischer, G., 2014. The East African Rift System. Aust. J. Earthsciences 107/1, 132–146

Rollinson, H.R., 1993. Using Geochemical Data: Evaluation, Presentation, Interpretation. Longman Scientific and Technical, England, 352 p

Rubatto, D., 2002. Zircon trace element geochemistry: partitioning with garnet and the link between U–Pb ages and metamorphism. Chemical Geology. 184 (2002), 123-138

Rudnick, R.L., Gao, S., 2013. Composition of the Continental Crust, 2nd ed, Treatise on Geochemistry: Second Edition. Elsevier Ltd. https://doi.org/10.1016/B978-0-08-095975-7.00301-6

Ruppel, C., 1995. Extensional processes in continental lithosphere. J. Geophys. Res. Solid Earth 100, 24187–24215. https://doi.org/10.1029/95JB02955

Sengör, A.M.C., Burke K., 1978. Relative timing of rifting and volcanism on earth and tectonic implications. Geophysical Research Letters, 5: 419-421

Sun, S. -s., McDonough, W.F., 1989. Chemical and isotopic systematics of oceanic basalts: implications for mantle composition and processes. Geol. Soc. London, Spec. Publ. 42, 313–345. https://doi.org/10.1144/GSL.SP.1989.042.01.19

Tanizaki, M.L.N., Campos, J.E.G., Dardenne, M.A., 2015. Estratigrafia do Grupo Araí: registro de rifteamento paleoproterozoico no Brasil Central. Brazilian J. Geol. 45, 95–108. https://doi.org/10.1590/23174889201500010007

Thybo, H., Nielsen, C.A., 2009. Magma-compensated crustal thinning in continental rift zones. Nature 457, 873–876. https://doi.org/10.1038/nature07688

Valeriano, C.M., Pimentel, M.M., Heilbron, M., Almeida, J.C.H., Trouw, R.A.J., 2008. Tectonic evolution of the Brasilia Belt, central Brazil, and earlyassembly of Gondwana. Geological Society, London Special Publication 294, 197-210

Valeriano, C.M., Dardenne, M.A., Fonseca, M.A., Simões, L.S.A., Seer, H.J., 2004.A evolução tectônica da Faixa Brasília. In: Mantesso Neto, V., Bartorelli, A.,Carneiro, C.D.R., Brito Neves, B.B. (Org.), Geologia do Continente Sul-Americano– Evolução da obra de Fernando Flávio Marques de Almeida. São Paulo, Beca. 575–592

Xia, L., Li, X., 2019. Basalt geochemistry as a diagnostic indicator of tectonic setting. Gondwana

Res. 65, 43–67. https://doi.org/10.1016/j.gr.2018.08.006

Xia, L., Xia, Z., Xu, X., Li, X., Ma, Z., 2013b. Late Paleoproterozoic rift-related magmatic rocks in the North China Craton: Geological records of rifting in the Columbia supercontinent. Earth-Science Rev. 125, 69–86. https://doi.org/10.1016/j.earscirev.2013.06.004

Xu, Z., Zheng, Y.F., Zhao, Z.F., 2017. The origin of Cenozoic continental basalts in east-central China: Constrained by linking Pb isotopes to other geochemical variables. Lithos 268–271, 302–319. https://doi.org/10.1016/j.lithos.2016.11.006

Wang, X.C., Wilde, S.A., Xu, B., Pang, C.J., 2016. Origin of arc-like continental basalts: Implications for deep-Earth fluid cycling and tectonic discrimination. Lithos 261, 5–45. https://doi.org/10.1016/j.lithos.2015.12.014

Wang, Y., Zhao, Z., Zheng, Y., Zhang, J., 2011. Lithos Geochemical constraints on the nature of mantle source for Cenozoic continental basalts in east-central China. LITHOS 125, 940–955. https://doi.org/10.1016/j.lithos.2011.05.007

Wiedenbeck, M., Allé, P., Corfu, F., Griffin, W.L., Meier, M., Oberli, F., Quadt, A. Von, Roddick, J.C., Spiegel, W., 1995. Three Natural Zircon Standards for U-Th-Pb, Lu-Hf, Trace Element and Ree Analyses. Geostand. Newsl. 19, 1–23. https://doi.org/10.1111/j.1751-908X.1995.tb00147.x

Wilson, M., 1995. Magmatic differentiation. Geol.Soc. London, Mem. 16, 205–218. https://doi.org/10.1144/GSL.MEM.1995.016.01.21

Wilson, M., 1989. Igneous petrology. A global tectonic approach, Unwin Hyman. Boston. 466 p

Winchester, J.A., Floyd, P.A., 1977. Geochemical Discrimination of Different Magma Series and Their Differentiation Product Using Immobile Elements. Chemical Geology, 20, 325-343. http://dx.doi.org/10.1016/0009-2541(77)90057-2

Wood, D.A., 1980. The application of a Th{single bond}Hf{single bond}Ta diagram to problems of tectonomagmatic classification and to establishing the nature of crustal contamination of basaltic lavas of the British Tertiary Volcanic Province. Earth Planet. Sci. Lett. 50, 11–30. https://doi.org/10.1016/0012-821X(80)90116-8

Zhang, Z., Mao, J., Saunders, A.D., Ai, Y., Li, Y., Zhao, L., 2009. Petrogenetic modeling of three mafic-ultramafic layered intrusions in the Emeishan large igneous province, SW China, based on isotopic and bulk chemical constraints. Lithos 113, 369–392. https://doi.org/10.1016/j.lithos.2009.04.023